TUNABLE-FILTER BASED MULTISPECTRAL IMAGING FOR DETECTION OF BLOOD STAINS ON CONSTRUCTION MATERIALS

SUWATWONG JANCHAYSANG

A THESIS SUBMITTED IN FULFILLMENT

OF THE REQUIREMENT FOR THE DEGREE OF

DOCTOR OF PHILOSOPHY OF SCIENCE IN APPLIED PHYSICS

FACULTY OF SCIENCE

KING MONGKUT'S INSTITUTE OF TECHNOLOGY LADKRABANG

2013

KMITL-2013-SC-D-030-037

หัวข้อวิทยานิพนธ์	การใช้ภาพหลายความยาวคลื่นโดยอาศัยตัวกรองแสงแบบปรับความยาวคลื่นได้ในการตรวจหาคราบเลือดบนพื้นผิววัสดุก่อสร้าง
นักศึกษา	พันโท สุวัฒน์วงศ์ จันทร์ฉายแสง
รหัสประจำตัว	49067003
ปริญญา	วิทยาศาสตร์คุษฎีบัณฑิต
สาขาวิชา	ฟิสิกส์ประยุกต์
พ.ศ.	2556
อาจารย์ที่ปรึกษาวิทยานิพนธ์	ดร.ประธาน บุรณศิริ ดร.ศรัณย์ สัมฤทธิ์เดชขจร

บทคัดย่อ

วิทยานิพนธ์ฉบับนี้ได้ทำการพัฒนาและสาธิตวิธีการในการตรวจหาคราบเลือด ซึ่งเปื้อนบนพื้นผิววัสดุก่อสร้างโดยใช้ระบบจับภาพหลายความยาวคลื่นแสง ในขั้นตอนแรกสุดได้ทำการวัดค่าสเปกตรัมการสะท้อนแสงของคราบต่างๆ บนพื้นผิวรองรับหลายชนิดโดยอาศัยวิธีการสอบเทียบอย่างง่าย และพบว่ารูปร่างของสเปกตรัมการสะท้อนแสงที่ได้จากคราบดังกล่าวได้รับอิทธิพลจากรูปร่างของสเปกตรัมการสะท้อนแสงของพื้นผิวรองรับ ต่อมาจึงใช้ทฤษฎีคูเบลกา-มังค์ (Kubelka-Munk) มาทำการแปลงสเปกตรัมการสะท้อนแสงดังกล่าว ให้เป็นสเปกตรัมการดูดกลืนแสงคูเบลกา-มังค์ (KM absorbance spectra) จากนั้นเกณฑ์การคัดแยกคราบเลือดซึ่งใช้ค่าพารามิเตอร์ทางสเปกตรัมของแสงต่างได้ถูกกำหนดขึ้น โดยมีพื้นฐานมาจากข้อมูลการทดลอง ต่อมาเกณฑ์ดังกล่าวได้ถูกทดสอบและปรับปรุงจนมีประสิทธิภาพ ในวิธีการที่ได้สร้างขึ้นนั้น การระบุคราบเลือดจะกระทำโดยใช้การตัดสินทางคณิตศาสตร์แบบตรรกะบูเลียน (Boolean logics) แทนวิธีการแบบดั้งเดิมในการเพิ่มความแตกต่างของเงาแสงบนภาพของคราบ วิธีการที่นำเสนอช่วยให้สามารถแยกแยะคราบเลือดได้ดียิ่งขึ้น ไม่ทำให้เกิดความเสียหายต่อหลักฐาน รวดเร็ว และสามารถนำไปพัฒนาต่อได้ง่าย ผลการทดลองระบุว่าเกณฑ์ในการตรวจหาคราบเลือดที่ถูกพัฒนาขึ้นสามารถตรวจหาคราบเลือด และสามารถแยกคราบเลือดจากคราบอื่นๆ บนผิววัสดุก่อสร้างได้ด้วยความแม่นยำ (Sensitivity) ในช่วง 0.60-0.95 แนวทางที่นำเสนอขึ้นยังได้นำมาสร้างเป็นระบบตรวจหาคราบเลือดแบบรวดเร็วโดยใช้

ภาพหลายความยาวคลื่น ระบบดังกล่าวจะทำการจับภาพหลายความยาวคลื่นโดยอัตโนมัติ ตรวจหาสเปกตรัมการสะท้อนแสงบนพื้นผิว และตรวจหาตำแหน่งของคราบเลือด จากนั้นจะแสดงตำแหน่งของคราบเลือดบนหน้าจอ ในการดำเนินการดังกล่าว มีกระบวนการที่สำคัญที่ได้คิดค้นขึ้น ได้แก่ (1) การปรับระยะเวลาในการเปิดหน้ากล้องแบบอัตโนมัติ เพื่อให้สอดคล้องกับพื้นผิวตัวอย่างและเพื่อป้องกันภาพหลายความยาวคลื่นมืดหรือมีแสงจ้าเกินไป (2) การตรวจหาตำแหน่งต่างๆ ที่ไม่มีการเปื้อนของคราบใดๆ บนพื้นผิวโดยอัตโนมัติเพื่อหาสเปกตรัมการสะท้อนแสงของพื้นผิวรองรับ (3) การจัดลำดับในการใช้เกณฑ์การคัดแยกต่างๆ เพื่อกำจัดการคำนวณซึ่งไม่จำเป็น และ (4) กระบวนการคู่ขนานระหว่างการจับภาพหลายความยาวคลื่นและการตรวจระบุคราบเลือดเพื่อช่วยลดเวลาในการตรวจพิสูจน์ ทั้งๆ ที่มีข้อมูลที่ต้องจัดการจำนวนมาก ระบบที่พัฒนาขึ้นสามารถตรวจพิสูจน์คราบเลือดเปรียบเทียบกับคราบสีน้ำตาลแดงอื่นๆ หลายชนิดบนพื้นผิวรองรับต่างๆ ด้วยเวลาเฉลี่ยในการตรวจพิสูจน์ในช่วง 23.3-28.7 วินาที ทั้งนี้รวมเวลาในการจับภาพไว้แล้ว

คำสำคัญ : การจับภาพหลายความยาวคลื่นแสง, การตรวจพิสูจน์คราบเลือด, ทฤษฎีดูเบลกา-มังค์, การประมวลผลภาพ, นิติวิทยาศาสตร์

Thesis Title	Tunable filter-based multispectral imaging for detection of blood stains on construction material substrates.
Student	Suwatwong Janchaysang
Student ID	49067003
Degree	Dotor of Philosophy
Program	Applied Physics
Year	2013
Thesis Advisors	Dr. Prathan Buranasiri Dr. Sarun Sumriddetchakajorn

Abstract

In this thesis, the method of using multispectral imaging system in rapid and less substrate-dependent detection of blood stains deposited on construction materials have been developed and demonstrated. First, a number of reflectance spectra of different stains on many substrates have been collected using a simple calibration method. It is found that the shapes of the blood stain reflectance spectra are much influenced by the reflectance spectrum of the substrate on which they are deposited. Kubelka Munk (KM) theory is applied to transform the acquired stains' reflectance spectra into the less substrate dependent KM absorbance spectra. Blood discrimination criteria based upon spectral parameters are then established from empirical data, tested, and refined. In our newly invented method, instead of introducing conventional contrast enhancement on the stain images, blood stain determination is executed mathematically via Boolean logics, resulting in more discriminative blood stain identification. This proposed approach allows for non-destructive, quick, discriminative, and easy-to-improve presumptive blood stain detection. Experimental results confirm that our blood stain discrimination criteria can be used to locate blood stains on several construction materials with high precision. True positive rates (sensitivity) from 0.60 to 0.95 are achieved depending on blood stain faintness and substrate types. Also, true negative rates (specificity) between 0.55 and 0.96 are accomplished. Based on the above

established criteria, all necessary tasks are then combined and organized to realize the multispectral imaging-based rapid blood stain detection system. To rapidly detect blood stains on the test surface, the developed system automatically captures the spectral images, extracts their spectral data, determines the positions of blood stains, and accurately highlights the positions of blood stains on the display. To achieve such a system, several tasks are newly introduced, including adjustment of camera exposure times to prevent image saturation or excessive darkness, the search for the sampled clean positions of the substrate in order to determine the substrate reflectance spectrum, and suitable detection procedures and proper arrangement of criteria in order to eliminate unnecessary calculations. Parallel processes between image capturing and blood stain identification help shorten the time for blood stain identifications despite a large amount of spectral data to be processed. The developed system can identify blood against several other reddish brown stains on several substrates. The measured average identification times on different test surfaces range from only 23.3 to 28.7 seconds including the image capturing process.

Keywords: Multispectral imaging system, Blood stain detection, Kubelka Munk theory, Image processing, Forensic science

Acknowledgement

Attempts that I made in my Ph.D. work have resulted in more failures than successes. There have been so many times, I felt like I was running in a labyrinth and couldn't find the way out. However, I had it my mind all along that I would never give up. Through the ups and downs, I knew that it would finally be a success.

I would like to thank Dr. Prathan Buranasiri and Dr. Sarun Sumriddetchakajorn, my advisors for their valuable suggestions and corrections, for the opportunity and for their patience they have had with me. I would like to thank the faculties, staff, and graduate committee at the Faculty of Science, King Mongkut's Intitute of Technology (KMITL), the thesis committee and especially the graduate committe for their support and for giving me time extension to finish my Ph.D work. I apologize for all the troubles I might have caused them.

I would like to thank fellows at Photonic Technology Lab (PTL) at NECTEC, namely Boonsong Sutapan, Yuttana Intarawane, Ratthasart Amarit, Kosom Chaitavon, Sataporn Chanhorm, Armote Somboonkaew, and Suwannee Phoojaruenchanachai and others whom I do not mention here for helping me on many occasions. Special Thanks for colleagues and brothers at Chulachomklao Royal Military Academy (CRMA), especially at the Physics Department and the Royal Thai Army for their support.

I would like to especially thank Thailand Graduate Institute of Science and Technology (TGISTS) for giving me scholarship, National Science and Technology Development Agency (NSTDA) and National Electronics and Computers Technology Center (NECTEC) for giving me a chance and resources to do this work. Without money support, all the though work would be ten times tougher.

I would like to thank my parents, and my relatives for their support and care. And I would like to apologize my wife Kwancheewa Janchaysang, and my kids Nattapat Janchaysang and Pimchanok Janchaysang for spending too much time with this work while I should have spent valuable time with them. They are the most precious thing in my life. I

lost many things I should not during doing my Ph.D. But it didn't matter at all since I still have my wife and kids. This success would be meaningless without them. So many days, I worked two jobs during the day and managed to be back home to be around my kids in the evening. After they went to bed, I drove 75 km to my work place, worked on my Ph.D. until I fell asleep, woke up and repeated the same routine for another day. There has almost never been a period that I worked for my Ph.D. without doing work for living. And, I know that there are many people who have been doing the same thing. I wish that they would succeed too. "If you just believe it, there's nothing to it."

Last but not least, I would like to thank and pay respect for all my teachers, who have ever taught me in my life, including Dr.Prathan and Dr.Sarun. I wouldn't have these days without them.

Table of contents

List of figures

List of tables

Chapter 1

Introduction

1.1 Motivations and research questions

The motivation of this thesis came from Kunying Pornthip Rojanasunand (M.D.) who stated the problems on her talk given at the National Electronics and Computer Technology Center (NECTEC) in 2009. One of the problems concerning presumptive blood stain detection occurred in the forensic investigation work in the southern provinces of Thailand. In their forensic investigation, presumptive tests for blood stain are performed using Luminol reagent. The main problem with Luminol is that the crime scene must be kept dark during the collection of pictures of the suspected areas. However, given the insurgency crisis in the southern provinces of Thailand, in some situations, collection of forensic evidence at night becomes a dangerous task. Quite often, the crimes take place in the open area, which makes the investigation more difficult. Moreover, the visible traces of blood as a consequence of Luminol testing appear within 30 seconds after the reagent is applied, making the picture capturing hard to perform. Even if the images of blood traces can be captured, it is still hard to resume the position of the blood stain via comparing the captured images with the real scene. During 2009, several works in multispectral imaging were going on in the Photonics Technology Laboratory (PTL) at NECTEC where the author has performed this doctoral thesis, so the knowledge and tools in multispectral imaging were somewhat available. With the awareness of the aforementioned problem and the available instruments in hand, we took the opportunity to explore the possibility of solving the above problem using a multispectral imaging system, which came the starting point of this thesis.

At the beginning of this research, we did not know much about forensic investigation. So, we asked ourselves several general questions. Some of these questions are stated as follows.

1. How do the current blood stain detection methods really work?
2. Are there existing blood stain detection methods that can solve the problem of the forensic team? If the methods exist, how do they work and what are their weaknesses?
3. Have the applications of the multispectral imaging in presumptive blood stain detection existed? If they exist, can they be used to solve the problems of the forensic teams? What are the advantages of multispectral imaging methods over the conventional methods? What are their limitations?
4. What can we do to improve the existing multispectral imaging methods and techniques to solve the problems for the forensic team?

Then, we started with the extensive literature review on the existing blood stain detection techniques, as will be discussed in detail in chapter 2. As we went deeper into it, we found that there are several existing methods for blood stain detections. Chemical methods are the most widespread ones. However, all the methods have weaknesses and no methods can really solve the problems of the forensic team. Furthermore, multispectral imaging methods in the presumptive investigation of blood stain are not prevalent. There are a few uses of the multispectral blood detection techniques in the laboratory. Nevertheless, there has been no use of multispectral techniques in real crime scenes yet.

Then, we continued our research by performing the initial experiments and analysis. We collected and studied a number of reflectance spectra of stains on several substrates. The details of these experiments will be discussed in chapter 4. Soon, the reasons why this field was on hold were uncovered. It was evident to us that the main problems of the multispectral imaging techniques have to do with the nature of staining of substances on substrates. There is the spectral mixing, both linear and nonlinear, between the stains and substrates. Providing the infinite possibilities of substrates profiles and the possibilities of stain thickness on the substrates, the spectra of the stains on substrates are very dependent on substrates. The problem had not been properly dealt with. The suitable blood stain detection method, therefore, could have not been established.

1.2 Objectives of the thesis

After the initial experiments, we realized that the main problem has to be fixed first. Hence, we have narrowed down the scope of our study in this thesis to just solving the main problem of using multispectral imaging technique for presumptive blood stain detection and to demonstrate that our invented method is valid and possible to become a presumptive blood stain detection method. Then, the goals of this study are officially set to the following tasks.

1. *Establish the presumptive blood stain detection method that is much more independent of substrate profiles using the multispectral imaging technique.*
2. *Demonstrate that the above technique can be used to achieve fast blood stain detection and have the potential to become the in-situ presumptive blood stain detection system.*

1.3 Overview of the thesis

This thesis is organized into six chapters, named as follows:

Chapter 1 Introduction
Chapter 2 Literature review on related theories and existing technologies
Chapter 3 Experimental framework
Chapter 4 Experiment Part I: Developing blood stain discrimination criteria
Chapter 5 Experiment Part II: Realization of rapid blood stain detection
Chapter 6 Conclusion

Here in Chapter 1, we state the motivations, problems, objectives, and overview of the research.

Chapter 2 gives the literature review on conventional blood stain detection techniques, basics on multispectral imaging system and blood stains, the existing applications of multispectral imaging system for blood stain discrimination, and related theories.

Chapter 3 describes the experimental frame work, which includes all the integrated instruments of the multispectral imaging system, on which this research is based, the calibration and spectral recovery methods.

Chapter 4 discusses the initial experiment, the problems with the existing multispectral imaging methods in blood stain detection, the method to solve the problem and the establishment of blood stain detection criteria and method. This chapter tells how effects of substrate reflectance on spectral is taken into account. The results of the proposed method were evaluated.

Chapter 5 shows how the proposed blood stain detection criteria and method established in chapter 4 can be applied to really make a fast blood stain detection system. In this chapter, the mechanisms which are specific to the method, including the quick substrate search and substrate reflectance determination, the data manipulation in matrix forms, the automatic exposure time adjustments were proposed, demonstrated, and evaluated.

Chapter 6 gives the conclusions, the future work, and the possible system architecture that would be achieved in real crime scene investigation according to the established blood stain detection method.

1.4 The potential benefits of the thesis

The thesis presents the novel method of forensically detecting blood stain using multispectral imaging system. With future modification of the method, the in situ presumptive blood detection devices may potentially be realized. The expected system will be portable, fast, reliable, and specific. The establish method still has the potential in detection of other substances such as ink or other stains.

Chapter 2

Literature review on existing technologies and related theories

In this chapter, the literature review on blood stain detection techniques, the natures of blood stains, the overview of multispectral imaging systems, the existing multispectral imaging blood stain detection techniques, and related theories are discussed.

2.1 Existing forensic blood stain detection methods

Presumptive blood stain detection and identification are essential in crime investigation. Efficient detection methods help bring justice to those people who are desperate for it, as well as save valuable time of the forensic investigators. Several methods are applied for this task including chemicals, light sources, and spectroscopic means. The review of these approaches is given in the following subsections.

2.1.1 Chemical based approaches

Several chemical approaches have been implemented for presumptive blood stain detections. Common chemical based tests include crystal tests and catalytic tests. In crystal test, haem groups, the red color proteins in hemoglobin, are crystallized when reacted with reagents [1]. Pyridine and acetic acid are among common reagents. This method requires microscopic observation and is accordingly unpractical in crime scenes.

Catalytic color tests are often employed at the crime scene to confirm visible stains whether they are truly blood. In this method, reagent and hydrogen peroxide are sprayed on samples. Hydrogen peroxide, catalyzed by haem group in blood, breaks down and causes the oxidation and color change in active reagents [2]. Benzidines, leucomalachite green, leucocrystal violet, phenolphthalein and ortho-tolidine are usually used as color-changing reagents. Another catalytic approach is based on fluorescence or chemiluminescence of reagents [3]. In this method, reagents and hydrogen peroxide are also simultaneously applied on samples. However, the breakdown of hydrogen peroxide by haem group causes reagents

to fluoresce or chemiluminesce instead of changing color. Fluoresceine and 3-aminophthalhydrazide (Luminol) are common reagents. The former exhibits fluorescence when oxidized, while the latter shows chemiluminescence. These tests are widely used to detect non-visible blood traces in the crime scene. However, the tests are not very specific to blood. Other substances such as detergents and bleach, as well as several animals' blood result in false positive chemiluminescense and fluorescence. Nevertheless, crime scene must be maintained very dark in order to detect faint fluorescent light from the blood. Figure 2.1 shows the example of photograph taken from tracing of blood by Luminol. Those faint fluorescent or chemiluminescent traces of blood occur within 30 seconds after reagents are applied, so capturing images is difficult in real crime scene. In some dangerous situation, the investigation cannot be kept dark or awaited until night time but must be performed under daylight. For all chemical based blood detection tests, application of chemical agents can wash away the crucial evidence in the scenes.

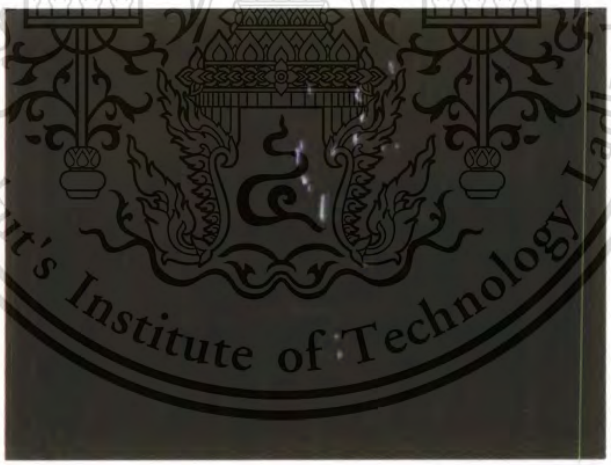

Figure 2.1 Sample Photograph of the scene traced by Luminol. Crime scene must be kept very dark. Problems occur due to the short-time range and low luminosity of the chemi-luminescense traces of the methods [4].

2.1.2 Ultraviolet light sources

For the above reasons, non-contact detection approaches via imaging technology are preferred. In the simplest non imaging method, forensic light sources make use of ultraviolet

(UV) light to detect fluorescent traces of body fluids, such as semen, urine, and saliva [5-6]. However, fluorescence emission of blood is not observed over the spectrum ranging from UV to near infrared regions. The use of UV light sources is therefore limited to making visible the blood spatters on some fluorescent substrates such as clothes, papers, and some painted surfaces. Moreover, UV light can possibly damage DNA evidence in blood.

2.1.3 Infrared photography

Infrared photography is another method used to detect blood stains. The method can enhance visibility of blood spatters on dark-colored clothes since blood strongly absorbs near infrared radiation (700-1000 nm) while most fabrics reflect it [7-8]. The mechanism of the devices in this method is simple. It consists of a camera with the optical filter that allows the IR to pass through the camera's lens. The method can be performed in broad daylight or with the normal light sources, which infrared radiation is always present. Nevertheless, the method is restricted to the detection of blood stains on fabrics and cannot effectively distinguish blood against many other stains.

2.1.4 Multimode imaging in thermal infrared

Recently, Morgan group [9-11] has combined the measurement of infrared reflectance, thermal emission, and thermal diffusion rates in multimode imaging to successfully detect faint blood against four other stains. According to the method, intense light source along with mechanical chopper provide periodic heating and cooling onto the surface. Figure 2.2 can be used to illustrate the principle of the method. The thermal infrared signals are detected from the surface as a function of time from the neat fabric, the fabric doped with dye and the gold reflectance standard. During the times that the surface is illuminated by the light, thermal emission, obtained via thermal imaging camera, can indicate the absorption properties of surface. It is seen that the part of the fabric doped by gold standard shows high infrared signal because high absorption and thermal emission of gold metal. The neat fabric and the fabric doped with dye show slower increase infrared signal, indicating lower thermal emission. The infrared signal, obtained at the times the surfaces is not illuminated by the light, can indicate thermal diffusion properties of surface. Similarly, the fabric doped with gold standard show the fastest thermal diffusion among the three surfaces. Also, the typical

diffuse reflectance in infrared region is measured for these samples. A combination of these three mode measurement is claimed to be used to enhance the chemical contrast on the surfaces and be able to detect faint blood stain out of four types of stains. However, the approach is still limited to the detection of blood stain on black acrylic fabric.

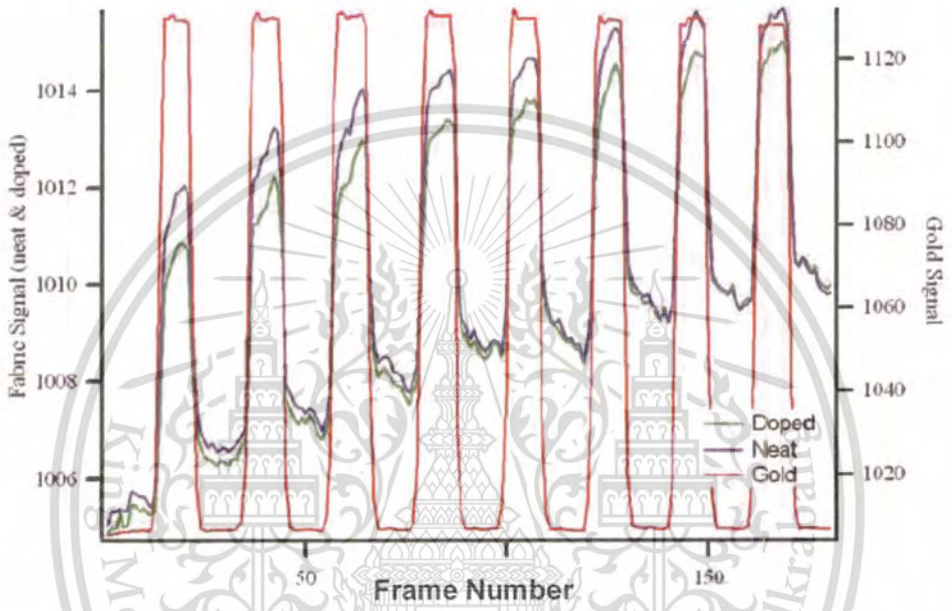

Figure 2.2 Periodic illumination with intense optical radiation provides a way of measuring thermal properties of the surfaces, which used to enhance chemical contrast on the surfaces [9]. [ต้องบอกแหล่งที่มาไหม]

2.2 Multispectral imaging

2.2.1 Overview of multispectral imaging system

Multispectral Imaging is a process through which the object of interest is imaged separately at different optical wavelengths of the electromagnetic spectrum. It is basically a type of spectroscopy. The number of wavelengths can vary from 2 up to more than one hundred. When the number of spectral images is large (more than 100), the method is usually called the hyperspectral imaging. The greater number of wavelengths, the more spectral details about the system can yield. However, the numbers of wavelengths to be used

depend mainly on the types and purposes of the applications. Multispectral imaging system can be either fluorescence based [12-13], or reflection based [14]. In this thesis, we focus only on reflection-based multispectral imaging. The imaging mechanism of the multispectral system is just the same as that of the normal imaging system. To obtain multispectral images, variable filter is attached in front of the camera to select certain spectral portion of light to it. Liquid crystal tunable filter (LCTF) [15-16], acousto-optic tunable filter [17-18], or filter wheel [19] can be used for this purpose. However, the LCTF based is the most common type of the multispectral imaging system. Alternatively, imaging using normal monochrome or trichromatic camera along with adjustable light sources can also review the spectral details of the imaged surfaces [20-22]. Multispectral imaging data can even extracted from a typical trichromatic camera by considering R G and B pixels of the image sensor array separately [23]. The obtained spectral details for multispectral system vary depending on the number of channels and bandwidth of the filter, the methods and algorithms of spectral recovery. For our multispectral imaging system, the LCTF is used. Currently, complete sets of handheld, ground-based, airborne, or even space-borne multispectral imaging systems are commercially available [24]. Costs and qualities of the systems differ. Figures of merit include the number of spectral channels, spectral resolution of the filter, speed, image resolutions, type of applications and equipped analytical programs.

The information obtained from the spectral images characterizes spectral properties of each location of the imaged surfaces. The multispectral images are understandably described by the 3-dimensional image cube. Two of the dimensions are spatial dimensions and one is a spectral dimension. The illustration of an image cube taken from a sampled surface in this research is illustrated in Figure 2.3. The figure shows only 5 spectral images for the purpose of delineation. In fact, the number of the spectral images taken by the devices in this thesis is up to 61 images.

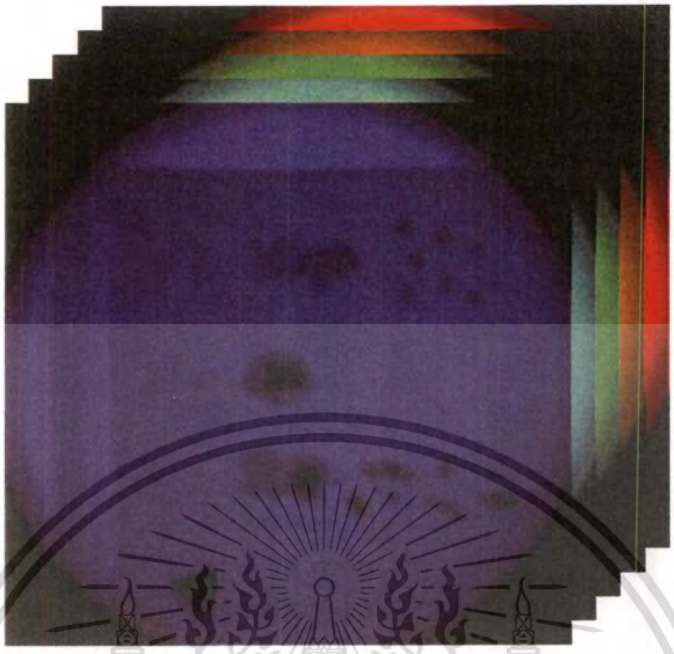

Figure 2.3 Three dimensional multispectral image cube consists of two spatial dimension and one spectral dimension.

2.2.2 Calibration and spectral reconstruction

The digital responses given by the camera in multispectral system do not reflect the true spectral identity of the imaged surfaces. Many instrumental factors are involved in the multispectral imaging process. To illustrate the mechanism of multispectral imaging, let's consider the propagation of light from a certain part of a typical diffuse object through a typical system to a single pixel, shown in Figure 2.4. The light incident on the imaged surface is reflected in all directions. Part of the reflected light propagates through the variable filter and the camera's aperture respectively, and is then mapped onto the corresponding sensor (either CCD or CMOS pixel) of the camera. The pixel collects the incoming photons and digitally registers the optical energy as the digital readout or pixel value. Therefore, the recorded pixel value of the pixel, denoted by $T_k(\lambda)$, depends on many factors, and can be expressed as:

$$T_k(\lambda) = \cdot \int i(\lambda) \cdot R(\lambda) \cdot o(\lambda) \cdot F_k(\lambda) \cdot \alpha(\lambda) d\lambda + n \tag{2.1}$$

where $i(\lambda)$ is the illuminant intensity falling on the surface at the area, $R(\lambda)$ spectral reflectance of the surface, $o(\lambda)$ is the spectral transmittance of the optical system in front of the detector array not including the tunable filter, $F_k(\lambda)$ is the spectral transmittance of tunable filter at the k-th spectral channel, $\alpha(\lambda)$ is the linear spectral sensitivity of the CCD camera's sensor and n is the noise present in the system.

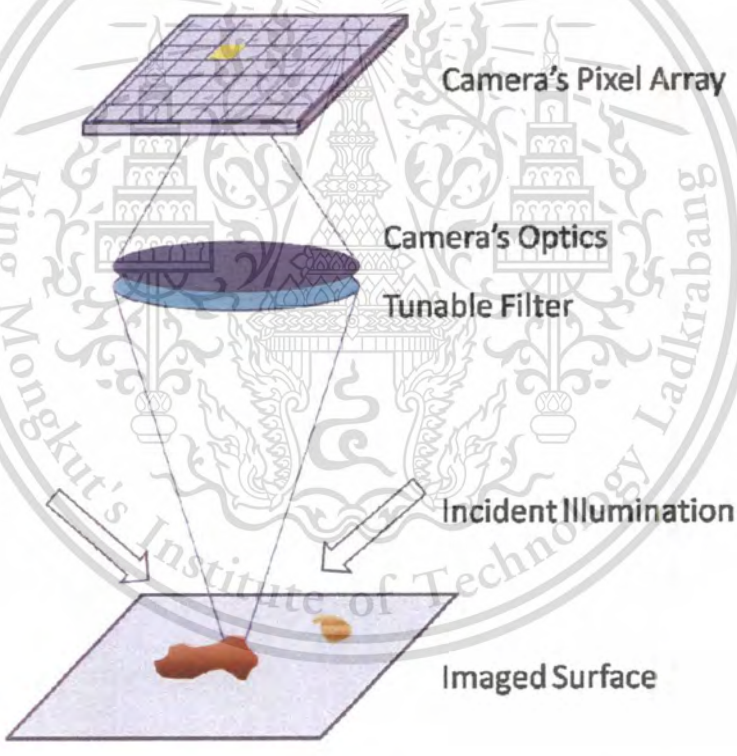

Figure 2.4 Mapping of a small area of the imaged object plane onto a single CCD pixel in the camera. Light has to pass through a series of the combining multispectral instruments before the digital readout of the camera can register the energy of radiation.

If the adjustable filter gives equal sample space of optical spectrum and the filter bandwidth is narrow enough, we can just treat $F_k(\lambda)$ as a rect function and drop the integral sign. The subscript k is then attached to λ as if the optical spectrum is interpolated. Then, equation 2.1 can be reduced to

$$T(\lambda_k) \approx \cdot i(\lambda_k) \cdot R(\lambda_k) \cdot o(\lambda_k) \cdot F(\lambda_k) \cdot \alpha(\lambda_k) + n \tag{2.2}$$

The process of spectral reconstruction is to recover the spectral reflectance values of the surface $R(\lambda_k)$. In some multispectral imaging applications, the digital readout of the camera can be used directly. However, for a majority of applications, calibration and spectral reconstruction are inevitable. The arguments $i(\lambda_k)$, $o(\lambda_k)$, $F(\lambda_k)$, and $\alpha(\lambda_k)$ are attributed to the properties of each individual system and the lighting environment. To know the response of the combined system, the surface of known spectral reflectance ($R(\lambda_k)$) must be used for calibration. Once the system is calibrated, it can be used to recover the spectral identity of the surfaces of interest. In many spectral reconstruction techniques, the above contributions are combined and equation 2.2 is written in matrix form. The reflectance spectra can then be solved with algebraic means.

In the fixed system and with the absence of noise, $R(\lambda_k)$ would be easy to recover. However, real world multispectral imaging systems would not naturally just give the true spectra of the surface because multispectral imaging systems are normally affected by all types of noise. For examples, in the outdoor applications, constant change in weather and sun direction during the day would alter illumination. Movement of instruments or imaged surface would bring change in optical path $o(\lambda_k)$. Even in the fixed and controlled system, noises are always present. The camera's responsivity $\alpha(\lambda_k)$ would also be altered by the temperature of the camera. Spectral reconstructions methods such as wiener filter [25-26], matrix R [27], smoothness [28] and neural network [29-30] are used to correct the errors in order to give preferable recovery of the surface's spectra. These methods are based on different assumptions and estimation techniques. Taking into account the noise of the system and unpredictable changes in environment, spectral reconstructions usually involve intensive

calculation, large database and comprehensive data training. In this research spectral recovery is performed by using calibration surface. With the system's instruments intact after calibration and constant illumination, the effect of noise in the system is minimized, and therefore ignored.

2.2.3 Spectral mixing

Spectral mixing occurs when more than one substance are imaged on to a single pixel on the image. As a result, several spectra are mixed together, accounting for the overall spectrum of the pixel. Reconsider the imaging of a certain part of the surface onto a single pixel in Figure 2.4. The objects whose sizes are smaller than the corresponding area of the pixel cannot be distinguished. If the types and spectra of all the mixing objects are known, the abundance of each object can possibly be estimated. The process is referred to as spectral un-mixing. Spectral un-mixing techniques are usually used in the multispectral imaging applications for aerial remote sensing in surveying of natural resources and agricultural areas. For our research, the focus is limited to the specific case of blood stains. The main coloring agents are the red blood cells (RBC). If magnified, the blood stain area mapped onto a specific pixel would be just as depicted in Figure 2.5. Microscopically, the RBCs are scattered all over the area. The mixing between light reflected from the area shaded and not shaded by RBCs causes linear spectral mixing. The linear mixing model can understandably be given by

$$R_{ST}(\lambda_k) = A_{RBC} \cdot R_{RBC}(\lambda_k) + A_s \cdot R_S(\lambda_k), \tag{2.3}$$

where $R_{ST}(\lambda_k)$ is the reflectance spectrum of stain recovered from the single pixel, A_{RBC} is the fractional area shaded by RBCs, $R_{RBC}(\lambda_k)$ is the reflectance spectrum over the RBC shaded area, is the fractional area not shaded by RBC and, is the reflectance spectrum of the substrates.

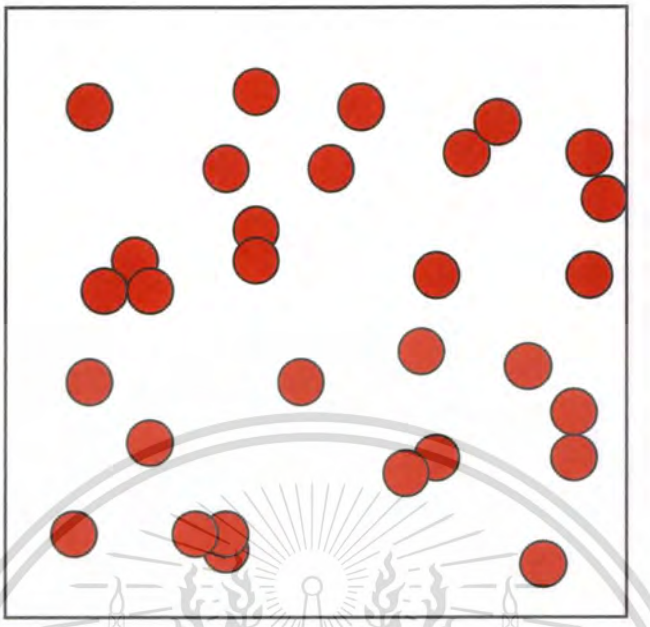

Figure 2.5 Illustration of RBCs scatted all over the area that is mapped onto a single pixel of the camera. As a results, linear and nonlinear spectral mixings occur.

On the other hand, the light, that is transmitted to or scattered from RBCs, can reflect back from the substrate. The light reflected back from the substrate can also scattered or transmitted through the RBCs. This back and forth reflections can occur several times. The process causes the spectral mixing that is non-linear. Several methods have been proposed for either linear or nonlinear spectral un-mixing [31-33]

2.2.4 Current applications of multispectral imaging

The spectral features provided by multispectral system allows for revelation of information impossibly seen by conventional imaging methods. Multispectral imaging has been used in a wide range of applications ranging from microscopy to satellite remote sensing, and in a wide variety of fields in academics and industries such as biology, environmental science, astronomy, medicine, agriculture and production industry. Currently, applications of the multispectral imaging are the active research topics around the world.

For the field of medicine and biology, multispectral imaging is utilized for several purposes, including diagnosis, evaluation of treatment, microscopy and studies of biology.

Especially, great benefits would results from the computer aided diagnosis. Different types and conditions of tissues may not be easily distinguished using normal medical imaging. Nevertheless, those differences can be observed using multispectral imagers. A majority of multispectral imaging applications in medicine are based on fluorescence. One or more fluorophores are injected into human beings or animals. Difference in fluorescent levels among tissues can then be detected with the multispectral imaging systems. For example, a multispectral imaging system has been used in visualization of blood vessels inside the tumors in mice [34]. A multispectral imaging system has been used to investigate the results of laser therapy on vascular cutaneous malformations [35]. The system works by visualization and mapping of pigmented and vascular lesions before and after the laser treatment. Using of multispectral system in estimation of chlorophyll in plant leaves has been demonstrated as well [36]. Some studies in biology using multispectral imaging are based on bioluminescence, a process in which living organisms emit light by themselves. However, this type of study is limited to certain types of organism. At present, the multispectral imaging system is commonly integrated as a part of the flow cytometry system. The multispectral images of the flowing cells can be helpful in the studies of cell classification and interaction [37].

Multispectral imaging has been used for food inspections to distinguish between good and defective, moist or burning products. It can also differentiate the real products against the counterfeit ones. The advantages of multispectral imaging over using the technician's visual inspection are that latent defects not visible to human eye can be recognized. Classification of foods usually depends on colors and spatial features on the products. A number of applications have been demonstrated, such as identification of different defects and diseases on raw French fries [38], Thai jasmine rice identification [39-40], two-dimensional (2-D) banana ripeness level indication [41], and detection of fecal and ingesta contaminations in poultry [42].

In remote sensing applications, multispectral or hyperspectral imaging systems are attached in the surveyor air-planes and satellites. Looking at objects or geological areas from different spectral bands provides several benefits such as material identification, location and

abundance determination. Remote sensing applications may be used for the purpose of geological mapping, vegetation, mineral and forest exploration, environmental monitoring, urban growth analysis and military. Airborne-multispectral images have been used to detect the spread of blight (a corn disease) in the fields across the United States [43]. In this application, spectral images were used to distinguish brown withered leaves that were interspersed in the fields of healthy green corn stalks. Hyperspectral images have also been used to identify vegetation species [44]. The detection of oil seep and oil impacted soil for remote sensing purpose has been demonstrated [45]. Remote sensing equipped with hyperspectral imaging system has been used to map out the commercial minerals of interest [46], and assist agricultural product management [47].

Multispectral imaging has also been used for military purposes. Many researches in this field have yet been kept in secret. Multispectral imaging either has been used or has the potential to gain information about battle fields, distinguish between targets and decoys, unveil camouflage, warn about long range missiles, detect of weapons of mass destruction and landmines, as well as monitor international treaty compliance [24].

Mentioned above are just a small portions of examples of the applications in multispectral and hyperspectral imaging. The number of new applications continues to increase and real commercial and industrial applications tends to grow considerably in the future.

2.2.5 Current applications of multispectral imaging for presumptive blood stain detection

Multispectral Imaging has been employed to test for the presence of blood or to enhance the existing chemical-based tests. Due to non-fluorescent nature of blood stains, all of the existing multispectral imaging-based blood stain detection methods are based on reflection. As discussed in section 2.2.3, unlike reflection-based imaging of plain surfaces, several complications occur when the substance of interest is just a blood stain deposited on a substrate. The main problem of using reflection-based spectral imaging method to identify blood stains is that the reflectance on the blood stain surface is substrate dependent. Granular nature of blood stains deposited on the substrates inevitably causes spectral mixing between

light reflected from blood stains and substrates. Given infinite possibility of substrate spectra and blood stain concentrations, blood stain detection criteria, universal to all substrates, have not been established. Current imaging methods have also considerable limitations in types of substrates and specificity in detecting blood against other stains.

Wagner et al [48-49] took advantage of the distinct narrow high-absorption band (i.e., Soret band) of heme proteins, centered around 415 nm. The arithmetic image divisions are performed between 415 nm and 440 nm spectral images, where blood exhibits steep spectral absorbance characteristics, in order to enhance the visibility of blood stains on the wood. Since a number of substances in real world exhibit high absorption around 400 nm wavelength, with the use of only two wavelengths, the proposed technique is not specific to blood stains and could result in false positive identification. In addition, camera response around Soret band is usually too low to overcome noise and distinguish one stain from another. The use of the method to detect blood on different substrates and to detect blood against other stains has not yet been demonstrated. Furthermore, the absorbance spectra of RBCs around Soret band are flatten the most by the packing effect. This effect is to be discussed in section 2.4.2.

The commercially available CONDOR™ wide field hyperspectral imaging (HIS) system [50-52] and its newest version HIS examiner™ systems [53] from ChemImage™ make use of hyperspectral imaging in forensic investigations, including visualization of fingerprints, questioned documents, inks, gun powder residue, and blood stains. However, for blood stain detection, the main focus of the systems is on visualization of the blood stain on dark fabrics using visible to near-infrared contrast enhancement techniques. The instrument can be only used in the laboratory. In addition, all the aforementioned spectral methods make use of traditional contrast enhancement through the pre-designed image operations, such as image subtraction, addition, and division among spectral images. Contrast enhancement has several limitations. For example, some substances may have different reflectance values from blood at one small part of the electromagnetic spectrum, and the other substances may at the other parts of the spectrum. It is, therefore, very difficult to enhance contrast for blood and eliminate contrast for all other stains at the same time.

Another limiting issue is that image operations are sensitive to saturation and undesired loss of information.

As of our knowledge, no existing multispectral imaging-based blood stain detection methods have thoroughly investigated the effect of substrate reflectance spectra. In addition, no imaging based blood stain detection systems have been demonstrated to distinguish blood from several stains on various substrates.

2.3 Blood stains

2.3.1 Blood stains' components and aging

The main components of blood inside human body are liquid plasma (~55% in volume), the RBCs (~40%-45%), white blood cells (~1%) , and platelets (<1%). The main component of plasma is water. However, the color of blood is not attributed to the plasma. Only the RBCs give the red color for the blood. The coloring agent of the RBC is the hemoglobin, the protein that is responsible for transportation of oxygen throughout the body. Hemoglobin can exist in several forms, such as oxyhemoglobin (HbO_2) and de-oxyhemoglobin. Inside the human body, the oxyhemoglobin makes up 90% of blood in arteries and 70% in veins. Right after blood comes out of human body, RBCs come into contact with the oxygen in the air and become 100% saturated with HbO_2. At this time, blood appears very red due to the HbO_2. Then the HbO_2 will gradually auto-oxidize into another form called the met-hemoglobin (met-Hb). The met-hemoglobin then slowly denatures into the hemichrome. Also, after a few days, the water in blood plasma would dry out. The dynamics of RBC after coming out of the body is shown in Figure 2.6

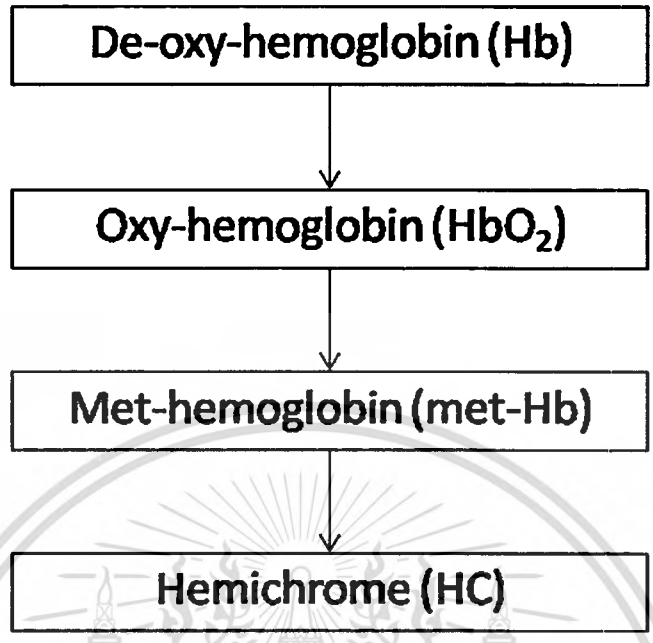

Figure 2.6 The dynamics of hemoglobin after coming out of the human body.

The average fraction of blood that changes over time is illustrated in Figure 2.7 [54]. Notice that just after the blood comes out of the body the main component of blood is hemoglobins. After 10-20 days, the main components of blood becomes the hemichrome.

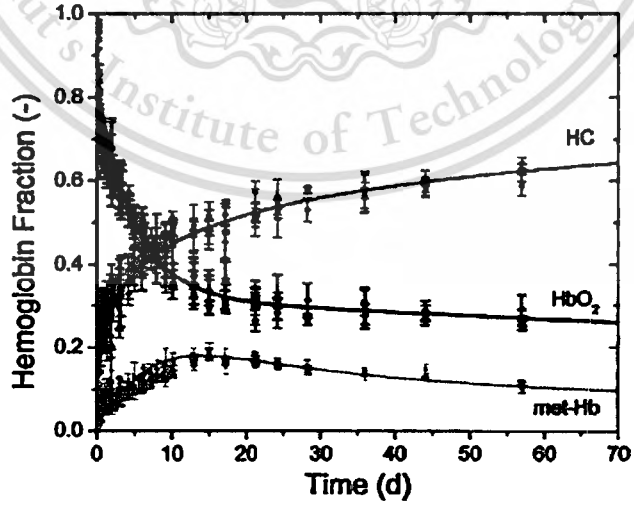

Figure 2.7 Fractions of hemoglobin forms in blood stains as a function of the age of blood stains in days (d). [54]

2.3.2 Blood stain absorbance spectra

Due to changes in forms of hemoglobin after blood comes out of human body, the color of blood stain changes over times. The absorbance spectra of the three hemoglobin derivatives are shown in Figure 2.8 [55-56]. It is seen that all forms of hemoglobin have high absorption in the blue region of the optical spectrum. Oxy-hemoglobin has the lowest absorbance between 600-700 nm, which results in a very red color. Higher absorbance in this spectral region occurs in met-hemoglobin and hemichrome. These hemoglobin derivatives, therefore, appear brown or reddish brown. The mixing components of blood yield various possible colors and shapes of blood absorbance spectra. The colors gradually change from red to reddish brown and brown over time. However, after a month, the colors change very slowly.

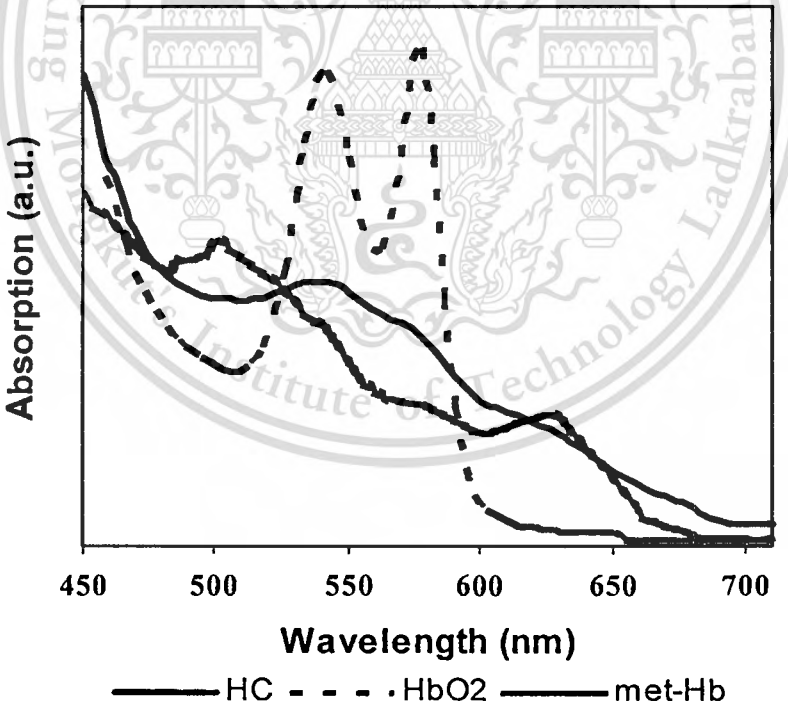

Figure 2.8 Absorbance Spectra of hemoglobin derivatives [55-56].

2.4 Related theories

2.4.1 Kubelka-Munk Theory

The Kubelka-Munk (KM) theory provides the relationship between diffuse reflectance spectra of the weakly absorbing materials [57-58]. This theory originates from considerations of paint layers on the paper substrates. There are several evaluation, utilization and modification of the theory [59-61]. This theory has also been used to successfully finding the age of blood stain samples that are deposited on the white cottons [54]. In this research, blood and other stains are treated as the thin layers of absorbing materials deposited onto the construction material substrates. The main equation of KM theory used in this research is

$$\frac{R_{ST}(\lambda)}{R_S(\lambda)} = 1 - \frac{K(\lambda)}{S(\lambda)}\left(\sqrt{1+\frac{2K(\lambda)}{S(\lambda)}}+1\right), \tag{2.4}$$

where $R_{ST}(\lambda)$, and $R_S(\lambda)$, are the reflectance spectra recovered from the absorbing layer, and the pure substrate surface, respectively, $K(\lambda)$ and $S(\lambda)$ are Kubelka Munk optical absorption and scattering, respectively. We use equation 2.4 to estimate the absorbance spectra of different stains on substrates. The equation 2.4 just yields the estimation of absorbance values of the stains, and by no means give the exact values.

2.4.2 Pigment packaging effect of red blood cells

Pigment packaging effect occurs as a result of confinement of pigment agents in high concentration solution. This effect was first explained by Duysens by measuring the absorption of Chlorophyll suspension [62]. The effect also results in the distortion of reflectance and absorption spectra shape between whole blood and blood vessels [63-64]. According to the theory, the absorbance of the substance is flattened more in the high absorption bands than the low absorption band when the pigments concentration becomes higher. The cause of the spectral flattening involves the shading among pigments themselves

in the concentrated solutions. In case of blood stains, the red blood cells are packed together and become concentrated as the blood serum dries off. The distortion factor is given by

$$Q = \frac{\mu_{sus}(\lambda)}{\mu_{sol}(\lambda)} = (1 - T_p) \cdot \frac{a_p}{\upsilon_p \cdot \mu_{sol}(\lambda)} \tag{2.6}$$

where $\mu_{sus}(\lambda)$ and $\mu_{sol}(\lambda)$ are absorption coefficients of the suspension and solution of blood respectively, T_p, a_p, and υ_p are the transmission, area and volume occupied by a single particle in the blood [64]. From Figure 2.7, it is seen that the absorption spectrum is flatten more at the spectral region where absorption coefficient is high.

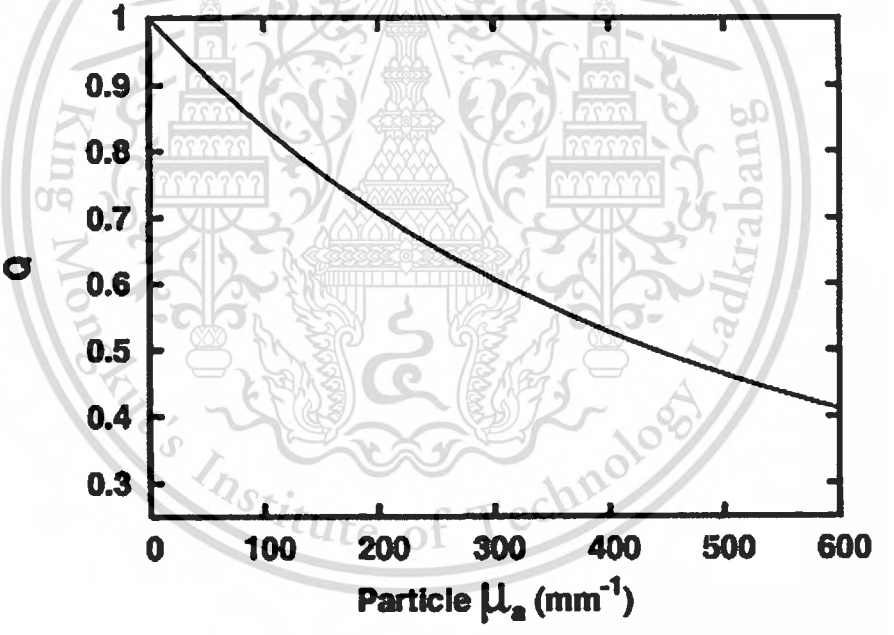

Figure 2.9 The distortion factor from the pigment packaging as a function of particle's absorption coefficient [23].

Figure 2.9 shows the experimental measurement of absorption of blood in solutions and suspension. These plots are compiled by Finlay and Foster from several sources [63-64]. It is evident that that the high absorption parts of the spectrum are flatten more than the low absorption parts. The Soret band (peaked around 415 nm) is distorted the most considering

the visible part of electromagnetic spectrum. For the blood stain deposited on a substrate, the packing effect is expected to be more evident, especially in high concentration blood, since the blood plasma should dried out and the RBC should be packed into a larger volume. In this research, the results of the calculation for the absorbance spectra of the blood stains given in chapter 4 will confirm the existence of the packaging effect in stain.

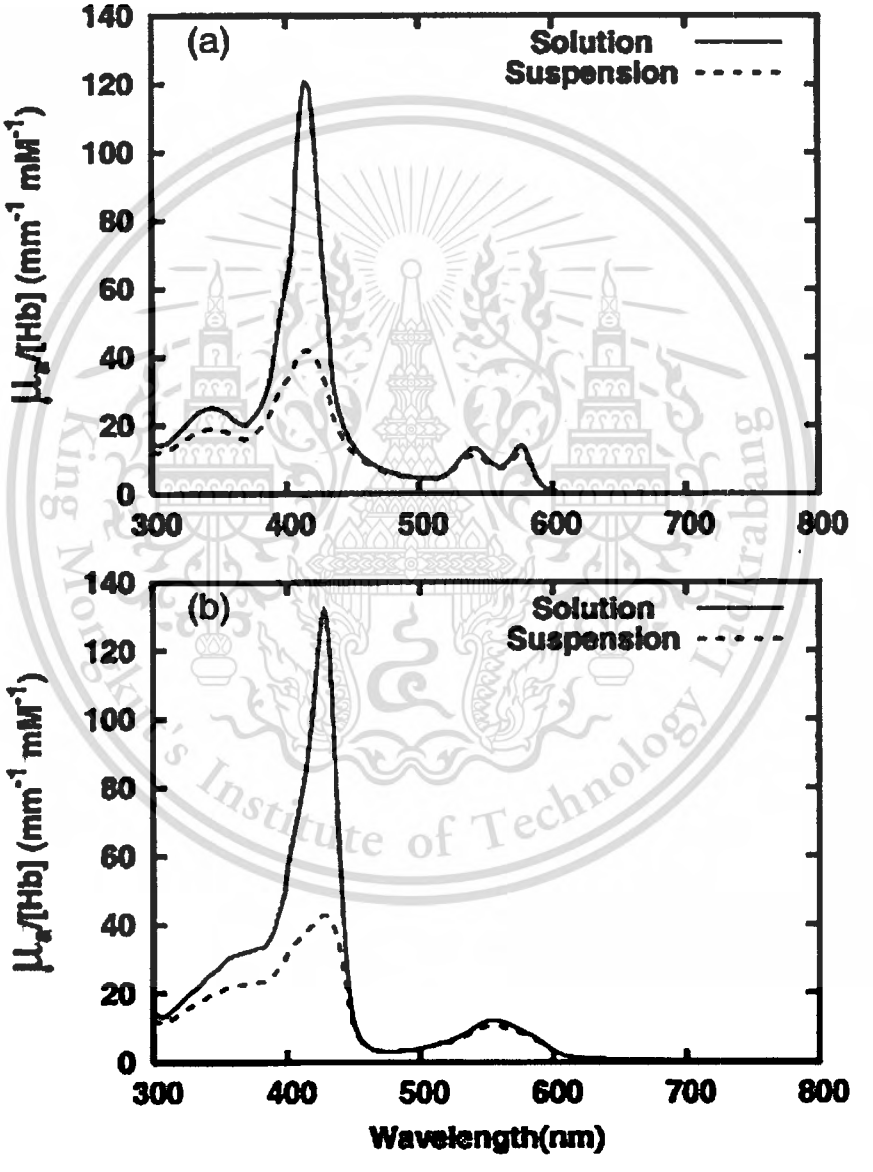

Figure 2.10 The absorbance spectra of 100 μM (a) oxyhemoglobin (b) deoxyhemoglobin in solution and suspended in spherical particle of 5 μm diameter [23].

2.4.3 Lorenz-Mie scattering

Lorenz-Mie Scattering refers to scattering of light from particles whose sizes are comparable to or greater than the wavelength of light, $(0.1\lambda < x < 100\lambda)$ where x is the size of the scattering particles [65]. The Mie scattering equation derives from the solution of the application of Maxwell's equation to the isotropic, homogeneous sphere. The Lorenz Mie scattering is responsible for the glare around the sun and the white color of the cloud and mist. The theory has also been used to study the property of the color pigments of paint layers. In case of stains deposited on the substrates, the pigment particles have the sizes in the range of a few microns. For examples, the color pigments of blood are packed inside the red blood cell particles whose sizes range between 2-3 μm where the wavelengths of the illumination range from 0.4-0.7 μm. In this research, we ignore the minute geometrical difference of scattering light at different spatial positions in the spectral images. In the most simplified form, the solution to the scattering equations is given by

$$S(\lambda) = S_0\left(\frac{\lambda}{\lambda_0}\right)^{-0.4} \tag{2.5}$$

where S_0 is a scattering coefficient at a specific wavelength λ_0. It is evident from equation (2.5) that Mie scattering is not strongly wavelength dependent. This equation is incorporated into the KM theory.

Chapter 3

Experimental framework

3.1 Experimental setup

Our multispectral imaging system for blood stain identification used in this thesis is shown in Figure. 3.1. The system is similar to other typical multispectral systems used for other material characterization. It consists of a camera coupled with an LCTF, light source and a control unit.

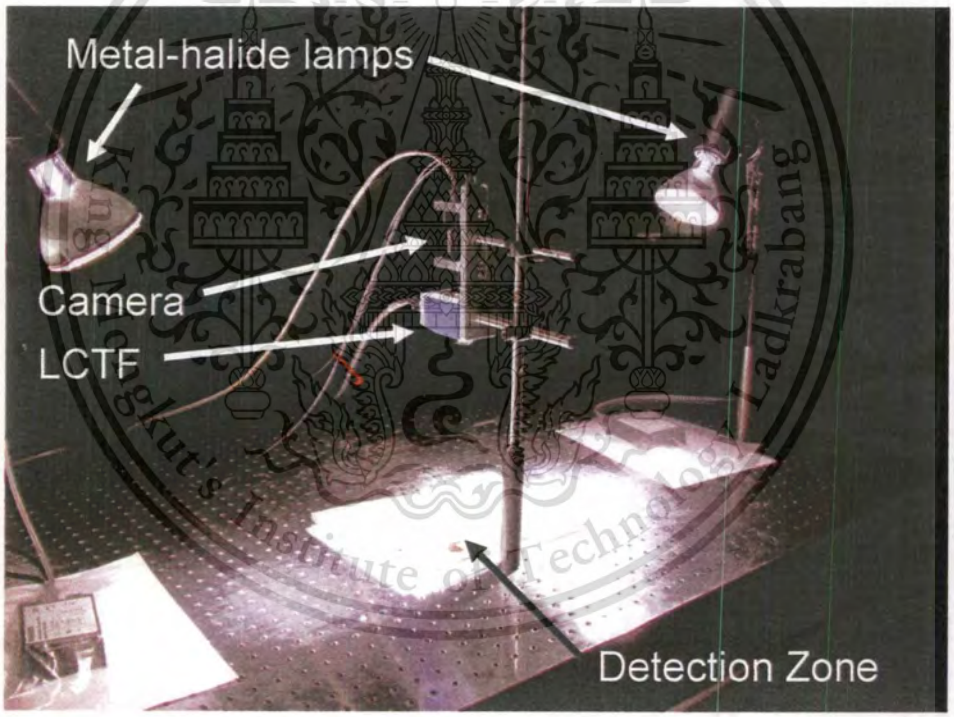

Figure 3.1 Multispectral imaging setup used in this experiment. LCTF: Liquid Crystal Tunable Filter.

Illumination is achieved using two metal halide lamps (Philips CDM–R 70W/942), which yield desired full spectral range over the visible region. The non-uniformity of the illumination on the image surface is kept to less than 25%. The incident angle of the

illumination is not necessarily limited, but preferably between 30°- 60°. However, the light source must be fixed in place for each session of the experiment for the calibration purpose. An 8-bit multispectral-grade color camera (Basler Scout scA750-60gc) is coupled with an LCTF (VariSpec, VIS 7-HC-20). The surface to be imaged is placed on the optical table just below the camera. A personal computer, equipped with LabVIEW program (as evident in Figure 3.2), is connected, so as to control image capturing of the camera and spectral scanning of the LCTF. The LCTF has a full-width half-maximum (FWHM) bandwidth of 7 nm, a wavelength scanning range from 400 nm to 720 nm wavelength, and a 20-mm circular aperture. The 2-D image sensor of the camera contains 750×480 pixels and it is set to operate in RGB mode. However, the camera's field of view is limited by the LCTF's circular aperture to ±7°. Since the camera is placed 30 cm above the sample surface, the image visibility is limited to a circular area of 10.5 cm in diameter. To lessen our calculation, we set the camera's area of interest (AOI) to 360×339 pixels, a rectangular area just to cover visible circular field of the images.

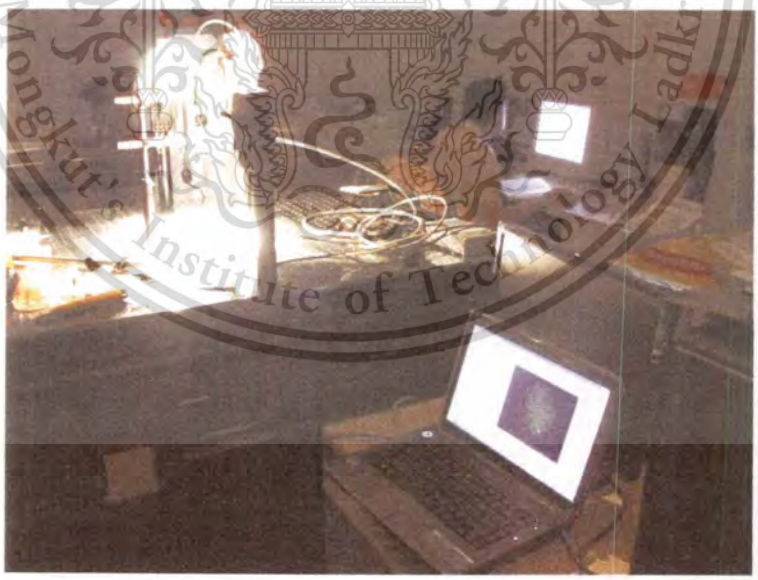

Figure 3.2 A personal laptop computer (on the lower right side) equipped with LabVIEW platform is the main controlling unit of the experiment.

3.2 Experimental setup instruments

In this section, all the instruments constituting our multispectral imaging setups are given in details.

3.2.1 Halogen lamps

Halogen light source has been tried in the experiments of this thesis many times due to its low price and availability. Multispectral imaging of the system works well in the spectral region around 500-700nm since the spectral illumination of the source is rich in the region. However, the halogen spectrum is minuscule at the lower end of the visible spectrum. This exacerbates the need to compensate for low spectral response of tunable filter. So, the halogen lamps have not been used for further part of the research.

3.2.2 Metal halide discharger lamps

In multispectral system, the spectral range of illumination should be match or even larger than the spectral range of the camera and the filters. In the initial data collection of this thesis, illumination was done by using halogen lamps. However, the halogen lamps give bright illumination only around 500-700 nm. Subsequently, multispectral image collection in this thesis is achieved by using 2 metal halide lamps (Philips CDM–R 70W/942) [66]. The illumination of the lamp is caused by an electric arc through a mixture of gases, including vaporized mercury and metal halides. The lamps are chosen because they yield full spectrum from 400-720 nm. The spectral power distribution, given from the manufacturer, is shown in Figure 3.3.

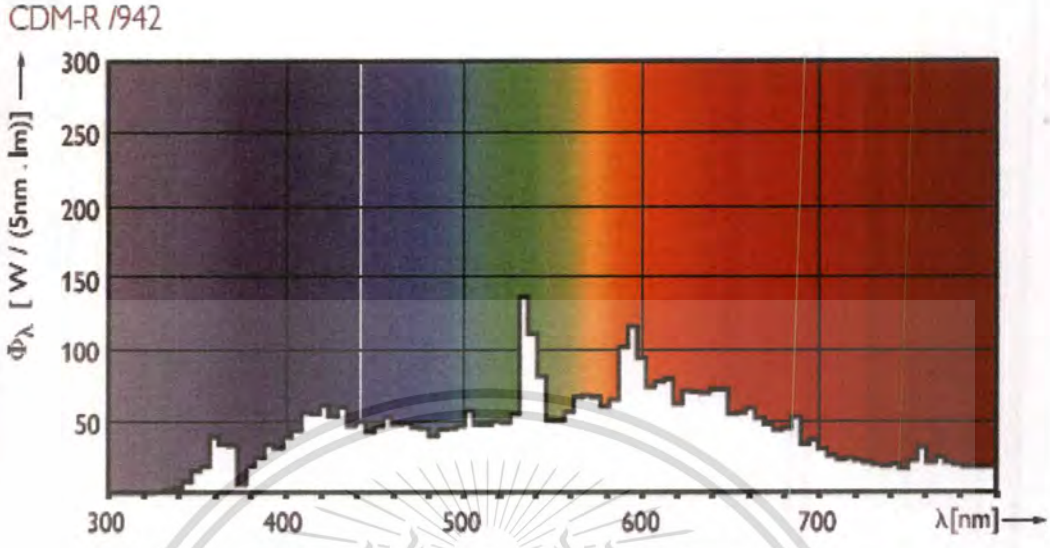

Figure 3.3 Spectral Power Distribution of the Philips CDM–R 70W/942 lamp [66].

However, the illumination of metal halide contains several spectral spikes. The largest spike is located around 538 nm. This causes many problems in the multispectral image collection because high illumination spectral regions tend to saturate the images while the low illumination regions cause the images to be too dark to give valuable information. In chapter 5, the solution of this problem will be presented. Low intensity at low wavelengths (400-440nm), combined with contribution of other instruments, also causes the system to give little response in this spectral range.

3.2.3 Liquid crystal tunable filter

In this thesis, the spectral tuning is accomplished using an LCTF. The LCTF allows us to electronically control the transmission of the light to the camera. The principle of LCTF is based on the variable retardation of liquid crystal wave plate [67]. LCTF usually consists of several stacking filter elements. Schematic diagram of an LCTF element is shown in Figure 3.4. In one LCTF element, the liquid crystal and the quartz are placed in between the two linear polarizers. Both liquid crystal and quartz are birefringent materials, which can act as wave retarders. The quartz acts as a fixed wave retarder. The nematic liquid crystal is contained in a transparent cell. There are transparent electrodes (usually made of indium tin

oxide, ITO) adhering to both sides of the cell. When the voltage is applied to the liquid crystal, its molecular alignments change. As a result, the degree of its birefringence By varying the applied voltage the instrument can act as a tunable filter. The select wavelength is the one at which the combined wave retarders exhibit a full wave plate. To achieve a preferable narrow-band filter shape, commercially available LCTF usually consists of a series of LCTF elements.

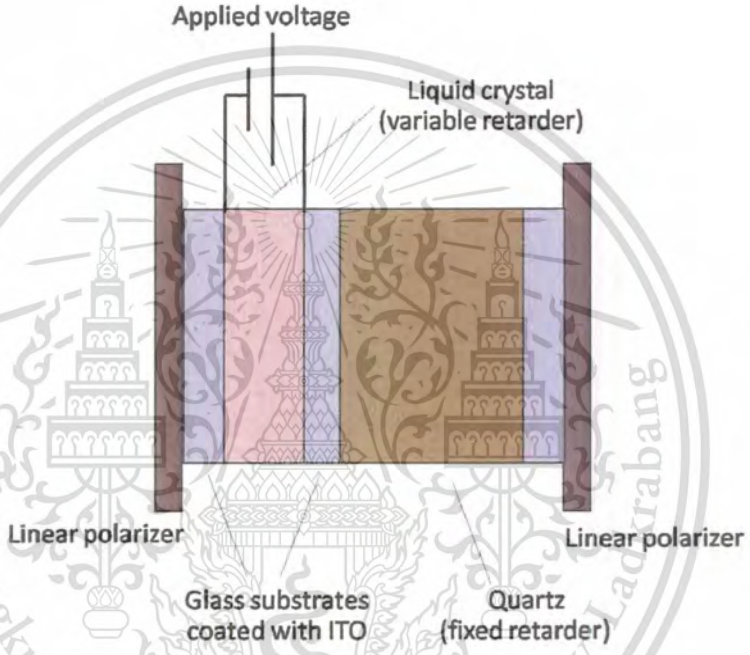

Figure 3.4 Scheme of typical LCTF element.

The advantages of the LCTF over other types of filters are that it has large field of view, high optical quality, efficient electronic tuning, wide tuning range, fast tuning time. The tuning time is usually in the order of tens of milliseconds. The disadvantage of the LCTF is that it has low transmission since light has to pass through polarizers. The maximum transmission at the selected wavelength is never greater than 50%.

The LCTF used in this experiment is the VariSpec model VIS 7-HC-20 [68]. The picture of the LCTF is shown in Figure 3.5. The LCTF has a full-width half-maximum (FWHM) bandwidth of 7 nm, a wavelength scanning range from 400 nm to 720 nm wavelength, and a 20-mm circular aperture. The slightly large bandwidth of LCTF causes

the illumination from the side channels to be filtered in the specific spectral images, which causes additional noise in the system.

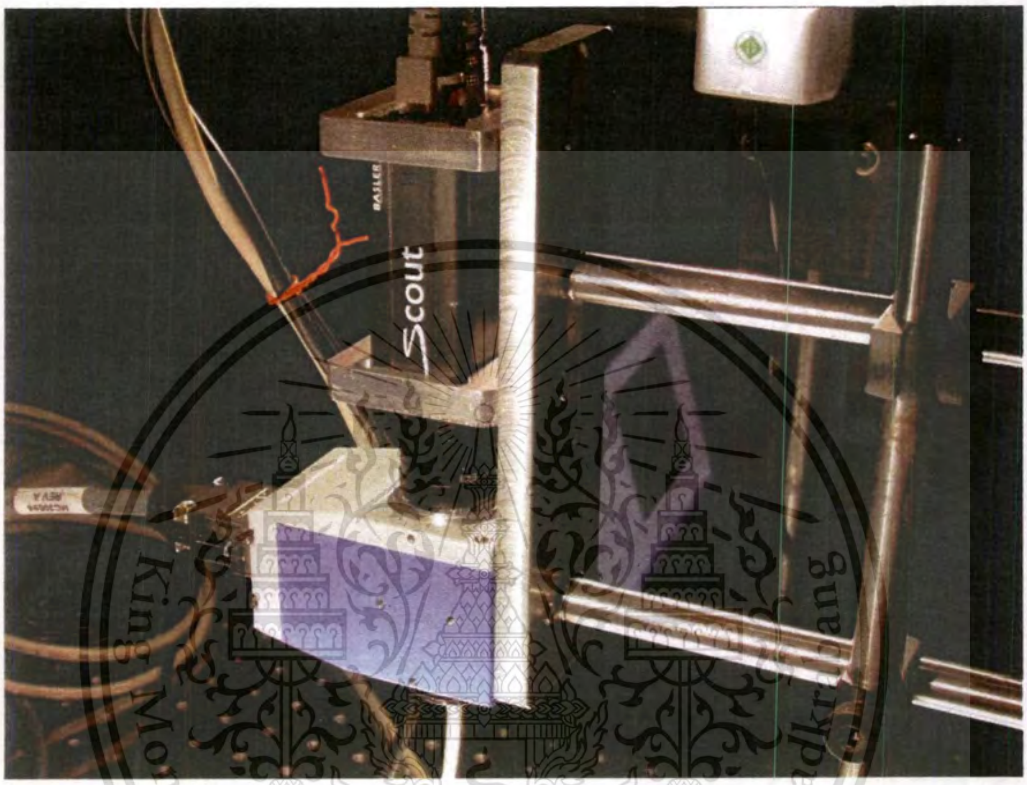

Figure 3.5 The Liquid Crystal Tunable Filter (bottom) used in this experiment is coupled with Basler Scout video camera (top).

The transmission of the LCTF, taken by the manufacturer is shown in Figure 3.6. Notice the low transmission from 400-500 nm. The low transmission at this spectral range along with that of other imaging instruments make low response in this part of the spectrm. The LCTF can be controlled by LabVIEW program. The response time of this LCTF model is 50 ms. However, for reliable results, after programmatically telling the LCTF to tune to a specific wavelength, the camera is set to wait at least 200 ms before capturing the image.

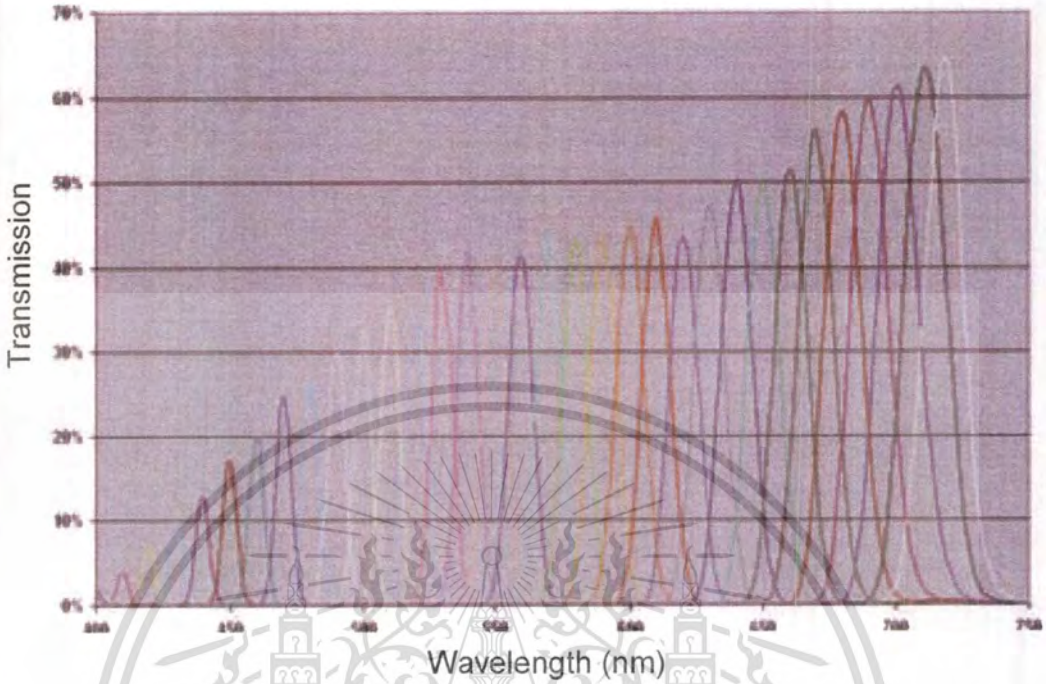

Figure 3.6 Transmission of LCTF [41].

3.2.4 Multispectral video camera

A multispectral-grade color camera (Basler Scout scA750-60gc) [69] is used in the experiments of this thesis. The prominent feature of this camera is that it allows electronic control of the camera via LabVIEW computer programs. The exposure time of the camera can also be programmatically controlled. The possible exposure times range from 124 μs to 125000 μs. However the pixel depth of this camera is only 8 bits, which gives spectral response ranging between 0-255. Compared with other models of multispectral camera, this model is more subject to the quantization noise. The spectral response in terms of quantum efficiency, given by the manufacturer is shown in Figure 3.7. Although the camera has spectral response from 370 nm to 1040 nm, this wide spectral range cannot be achieved in this research since the system is limited by spectral range of other instruments. For example, the LCTF can pass the highest wavelength of only 720 nm.

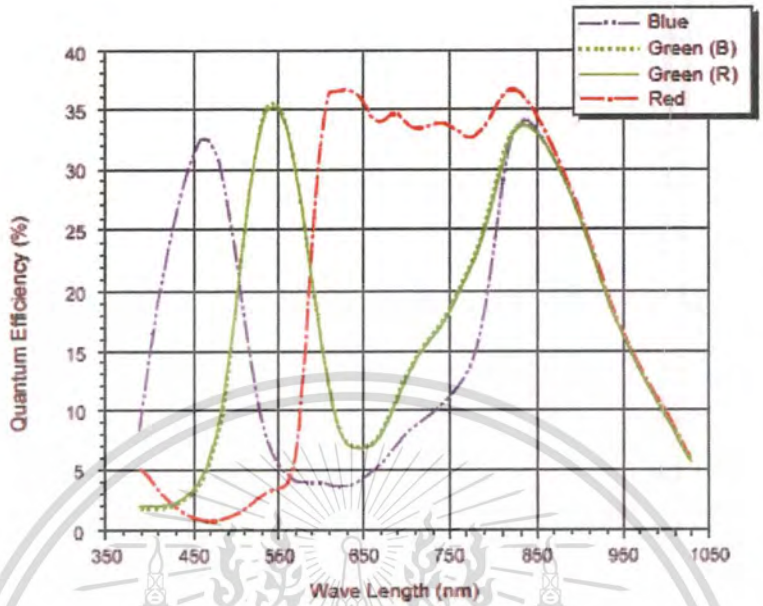

Figure 3.7 RGB spectral response of Basler Scout scA750-60gc [42].

3.3 LabVIEW programming

LabVIEW is a visual programming platform from National Instruments. LabVIEW stands for Laboratory Virtual Instrumentation Engineering Workbench. In this thesis, LabVIEW 2011 is used in all stages of data collection, analysis and even developments of the real blood stain detection system. In doing so, LabVIEW allows us to

1. control the capturing of the video camera,
2. control the exposure time of the camera capturing,
3. control the multispectral scanning of LCTF,
4. coordinate the image acquisition between camera and LCTF,
5. extract spectral data from the captured image cubes,
6. analyze spectral data using mathematical functions, and
7. store and display the results in the thesis.

The visual-based platform of Labview makes the programing for the experiment easy compared to character based programming. This allows several tasks to run in parallel.

3.4 Image capturing

To capture desired multispectral images, the LCTF is programmatically tuned to uniformly sample 61 wavelength images, ranging from 458 nm to 710 nm wavelength with the tuning step of 4 nm wavelength. For each captured scene, the camera catches 58 images, one image for each tuning wavelength, to form a 3-D image cube that contains information in two spatial dimensions and one spectral dimension. The 3-D image cube therefore has the size of 360×339×58 pixels. Since the spectral response of our multispectral-imaging system is spiky and the surfaces on which we look for blood stains can be of any types or reflectance spectra, the spectral images can easily be saturated or too dark to recover their true spectra. To solve the problem, during capturing one spectral image, we propose to capture several 3-D image cubes of the same scene with different exposure times ranging from 10,000 to 120,000 μs. Then the set of spectral images whose exposure times give suitable bright image, but not saturated or not too dark, are selected so that true reflectance spectra of the surface are obtained.

3.5 Calibration and spectral reconstruction method

When capturing multispectral images, the system does not automatically give the reflectance spectra of the surface. As mentioned in chapter 2, the camera digital responses result from a combination of surface reflectance, all multispectral instruments, illumination, and noise. The raw digital response taken from some points on different stains on gypsum substrate are shown in Figure 3.8. It is evident that without calibration, the true spectral identities of the surface will never be recognized.

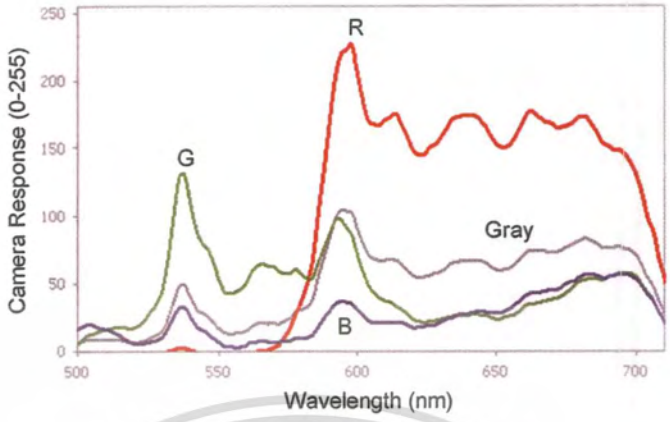

(a)

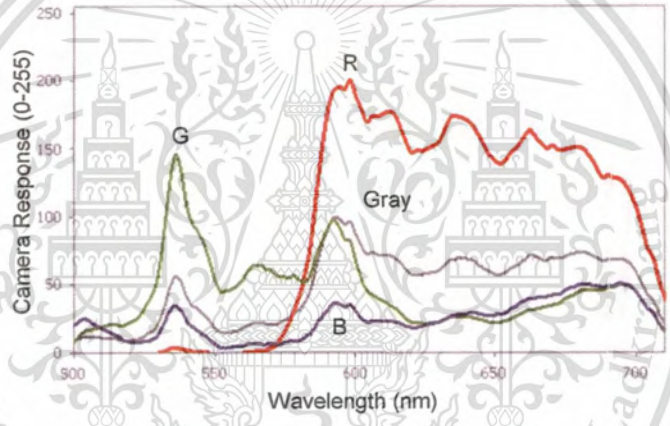

(b)

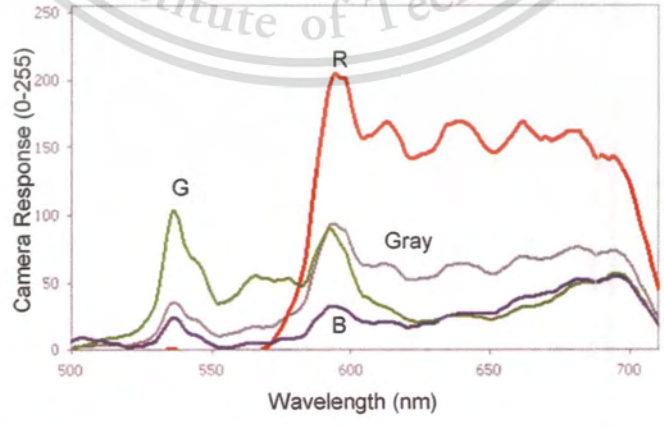

(c)

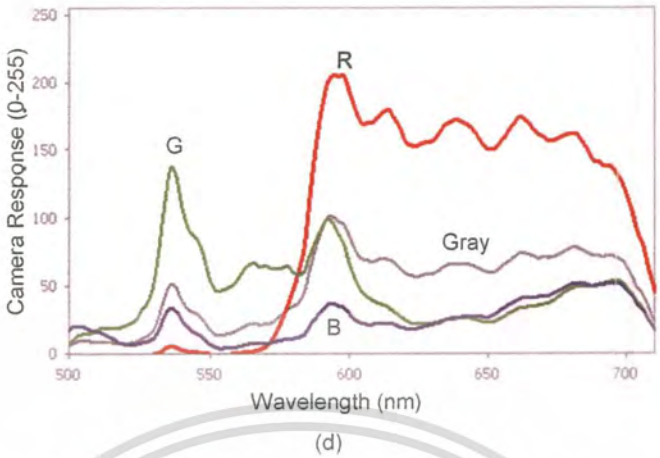

Figure 3.8 Examples of digital response of the camera when capturing (a) blood stain, (b) coffee stain, (c) ketchup stain, (d) mud stain on gypsum substrates. The R, G, B, or gray labels indicate the red, green, blue, or gray scale values of the camera response.

In this research, the widely-accepted white reference calibration method [70-72] is performed to calibrate the system and recover diffuse spectral reflectance of the test surfaces. The technique is achieved by comparing the highly reflective lambertian surface of known spectral reflectance with the test surfaces. At the beginning of this research, we used the white reference standard tile, modeled SRS 99, from Labsphere with known reflectance spectra, shown in Figure 3.9. The surface allows reflection over 98% all over the visible spectrum and can be used efficiently for the calibration purpose.

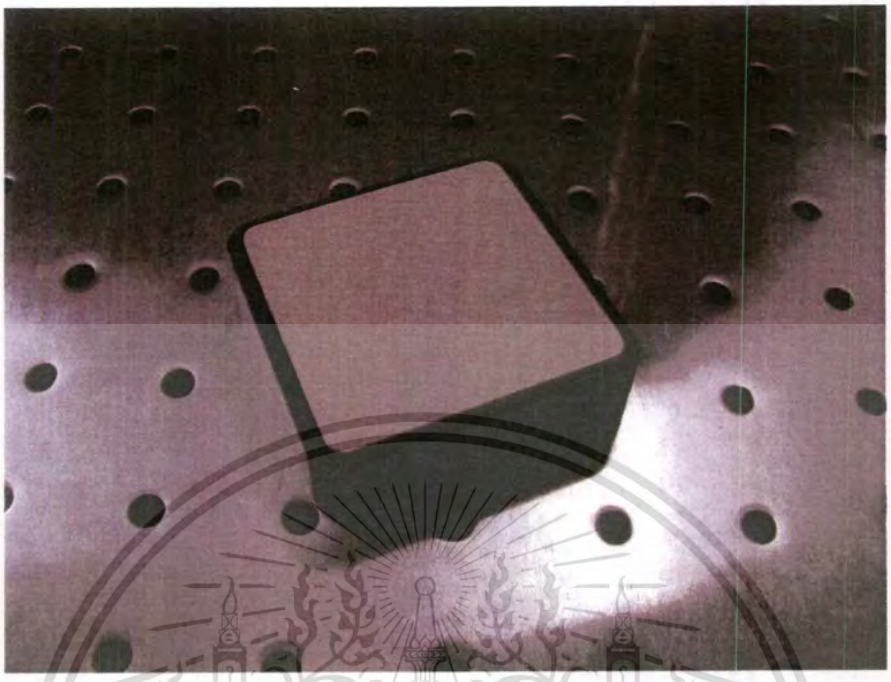

Figure 3.9 White reference tile used for calibration at the beginning of the experiment. Problems in occur since the size of the surfade is smaller than the field of view of the camera and the surface could be tarnished if used often.

However, by taking into account cost and handling issues in real world scenario, we propose to use a stack of spatially uniform white bleached paper of known reflectance spectrum, instead of a commercially expensive and careful-handling white reference tile. The white bleached paper used in this research is just the commercial-grade, A4-sized paper, typically used in office work. First, to known the spectral reflectance of the white paper, it must be calibrated using the white reflectance standard tile. Once this is achieved, the white paper can be used for calibration of other surfaces. To calibrate the multispectral images, the white bleached paper is placed on the detection zone in such a way that all pixels in the image field of view can capture the desired spectral images of the white bleached paper ($R_W(\lambda_k)$). After removing the white bleached paper, many sets of spectral images of the test surfaces can be taken as long as all illumination and imaging instruments are kept intact. With the incorporation of exposure time, the spectral reflectance at any pixel on the test surface $R_T(\lambda_k)$ can be expressed as

$$R_T(\lambda_k) = \frac{\left[(T(\lambda_k) - D)/\tau_T(\lambda_k)\right]}{\left[(W(\lambda_k) - D)/\tau_W(\lambda_k)\right]} \cdot R_W(\lambda_k), \tag{3.1}$$

where $T(\lambda_k)$ and $W(\lambda_k)$ are the digital responses from the test surface image pixel and the white bleached paper image pixel, respectively. The variables $\tau_T(\lambda_k)$ and $\tau_W(\lambda_k)$ are the camera's exposure times when capturing the test surface and the white bleached paper, respectively and D is the dark response of the camera. For our 8-bit camera, $T(\lambda_k)$ and $W(\lambda_k)$ range from 0-255. They can be taken from either R, G, B, or grey scale digital responses as long as the pixel values are in the linear response range. For our LCTF-based multispectral imaging system, it is suitable that the digital responses are extracted from the blue color plane for wavelength channels from 458 nm to 498 nm and from the green color plane for wavelength channels from 502 nm to 710 nm. Dark response, originating from dark current present in the detector array, can be determined by capturing the image while the camera's slip is covered.

There are advantages of using white bleached paper for our calibration method. First, the paper is cheap, replaceable if tarnished, and reusable for other work. Secondly, since the paper is large enough to cover the camera field of view, all pixels in the image are readily calibrated without further correction for spatial non-uniformity of illumination and for geometrical difference between reference and test surfaces.

To validate our proposed calibration and spectral reconstruction method, we use the technique to find the spectral reflectance of the standard color pads of the x-rite color checker shown in Figure 3.10. The checker's pad has the colors that are standardized according to the Munsell color standard established by the Munsell Color Science Laboratory. Figure 3.11 shows the results of spectral recovery of 4 color patches, including cyan, magneta, orange yellow, and yellow green, from the color checker. The solid lines indicate the true reflectance spectra while the dashed lines are the spectra recovered by our method. Our method yields the spectra with the error of less than 5% all over the spectrum. The accuracy is good enough to continue our research.

Figure 3.10 The x-rite color checker used for the testing of our calibration method. The color checker gives the standardized color references according to the Munsell color standard.

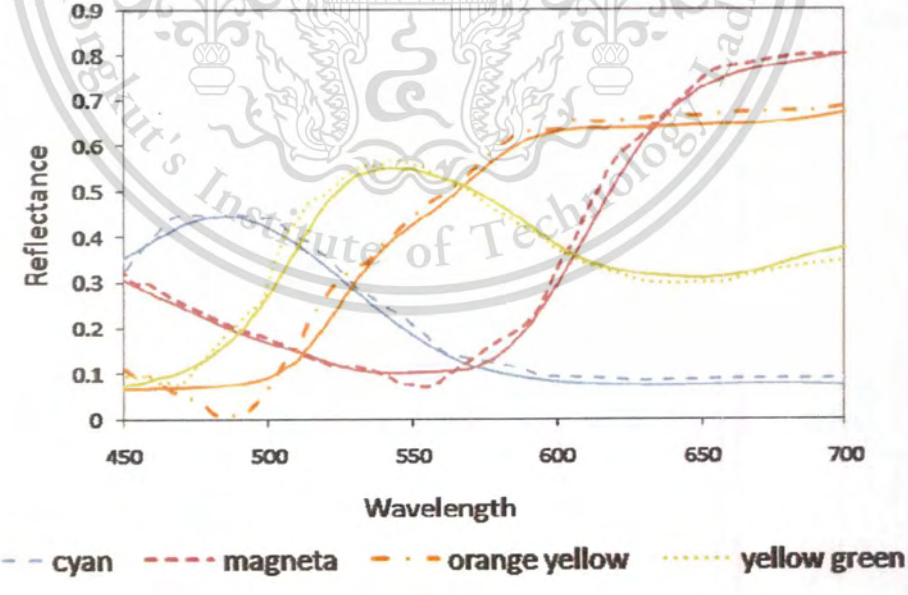

Figure 3.11 The results of our spectral reconstruction tested from 4 color patches from the x-rite color checker. The solid lines are the true reflectance spectra and the dotted lines are the recovered reflectance specta.

As will be evident in later sections of this thesis, since the detection of blood stain involves complicated mathematical calculations, processing the images directly is not suitable. So, we transform the data in an image cube into an array. To do this, digital responses of 3 by 3 adjacent pixels in any image are extracted and averaged into a single number before becoming a single element of the array, yielding measured spatial resolution of blood stain detection of 0.9 ×.9 mm^2. The 3-D image cube of size 360×339×58 = 7,078,320 elements is therefore compressed and transformed into the 3-D array with the corresponding size of 120×113×58 = 786,480 elements. Two spatial dimensions are further reshaped into a 1-D, giving the final size of the 2-D array of 13,560×58 = 786,480 elements. From Eq(1), it can be clearly seen that each element obtained under our white reference array is represented by a calibration number of

$$w = \frac{\left[(W(\lambda_k) - D)/\tau_W(\lambda_k)\right]}{R_W(\lambda_k)}. \tag{3.2}$$

For the test surface array, each element is represented by

$$t = \left[(T(\lambda_k) - D)/\tau_T(\lambda_k)\right]. \tag{3.3}$$

In this way, the spectral reflectance of the surface can be calculated directly from

$$R = t/w. \tag{3.4}$$

There are several pros of transformation of the 3-D image cube into an array. First, averaging responses from 3 by 3 pixels into one element before further calculations can reduce noise, and lessen system computational load and memory, thus improving speed of the detection system. Secondly, calibration data in the form of an array can rapidly be stored and extracted from a single text file. Thirdly, with multispectral data arrays, unnecessary data from spatial points that have been identified as non-blood can immediately be removed

from the array without further consideration. This will considerably help reduce computational load in real blood stain detection system. Lastly, image processing also unnecessarily processes all R, G, and B pixels in the image as our calibration and spectral recovery scheme requires only spectral data in either R or G or B color planes.

3.6 Dark current compensation

Dark response of the camera originates from dark current in CCD array [73]. The noise changes slightly over the image brightness and vary slightly from pixel to pixels. In fact, noise in the images come from all instruments and environment, including, the illumination lamps, the ambient lights, the impurity of thee reference and test surfaces, the tunable filter, and the camera. For simplicity, we represent the camera dark responses by one single value for all pixels and spectral images. We take camera dark noise as the only noise in the system. For our experiment, dark noise can be determined by 2 methods. In the first method, the dark noise is simply determined by capturing the image while the camera's slip is covered. In this way light intensity falling on to the CCD array of the camera is near zero. The spectral responses of the camera originate purely from the dark current in this case. In the second method, the dark responses is determined either before or during calibration stage by taking two consecutive images of the reference paper for each channel at different exposure times. Dark noise can be derived as

$$D \approx \frac{\tau_l \cdot W_h(\lambda_k) - \tau_h \cdot W_l(\lambda_k)}{\tau_h - \tau_l} \tag{3.5}$$

where subscripts l and h indicate that the image is taken at low or high exposure time respectively. One condition that must be satisfied is that the image must not be saturated.
For our 8 bit camera, camera responses can range from 0-255. For blue pixels, dark responses usually range from 7 to 10 with the average of 8.9 for, and from 5 – 7 with the average of 5.9 for green pixels. Although, dark responses vary slightly with image brightness, we take the above average values in our calculation.

Chapter 4

Experiment part I:

Developing blood stain discrimination criteria

4.1 Overview of the experiment

Detection of blood stains based on spectral reflectance has several limitations since the shape of the blood stain reflectance spectra is much influenced by the reflectance spectrum of the substrate on which it is deposited. In this experiment, we develop substrate-independent blood stain detection criteria for use in a liquid crystal tunable filter-based multispectral imaging system. Key features include substrate contribution reduction through KM theory and criteria establishment based upon empirical data and blood discrimination criteria, which identify the blood stains using mathematical inequalities and Boolean logics. By applying our simple calibration method along with the KM theory, absorbance spectra at any image points of the test surfaces can be estimated. Blood discrimination criteria based upon the acquired absorbance spectra are then established and tested. Experimental results confirm that our blood stain discrimination criteria can be used to locate blood stains on several construction materials with high precision. Our proposed approach allows for possible non-destructive, quick, and easy-to-improve blood stain detection. Sensitivity from 0.60 to 0.95 is achieved depending on blood stain concentration and substrate type. Also specificity between 0.55 and 0.96 and identification time of 4-5 minutes are accomplished, respectively. The established blood stain discrimination criteria will be incorporated in a real blood stain detection system in Chapter 5 of this thesis where system design and considerations as well as speed issues are discussed. In sections 4.2-4.3, we discuss the experimental details and procedure for establishment of blood stain criteria. In section 4.4, we demonstrate that the strain reflectance spectra really depend on substrate spectra and section 4.5 shows that KM theory can reduce the dependence of stain reflectance spectra on substrates. Then, in the sections 4.6-4.8, we describe in detail how the blood detection criteria can be established and evaluated.

4.2 Sample materials

To establish efficient blood stain detection criteria, we must collect enough sample spectra of blood and other stains on a variety of substrate materials to be certain that true spectral characteristics of blood stains are appreciated. In this work, several common construction materials including gypsum boards, concrete boards, green tiles, white tiles, and wood planks are used as substrates. We also use bovine blood instead of human blood as it possesses absorption spectra comparable to human blood [74]. Other stains under our study include coffee, cocoa drink, ketchup, soy sauce, mud, soil, and oyster sauce. For the purpose of spectra collection, each substance is stained so that different concentrations of each substance are deposited on the substrates. Figure 4.1 shows some of our sample surfaces, including gypsum boards, wood planks, white tiles, and concretes. Several multispectral images of these surfaces are captured with our aforementioned multispectral system.

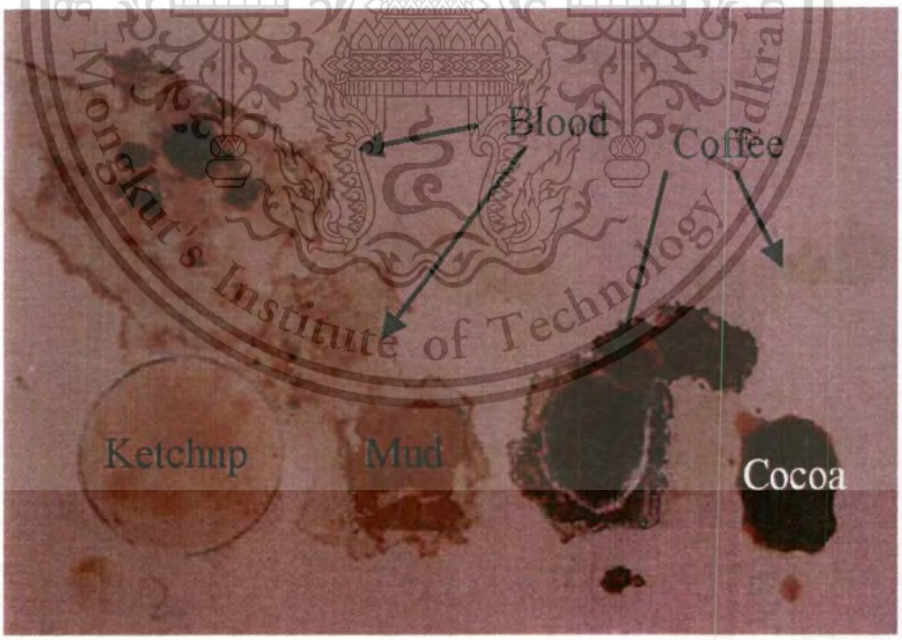

(a)

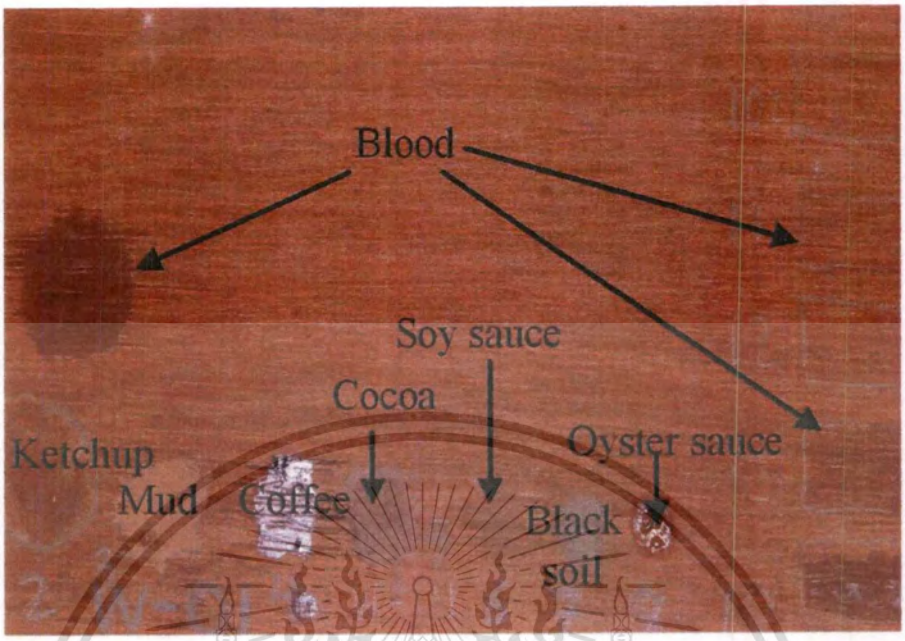

(b)

(c)

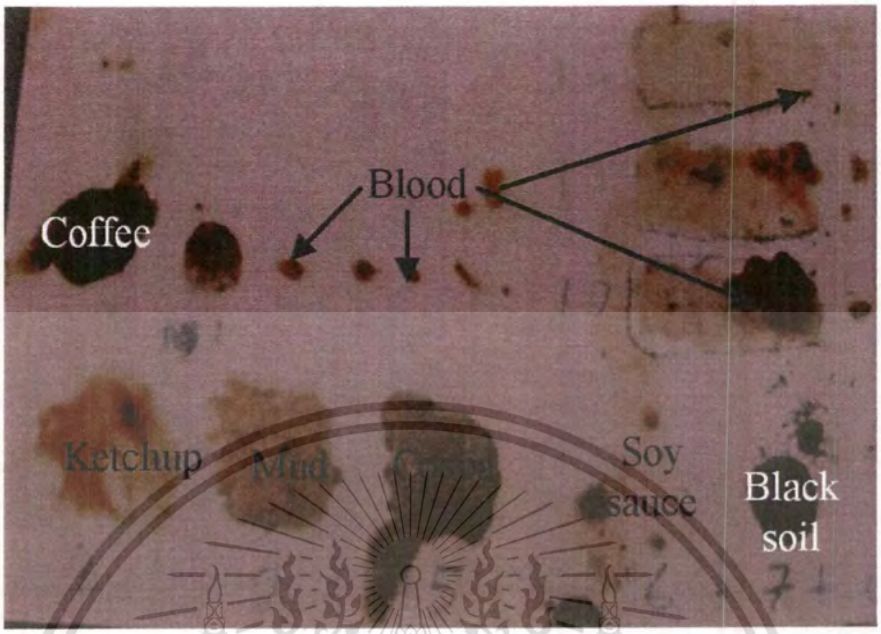

(d)

Figure 4.1 Examples of our stain samples on a variety of substrate surfaces including (a) gypsum, (b) wood, (c) rough surface orange tile, and (d) white tile. Each substrate has different concentration of blood and other stains deposited on them.

4.3 Procedure for establishing blood stain discrimination criteria

Since absorbance of substance is substrate independent, it is likely that absorbance could be the base for detection blood stain. Although we cannot physically measure absorbance spectra from multispectral imaging system, KM theory allows us to indirectly estimate absorbance from the measured reflectance. To develop blood stain discrimination criteria, the procedure in Figure 4.2 is proposed and performed.

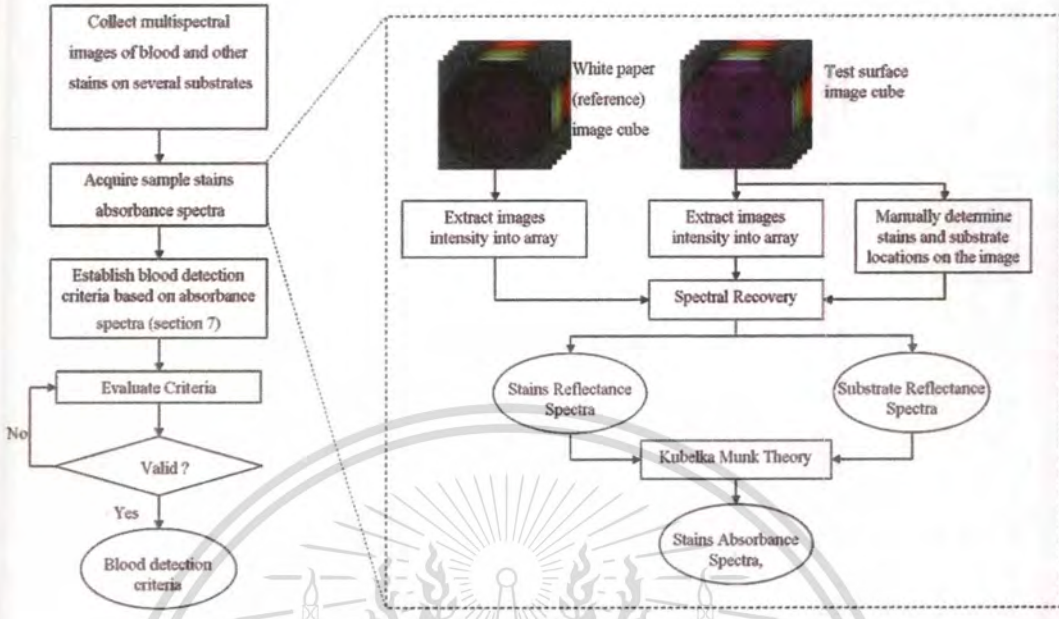

Figure 4.2 Proposed procedure in development of blood detection criteria.

First, we collect many sets of multispectral images of blood and other stains samples on different substrates. Then, we use our proposed calibration and spectral recovery method, and later on apply KM theory to obtain absorbance spectra of each stain. Based upon these absorbance spectra, blood detection criteria can be established. In the following sections, we describe in detail the step by step developments of blood detection methodology according to our proposed idea.

4.4 Stains' reflectance spectra

Sample reflectance spectra of stains are collected by manually locating the image coordinates where stains are deposited and then, with simple array manipulation, reflectance spectra from those coordinates are extracted. Figure 4.3 (a) shows reflectance spectra of different stain types, deposited on gypsum and wood substrates.

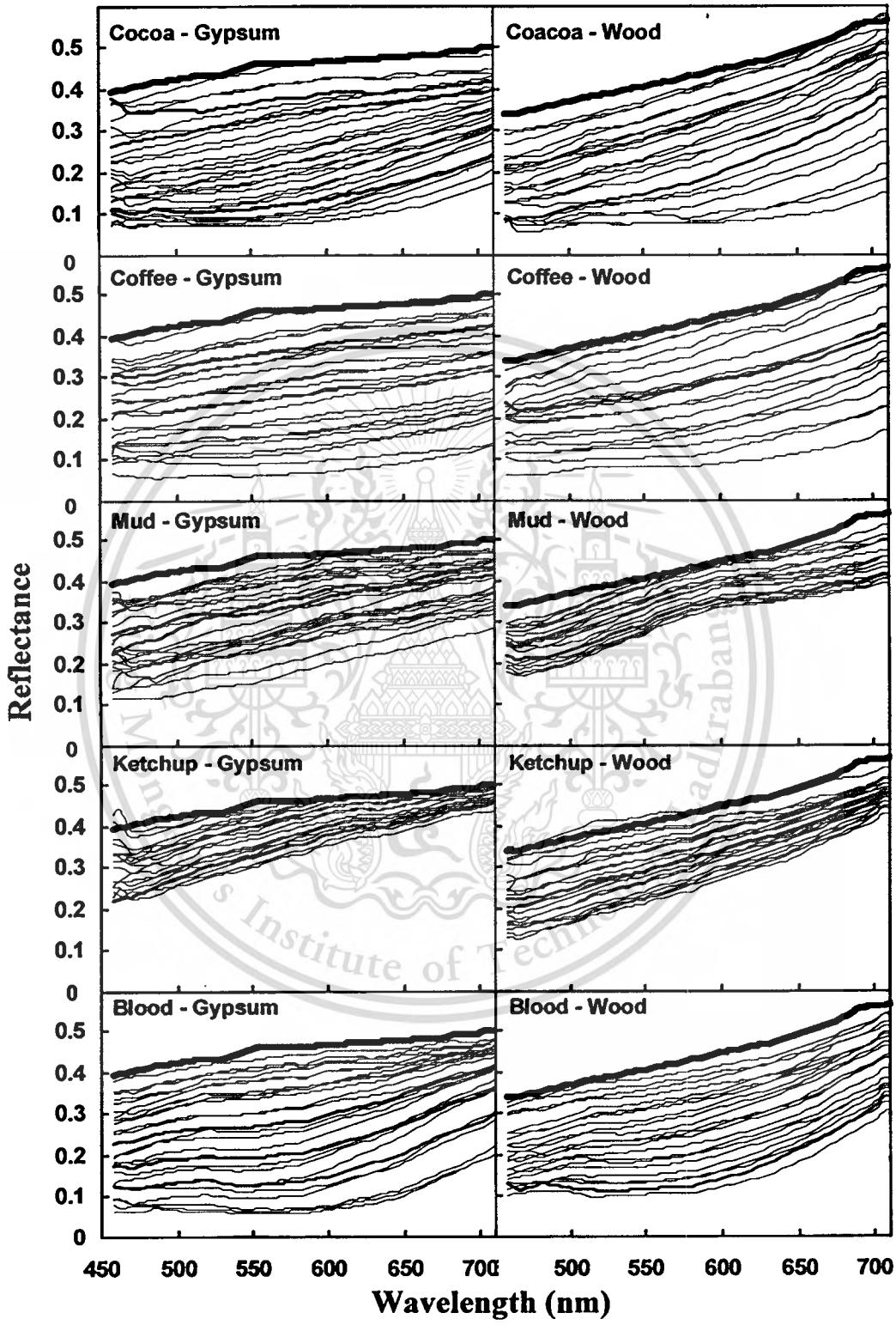

(a)

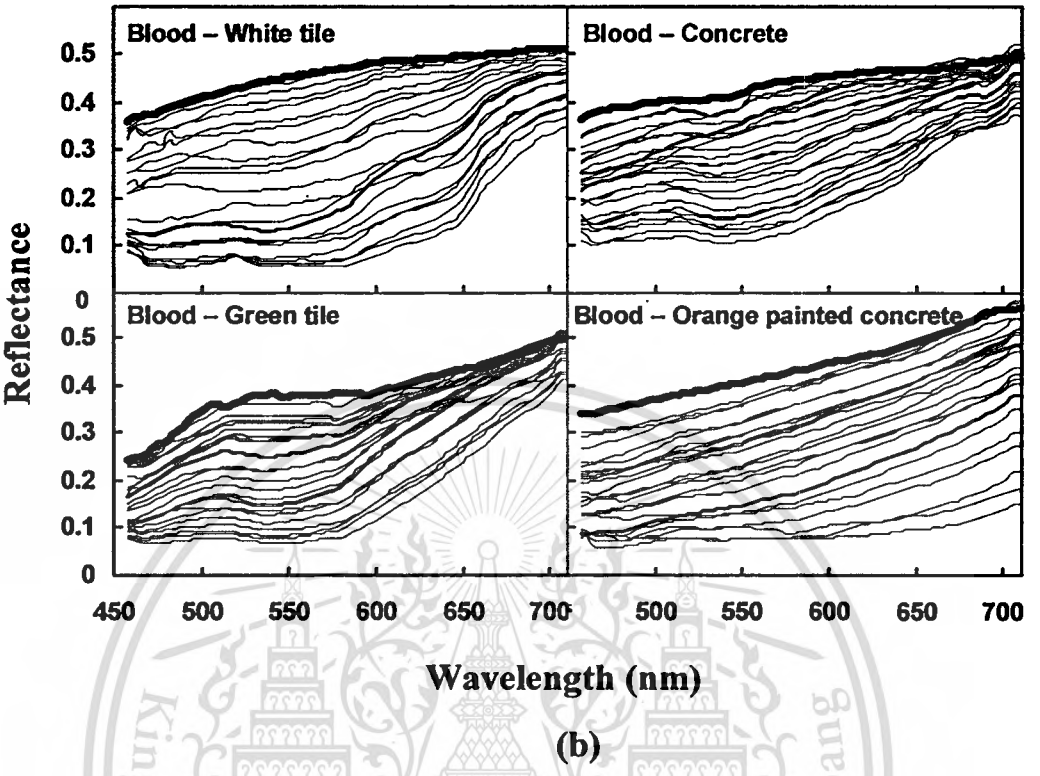

Figure 4.3 Recovered reflectance spectra of (a) blood and other stains on gypsum andwood substrates and (b) blood stains on different substrates. Bold lines are reflectance spectra of substrate while solid lines are those of stains.

It is clear that there are a number of possible reflectance curves for each stain type, depending on stain concentration. The highest reflectance curve (a bold line) in each chart belongs to the substrate while lower curves (thin solid lines) belong to the stain. The higher stains' reflectance curves also indicate thin or low-concentration stains, while the lower curves belong to thick or high-concentration stains. In addition, differences in curve tendency are also observed among different stain types. When the substrate changes, differences in spectral shape of the blood stains can be observed as shown in Figure 4.3 (b), pointing out that the shape of blood stain reflectance spectra is much influenced by the reflectance spectra of the substrates. The reason behind this phenomenon is that granular nature of stains, deposited on the substrates, inevitably causes spectral mixing between light reflected from stains and that from substrates. The fainter the stains are, the larger the

contribution of substrate is to the reflectance spectra. Since substrates in real world may be anything and may exhibit infinitely possible shape of reflectance spectra, the blood stain reflectance spectra on the substrates can also be of any shapes. Blood stain detection system based upon reflectance spectra is therefore improbable.

4.5 Estimation of stains' absorbance spectra

Since absorbance of substance is substrate independent, it is likely that spectral absorbance could be the base for detection blood stain. Although we cannot physically measure absorbance spectra from a multispectral imaging system, KMtheory allows us to indirectly estimate spectral absorbance from the measured reflectance. In this section we use KM theory to obtain absorbance spectra of stain samples. Note that KM formulae has been successfully used by Bremmer et al to obtain blood stain absorption spectra on white cotton substrate in order to determine the age of the blood [61]. Here, we apply same formulae to the spectral reflectance recovered in the previous section.

$$\frac{R_{ST}(\lambda)}{R_S(\lambda)} = 1 - \frac{K(\lambda)}{S(\lambda)}\left(\sqrt{1+\frac{2K(\lambda)}{S(\lambda)}}+1\right) \tag{4.2}$$

where $R_{ST}(\lambda)$ and $R_S(\lambda)$ are the reflectance spectra recovered from the stain and pure substrate surface, respectively. This equation has been, in fact, stated as equation 2.4 when KM theory is mentioned. The variables $K(\lambda)$ and $S(\lambda)$ relate to stain optical absorption and scattering, respectively. To find $R_S(\lambda)$, we manually locate the known pure substrates areas in the image, extract reflectance values at all corresponding points, and average them to get the substrate spectrum. A Lorentz-Mie scattering concept (equation 2.5 in chapter 2) is also applied during our estimation of stain absorbance spectra.

$$S(\lambda) = S_0\left(\frac{\lambda}{\lambda_0}\right)^{-0.4}. \tag{4.3}$$

Here, we take $\lambda_0 = 450$ nm and $S_0 = 1$ for all stain samples. Hence, unit of $K(\lambda)$ becomes arbitrary. Some resultant absorbance spectra of the different stains on gypsum and wood substrates are shown in Figure 4.4 (a) (compare with Figure 4.3 (a)). Also, some blood stain absorbance spectra on different substrates are shown in Figure 4.4 (b) (compare with Figure 4.3 (b)). These absorption curves are not necessarily taken from the same stain locations as those reflectance curves in Figure 4.3 They are chosen in such a way that the curves are clearly distributed and that the tendency of the curves can be clearly observed on the chart. Higher absorbance curves on each chart are associated with thick or high-concentration stains, while lower absorbance curves belong to faint stains. From the shape of blood stain absorbance spectra on all six substrates in Figure 4.4, more distinguished spectral features can be clearly observed from blood stain absorbance curves than from reflectance curves. It is obvious that blood stain absorbance spectra show similar curve tendency among all six substrates. Prominent spectral features include the steep down-slope at low wavelengths (458-510nm), the up-slope roughly from 514 nm to 542 nm wavelength, the down slope from 546 to 690 nm wavelength and very low absorbance at the red end of visible spectrum. Tendencies in deflection or concavity of the curves are also evident. Inconsistency on absorbance curves at low wavelengths (e.g., 458-466 nm) is observed because of low intensity of illumination as well as low response of our multispectral system at this spectral range. Thereby, the criteria that will be established in section 7, must be based on 470-710 nm wavelength only.

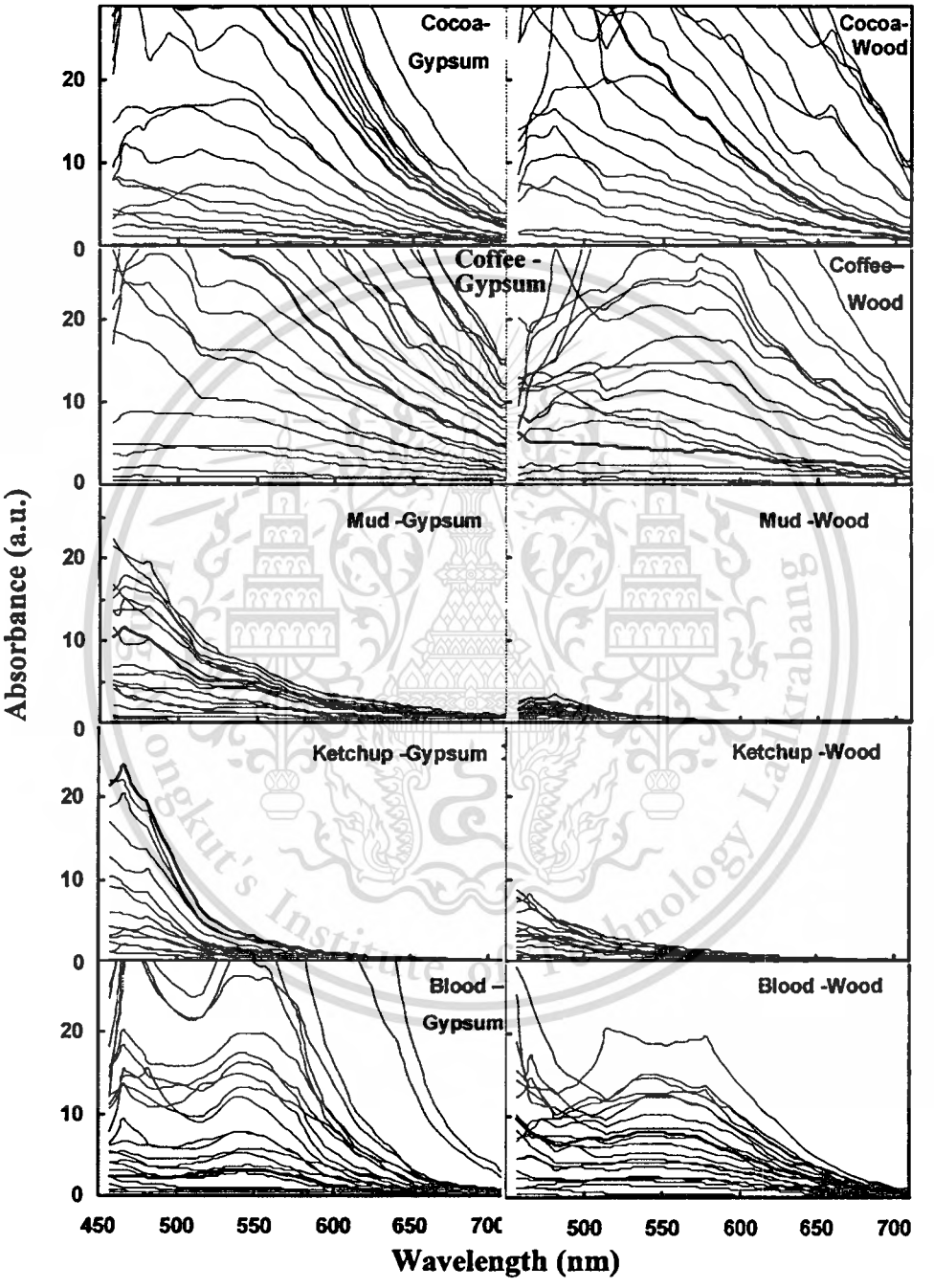

(a)

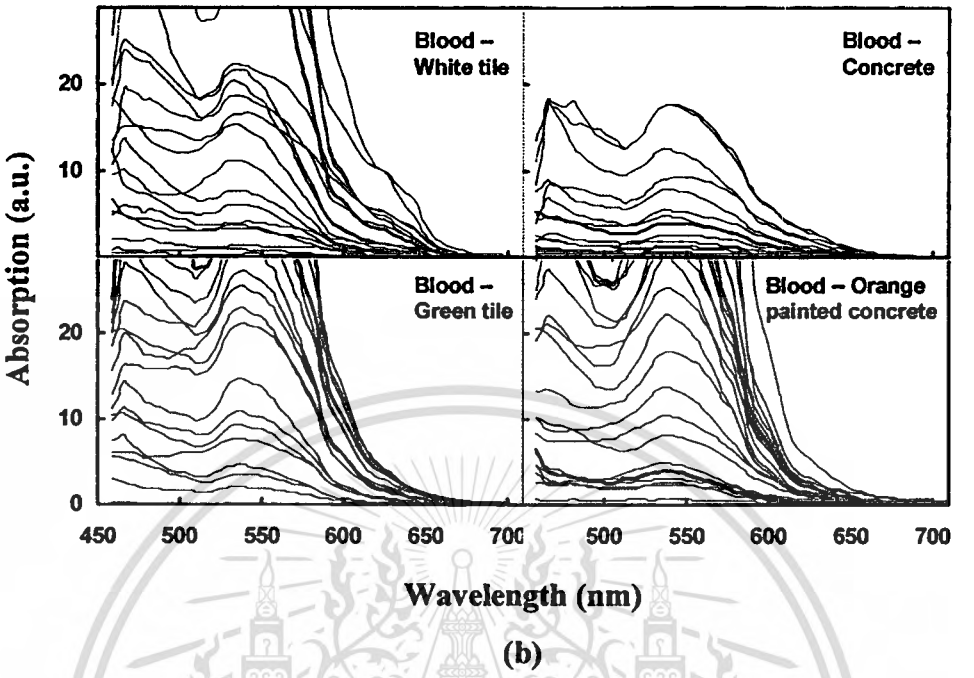

Figure 4.4 Recovered absorbance spectra of (a) blood and other stains on gypsum and wood substrates (compare with Figure 4.3 (a)) and (b) blood stains on different substrates (compare with Figure 4.3 (b)).

At the time the spectral images are taken, blood stains are a few weeks to several months old. At this time range, major constituents of blood pigments are hemichrome (50-70%) and oxy-hemoglobin (20-30%) [61]. Hence, the absorbance spectra are influenced most by the spectrum of hemichrome. The K-M absorbance spectra experimentally recovered from blood stains shown in Figure 4.4 are in good agreement with the absorbance spectra shown in Figure 2.8, which indicates that RBC pigment at the period of analysis should consist mainly of hemichrome and oxyhemoglobin.

4.6 Establishment of blood stain detection

In our real fully-developed detection system, spectral parameters from all spatial points on images of a test surface will be programmatically extracted and tested by a series of our blood stain discrimination criteria. The criteria are simply the mathematical inequalities involving the spectral parameters purposely made in the way that they would pass the spatial points in the image that possibly correspond to the blood stain and at the same time prevent

the points ascertained as definitely not corresponding to blood. Spectral parameters include reflectance values, absorbance values, arithmetic operations of these values, and polynomial coefficients of absorbance spectra. The spatial locations on the test surface that pass all of our criteria will be finally identified as the blood stain. To establish the criteria, we first choose spectral parameters that can intuitively reflect the distinct spectral characteristics of blood stains reflectance and absorbance curves as well as can simultaneously eliminate other stains. Simplest criteria make use of only a single spectral parameter. For example, since we see that blood stain absorbance is very small at the red end of the visible spectrum, we make a criterion that the absorbance at 710 nm wavelength must be less than 1 (i.e., $K(710\text{nm}) < 1$, see absorption values at 710 nm wavelength shown in Figure 4.4) In this way, we can exclude many spatial points corresponding to coffee and cocoa stains. In another criterion example, we exclude spatial points whose reflectance values are close to the reflectance of the substrate in order to eliminate the substrate locations, $(R_{ST}(470\text{nm}) / R_S(470\text{nm}) \leq 0.98$, consider reflectance values at 470 nm wavelength on the charts in Figure 4.3) In a more complex criterion, two extracted spectral parameters are plotted on the x and y axes of a scatter chart. Four examples of these charts are shown in Figure 4.5. Each data point on the charts corresponds to the stain type indicated by the shape of marker. The substrate type is indicated by the color of the marker. For clarity, the separate charts on the right side show data points corresponding to only the blood stain whose trend can clearly observed. Criterion boundaries are manually selected to loosely encompass the blood stain region. Each boundary is drawn with joining straight line segments so that criteria expressed in simple linear inequalities (i.e., $y > mx + c$ or $y < mx + c$) can be applied, where m is the slope and c is the y intercept of the line segment. The correct marks and cross marks indicate the regions to be selected and deselected by our proposed criteria, respectively. We normally make slightly loose criteria to spare for noise in the system. However, the data points from blood stains that considerably deviate from the trend possibly due to large noise or impurity have to be excluded. Otherwise, specificity of the system must be sacrificed. Although spectral parameters made from reflectance and absorbance values of a few wavelengths (Figure 4.5 (a)-(d) are quick to

process and useful to preliminarily exclude some stains, they are not discriminative enough to exclude all other stains. More discriminative spectral parameters take advantage of polynomial coefficients (Figure 4.5 (e)-(i) since they are established from more wavelengths and hence less subject to system's noise. To make the criteria, we apply polynomial fits (up to the 3rd order) to selected portions of the absorbance spectra. For instance, since blood stain absorbance curves have prominent concave downward shape along 514-586 nm and centered around 550 nm wavelength, we estimate that the 2^{nd} order coefficients of this curve section for the blood stain must be some negative values. Accordingly, we apply polynomial fit to this curve section, which we let the center be at 546 nm and adjust the x scale so that the distribution of data points is clearly observed. Then, we plot the 2^{nd} order coefficients against the 0^{th} order coefficients (Figure 4.5 (g). Figure 4.5(i) shows a criterion associated with the 3^{rd} order polynomial coefficient. The criterion seems to not to be very discriminative at low stain concentrations (the points near the origin). However, we can still use it to distinguish blood at higher concentrations ($K(546\text{nm}) > 16$). The distribution of data points on many scattering charts for each stain usually has imperfect triangle-like shape with one tip at the origin. The points closer to the origin belong to thin stains. One criterion may be able to exclude only some stains or some concentrations of stains. Taken into account the interest of forensic investigation and based on 2-D spectral data from 470-710 nm wavelength, we currently make as many as 26 criteria in order to take out as many different stain points as possible. The details of the criteria can be found in the Appendix at the end of this thesis. Although several criteria may exclude many same spatial points in the image, we rely on the fact that if some spatial points of other stains are misidentified by a criterion, there may be another criterion that can exclude the points. Having many criteria may not hurt the speed of the system much, because criteria can be cascaded so that the excluded spatial points will not be calculated again in the later criteria. One advantage of this detection system is that system specificity can always be improved by finding more criteria, refining existing criteria, or even remove some redundant criteria.

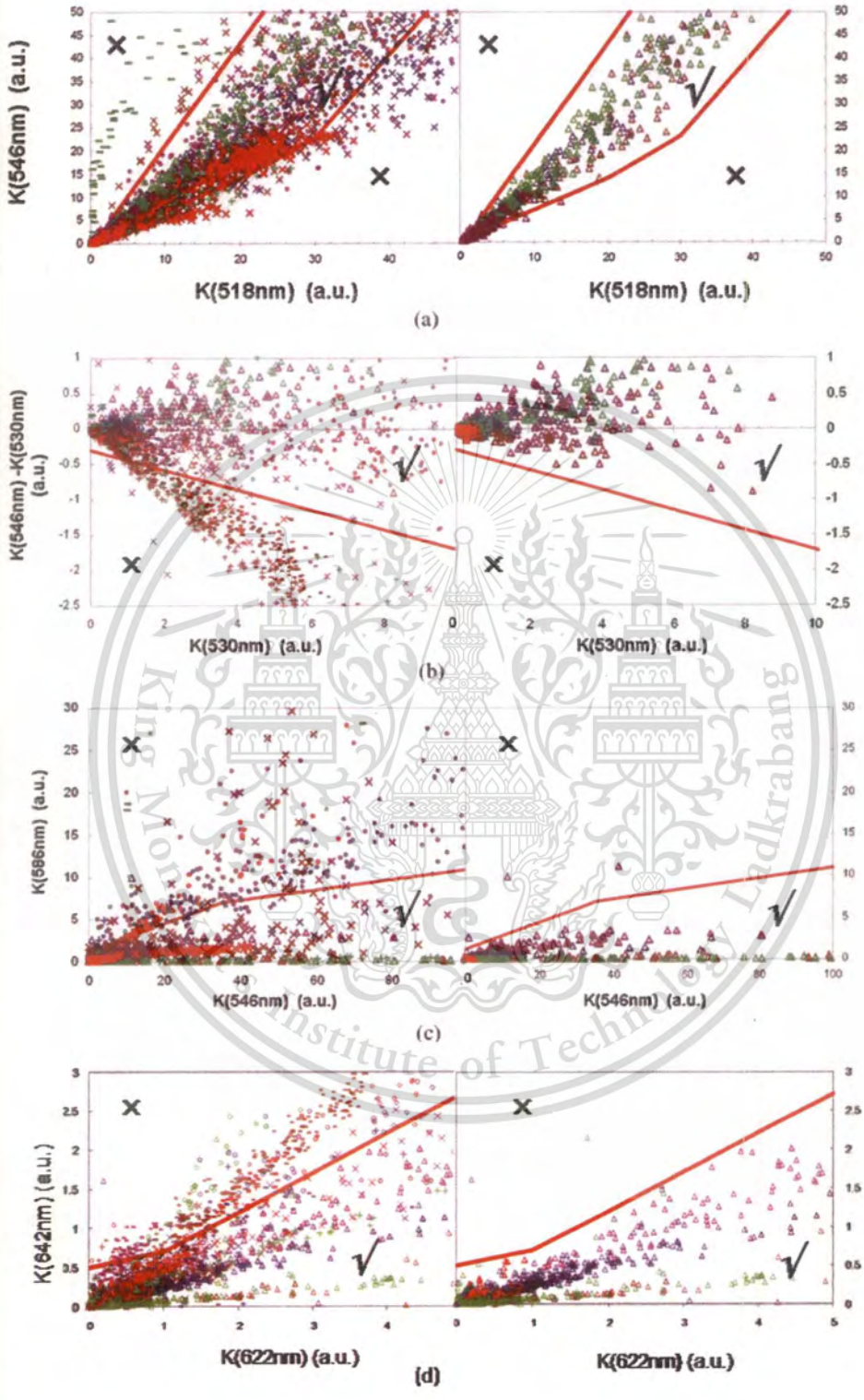

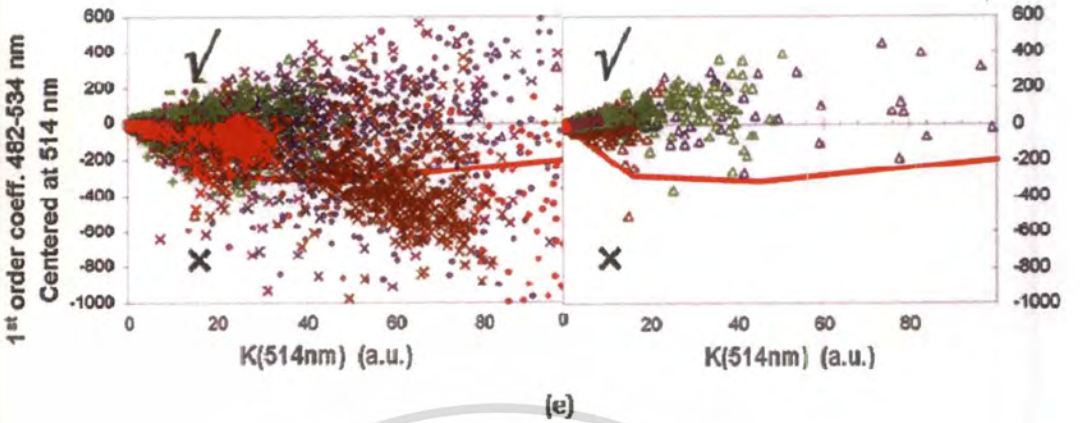

(e)

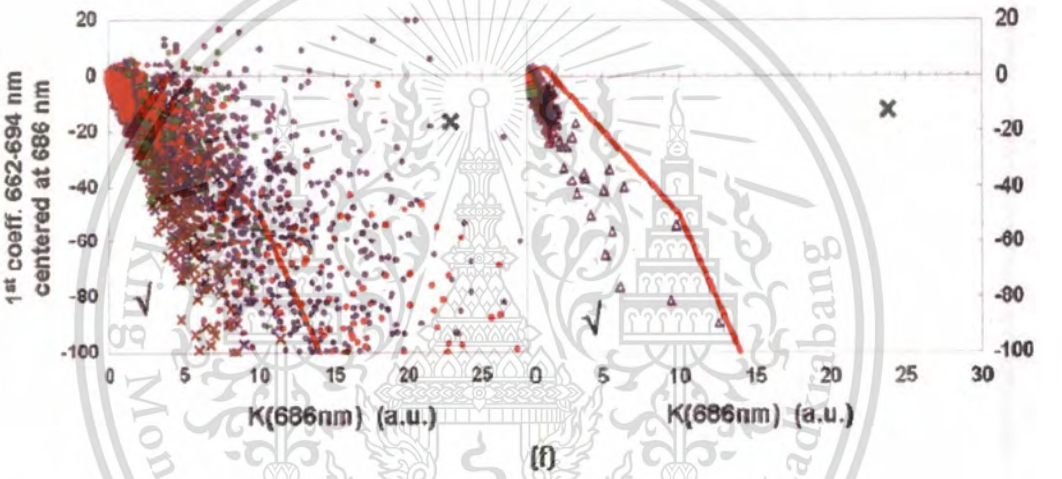

(f)

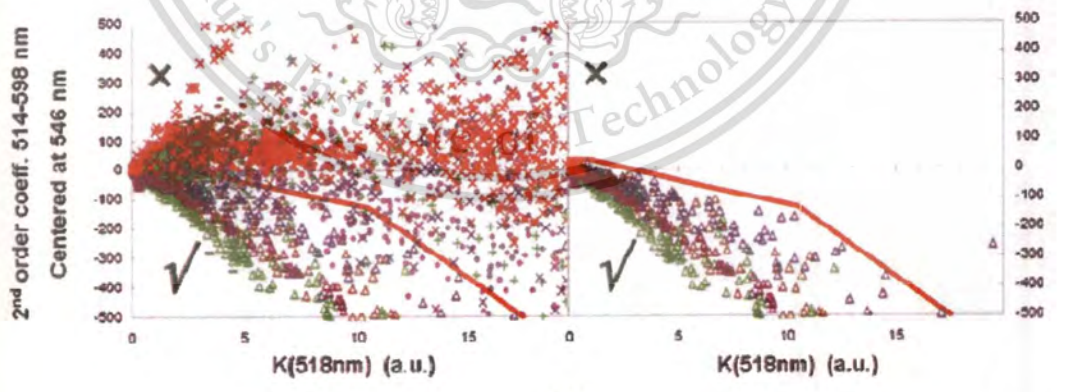

(g)

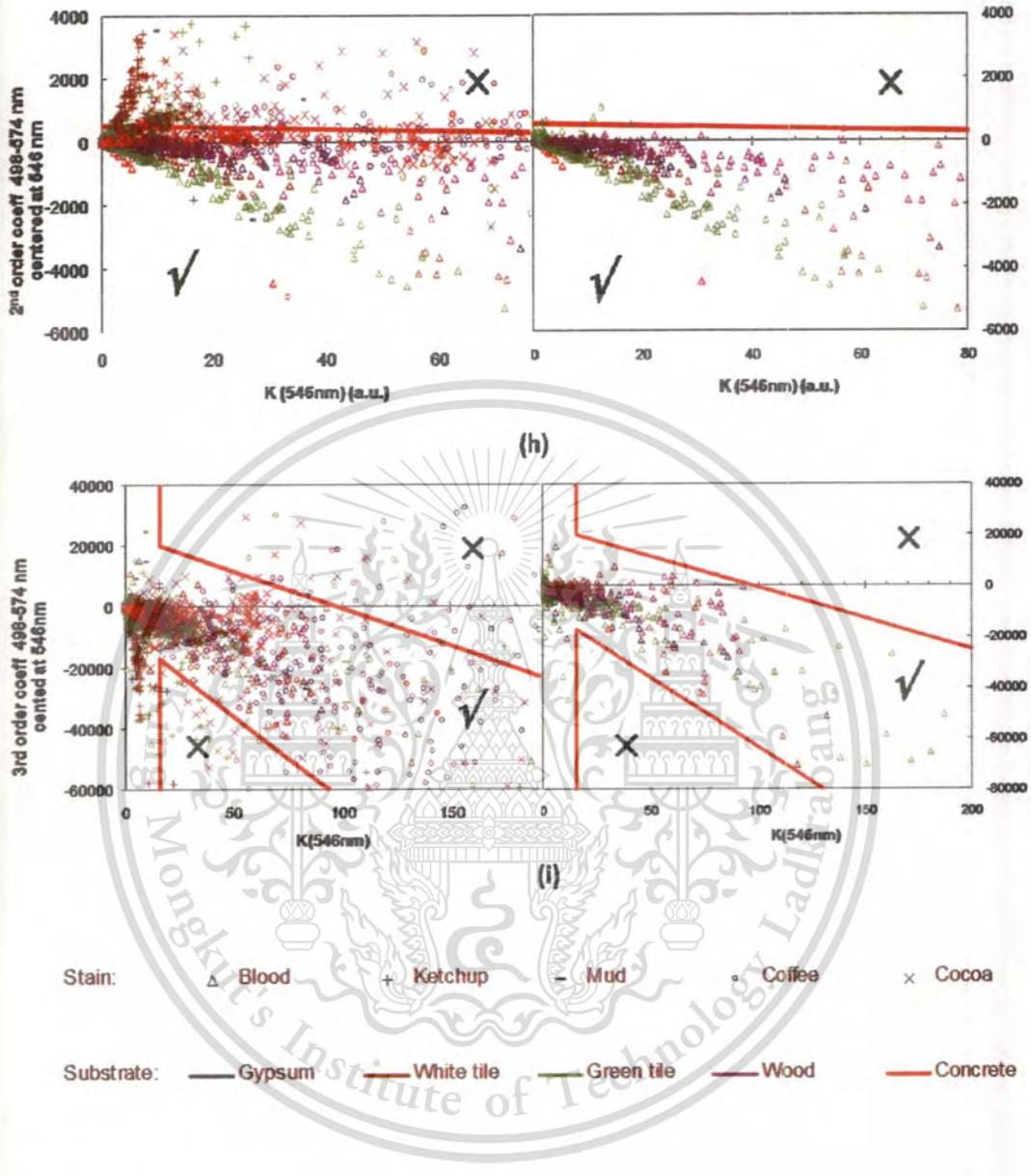

Figure 4.5 Examples of blood detection criteria, each based on two spectral parameters. (a)-(d) are preliminary criteria, (e)-(i) are different order of polynomial coefficients on different curve segments vs absorbance values at selected wavelengths. Charts on the left side show data points from all stains while on the right side show those from blood stains only. Criterion boundaries are drawn with straight line segments to cover the blood stain region.

4.7 Experimental verification for the established criteria

To evaluate our detection criteria for the blood stain, we capture several other multispectral image cubes of stain samples and perform blood stain detection with our established criteria on those new image cubes. The image cubes are transformed into arrays and calibrated by the method described in sections 5 and 6. The detection program operating under LabVIEW 2011 is designed such that the required spectral parameters for every spatial point are extracted. Then, all spatial points are sequentially tested by all 26 criteria established in section 7. Only the spatial points that pass all criteria are identified as possible blood stains. Although this is not a computationally efficient method of detecting blood, the purpose of this Chapter is to establish and refine our detection criteria for the blood stain. In Chapter 5, we will propose and experimentally show the method to eliminate unnecessary calculation steps in real blood detection system. Figure 4.6 shows result images after they pass through our blood detection criteria. The points identified as blood stains are masked with 2×2-pixels pseudo-red color on the original 530 nm images.

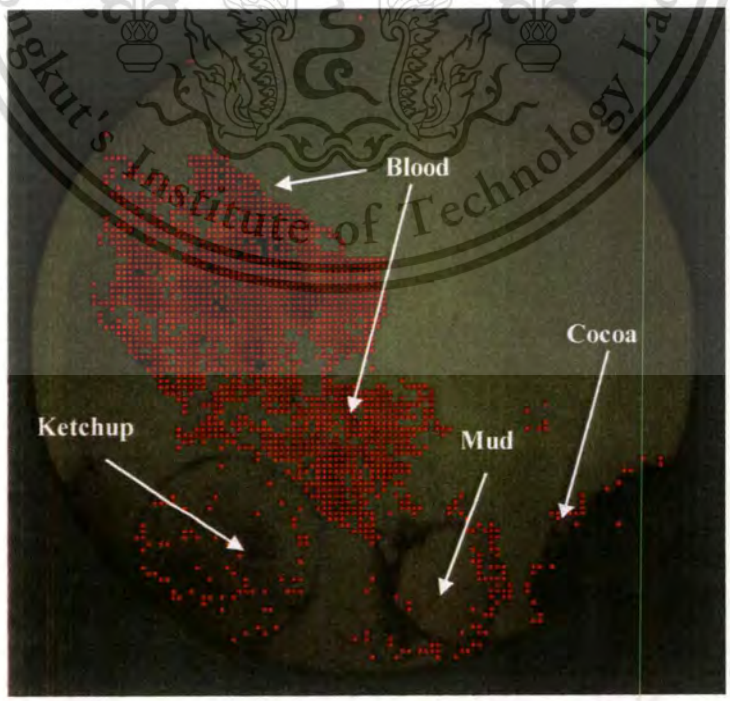

(a)

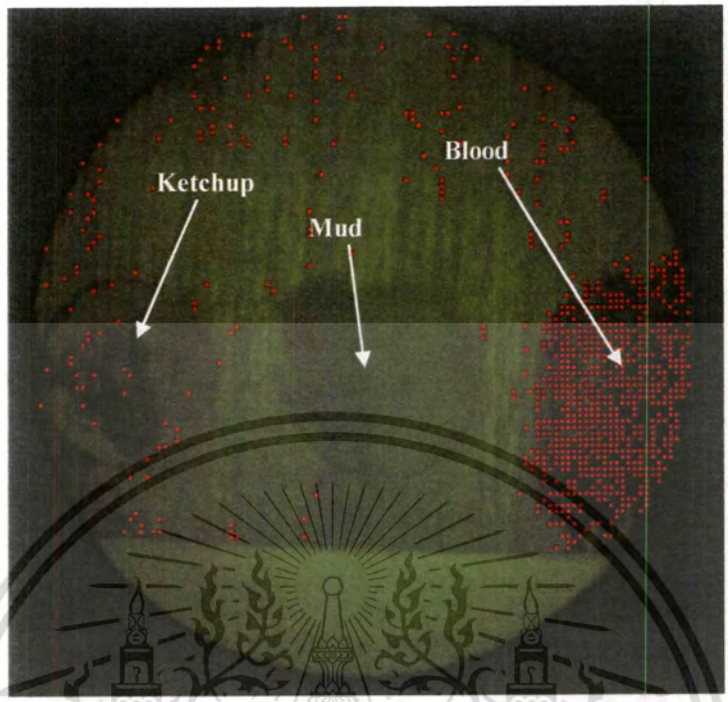

(b)

(c)

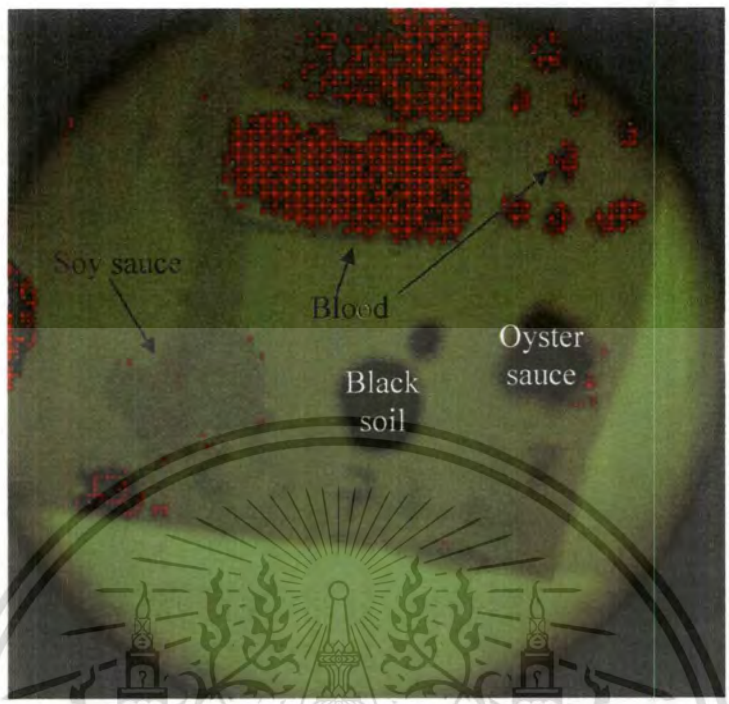

(d)

Figure 4.6 Examples result images for blood stain detection on (a) gypsum (b) wood (c) green tile and (d) white tile. Spatial points identified as blood are masked with 2 by 2 pixel pseudo red color on the original 530 nm spectral images.

4.8 Experimental results

Performance of the detection system is appraised by its sensitivity, specificity, and speed [75]. Since we know the true locations of our blood stain samples on the result images, the system sensitivity can be described in terms of true positive rate (TPR). Because sensitivity of blood stain detection depends on stain concentration, plotting the TPR versus stain concentration is appropriate. As discussed earlier, though stain concentration at each spatial point cannot directly be measured, the height of the stain reflectance curves (section 5) or absorbance curves (section 6) can indicate the concentration of the stain. In our scheme, the absorbance values do not give the intuitive measurement of strain concentration since their units are arbitrary. So, we turn to the reflectance curve. We choose to plot TPR versus $R_{ST}(470nm)/R_S(470nm)$ (see Figure 4.7 (a)) because reflectance curve separations are typically larger at low wavelengths and the lowest available wavelength that

gives consistent measurement in our system is 470 nm (see Figure 4.4.) For most reddish brown stains, the stains are darker than the substrates and the value of $R_{ST}(470nm)/R_S(470nm)$ usually ranges from 0 to 1. The closer the value is to 1, the closer the stain looks like the substrate; and hence the more difficult the stain is to be told by naked eyes.

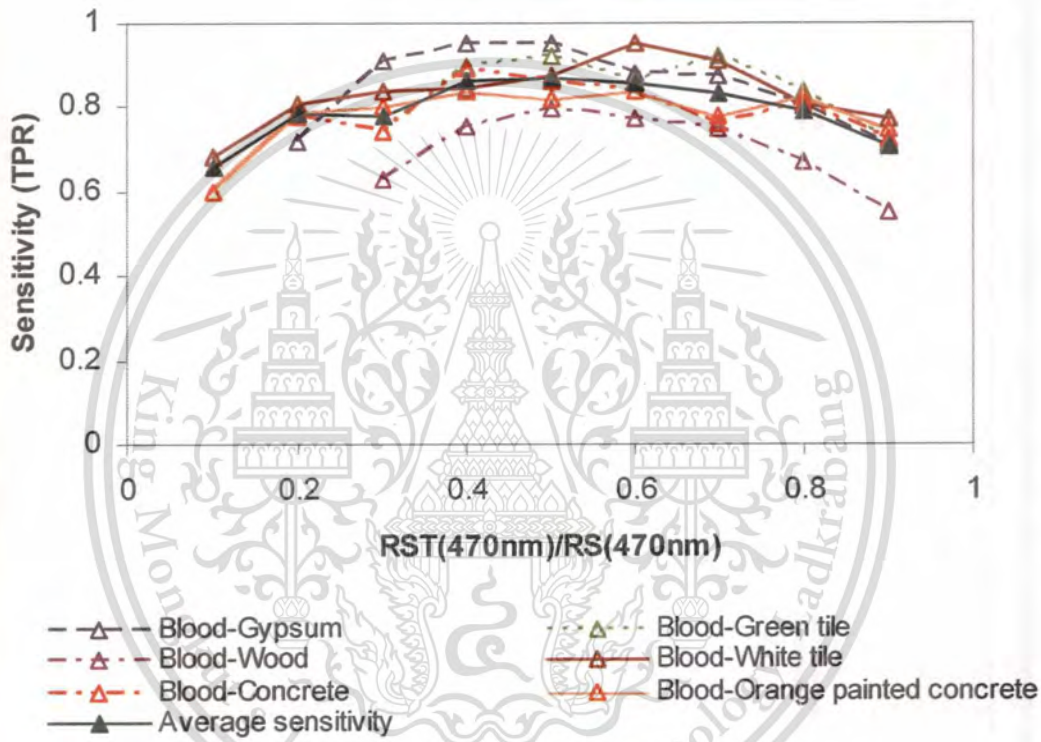

Figure 4.7 System performance of our blood stain detection described in sensitivity.

According to Figure 4.7, the values of $R_{ST}(470nm)/R_S(470nm)$ are grouped into class intervals just like in histograms, with the interval size of 0.1. The markers represent the middle value of their classes. For example markers at 0.9 represent $R_{ST}(470nm)/R_S(470nm)$ values between 0.85-0.95. TPR is determined for each class. For all substrates, high sensitivity (0.7<TPR<0.95) is achieved at medium to high blood concentration ($0.3 < R_{ST}(470nm)/R_S(470nm) < 0.7$). This medium concentration blood stains have high SNR levels and are easiest to identify. The highest sensitivity for blood station detection is observed on gypsum substrate (0.8<TPR<0.95), while the lowest is

on wood (0.6<TPR<0.79), because of high local variation of wood substrate profile. For thin or low concentration of blood stains $(0.8 < R_{ST}(470nm)/R_S(470nm) < 0.9)$, sensitivity is lower (0.55<TPR<0.84) with the average of 0.74 because small spectral signals from thin blood stains' absorbance spectra are embedded in larger signals from the substrate spectra resulting in lower SNR values. For thick or high concentration of blood stains $((0.1 < R_{ST}(470nm)/R_S(470nm) < 0.2))$, sensitivity is also low (0.60<TPR<0.81) with the average of 0.73, because original digital response values are very low, especially at low wavelength (λ<500 nm), which also causes lower SNR values. Furthermore, thick stains are more subjected to packing effect of pigment particles in stains [64], which distorts the high absorbance parts of the spectra far more than lower parts.

The system specificity can be determined via the relationship between the true negative rate (TNR) and $R_{ST}(470nm)/R_S(470nm)$ by using the same method as above. For our system, specificity is the ability to exclude other stains from blood. For each stain type, we determine TNR for each substrate and take average of TNR values from all substrates. The TNR values as a function of $R_{ST}(470nm)/R_S(470nm)$ are shown in Figure 4.8. High specificity (0.8<TNR<0.96) is achieved at medium and high stain concentrations. Highest specificity is obtained in mud stains (0.86<TNR<0.96) and lowest in ketchup stains (0.78<TNR<0.88). For the same reasons as sensitivity measurement, at low and high stain concentrations, specificities for all stains reduces. The average TNR value at low concentration $(0.8 < R_{ST}(470nm)/R_S(470nm) < 0.9)$ is 0.75, and at high concentration $(0.1 < R_{ST}(470nm)/R_S(470nm) < 0.2)$ is 0.77. In this chapter, the identification process take 4-5 minutes for each image cubes because at all spatial points, all required parameters are extracted and tested by all criteria. In Chater 5 of this thesis, we will take into account the speed issues and evaluate speed when we employ the criteria established in this Chapter to make rapid blood stain detection system.

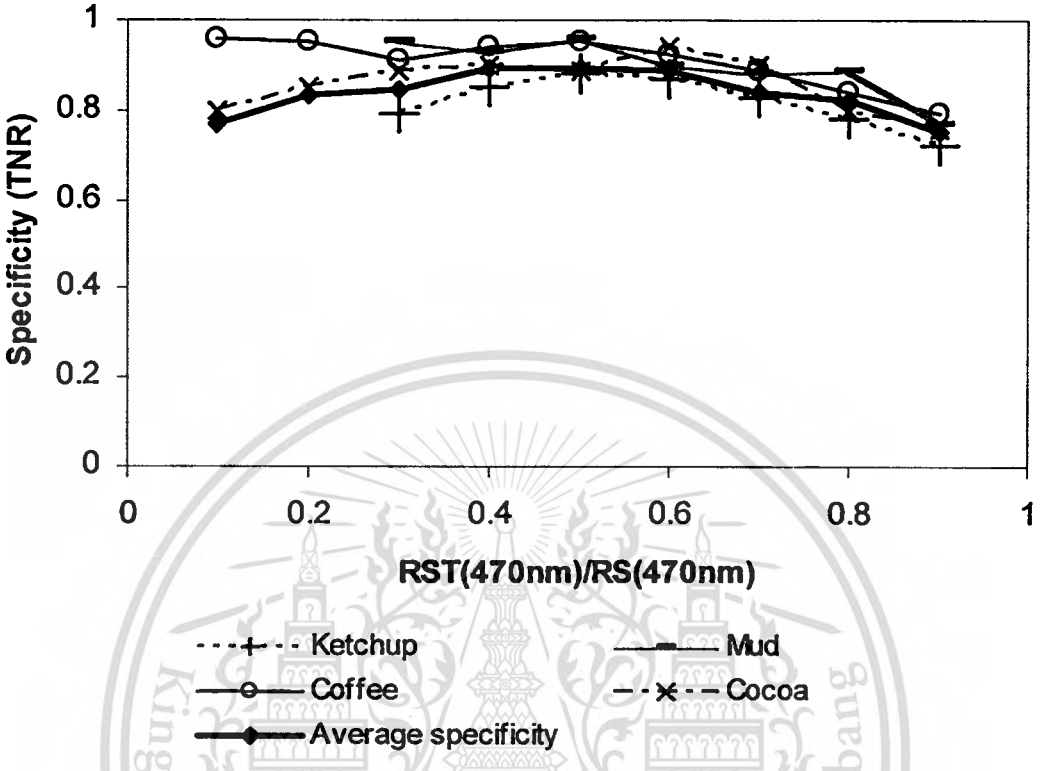

Figure 4.8 System performance of our blood stain detection described in specificity.

Chapter 5

Experiment part II:

Realization of rapid blood stain detection

5.1 Overview of the experiment

Based on the blood stain detection criteria established in chapter 4, we combine and organize all necessary tasks to realize rapid blood stain detection system. The developed system automatically adjusts camera exposure times to prevent saturation or excessive darkness in spectral images, searches for the clean positions on the substrate, determines the reflectance spectra, applies the criteria, and accurately pinpoints positions of blood stains. Parallel processes between image capturing and blood stain identification shorten the times for blood stain identifications, while proper arrangement of the criteria and image capturing order allows the system to eliminate unnecessary calculations despite a large amount of data to be processed. The developed system can identify blood against several other stains on several substrates, and then rapidly display positions of possible blood stains on the display. The measured average identification times on different test surfaces range from only 23.3 to 28.7 seconds excluding the image capturing process.

In realization of a blood stain detection system, several issues arise in making the technique practical. Firstly, the multispectral imaging blood stain detection system involves several data processing steps and a large amount of multispectral data to be accounted for. To make the blood stain detection system rapid, the detection procedure must be well planned. Since our blood stain detection method is basically operated by gradually eliminating spatial points (a group of 3×3 adjacent pixels) identified as not corresponding to blood using a series of criteria, the criteria and the image capturing order must be appropriately arranged such that the criteria with more specificity would be applied earlier. Secondly, because our blood detection process proposed in chapter 4 requires determination of the substrate reflectance spectrum, the system should efficiently search for locations of the clean substrate and determine its reflectance spectrum. Thirdly, crime scene investigation

may cover large search areas and a wide variety of colors and textures of substrates. Given usually spiky spectral shape of the combined response of the multispectral imaging instruments, the captured spectral image can be easily saturated or darken, implying that obtaining suitable multispectral data is nontrivial. In addition, forensic investigators should not waste much of their valuable times setting up or adjusting lighting conditions to suit each scene by themselves. Hence, the ideal blood stain detection system should be automatically adjusted itself for any kinds of substrates and environmental conditions. Moreover, the imaged test surface may contain bright and dark stain spots that could potentially correspond to blood. Detection system should adapt its image capturing to collect usable spectral data from all those bright and dark spots in the field of view as well. In this experiment, we propose the system that can correct the above problems and realize the rapid blood stain detection based on our blood detection criteria established in chapter. This chapter briefly reviews the physical system, describes the calibration procedure and then discusses the proposed rapid blood stain detection procedure. Along the discussion, we explain how the above problems are dealt with, to make rapid blood stain detection system possible. The key features include our special data manipulation in the form of multispectral data array, automatic search for substrate positions on the test surface images, automatic determination of substrate reflectance, and automatic adjustment of camera exposure times.

5.2 Sample materials

We use the same experimental setup described in chapter 4. The only difference is the newly written program, developed to control the acquisition of the spectral images and quickly identify position of blood stains on the screen. In this experiment, new sets of substrates and stain samples, shown in Figure 5.1, are prepared in order to show that the criteria, established chapter 4, can be applied to different samples and substrates. The stains include bovine blood, coffee, rust, cocoa drink, dirt, tea, and chicken essence soup. The substrates used in the experiment are chosen to have a variety of colors and textures, including a gypsum board, tiles (white, blue, and brown), a white-painted concrete, and an artificial wood board. The sample arrangement (Figure 5.2) is similar for all substrates.

Thirty six stain spots are arranged in a 6×6 cm2 rectangular area so that they can be seen at the same time in one image. The size of the stain spots varies between 0.2-0.5 cm in diameter. The horizontal and vertical distances between each pair of stain spots are about 1.2 cm apart. Each substance is stained with different, but unspecified, concentration values. We also put four extra long stains from blood, coffee, cocoa, and chicken essence soup outside the above area.

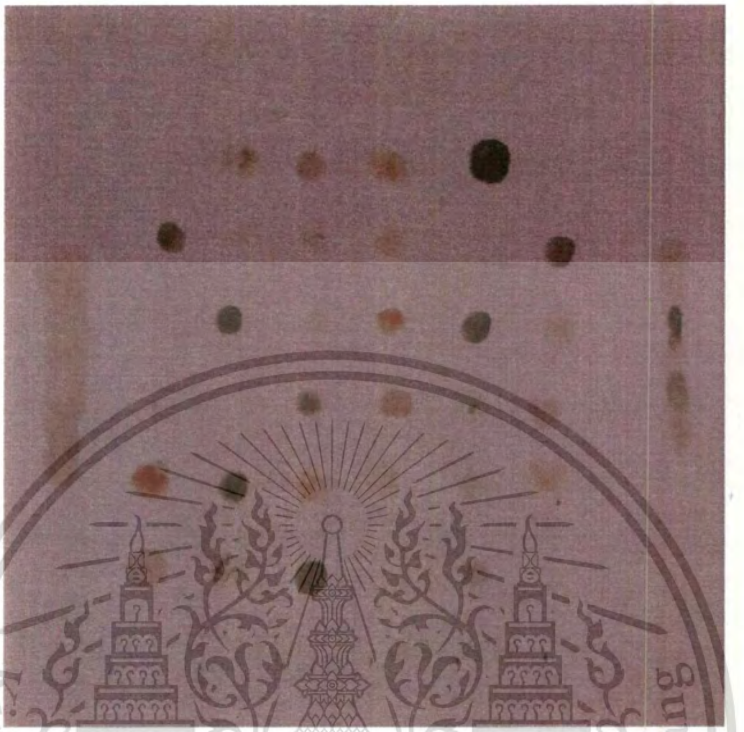

(a)

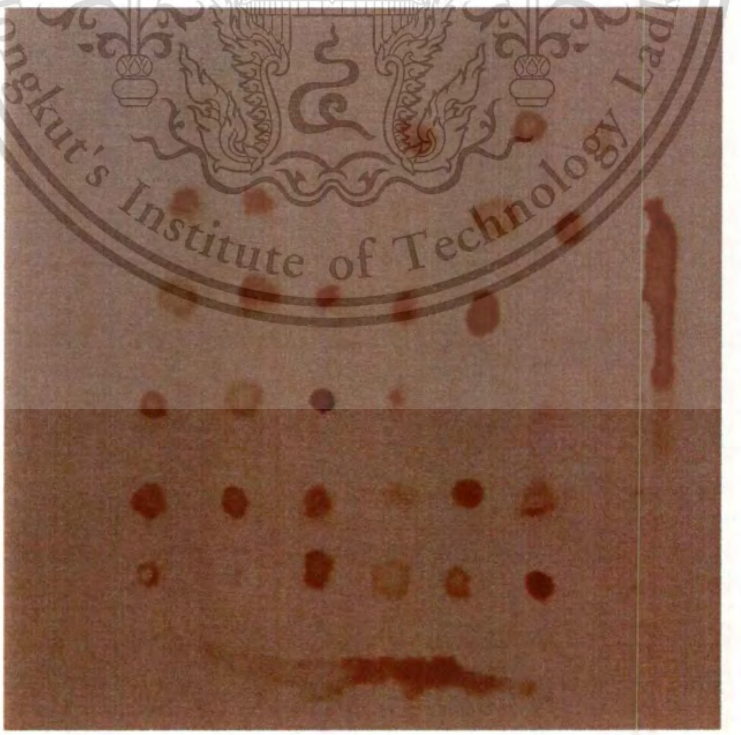

(b)

(c)

(d)

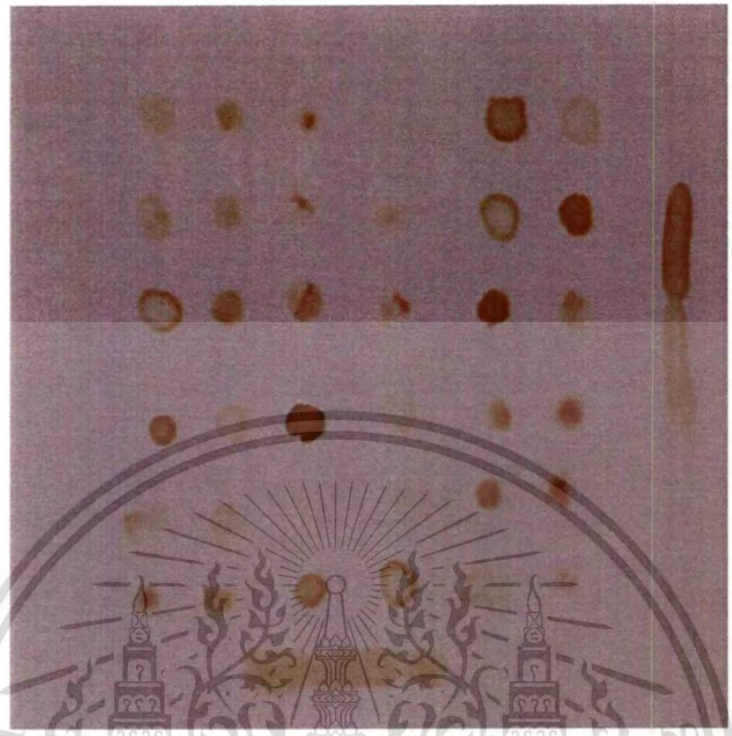

(e)

(f)

Figure 5.1 Six test surfaces including (a) gypsum, (b) brown artificial wood, (c) white painted concrete, (d) white tile, (e) blue tile, and (f) rough brown tile. Each substrate is stained with blood and 6 other substances.

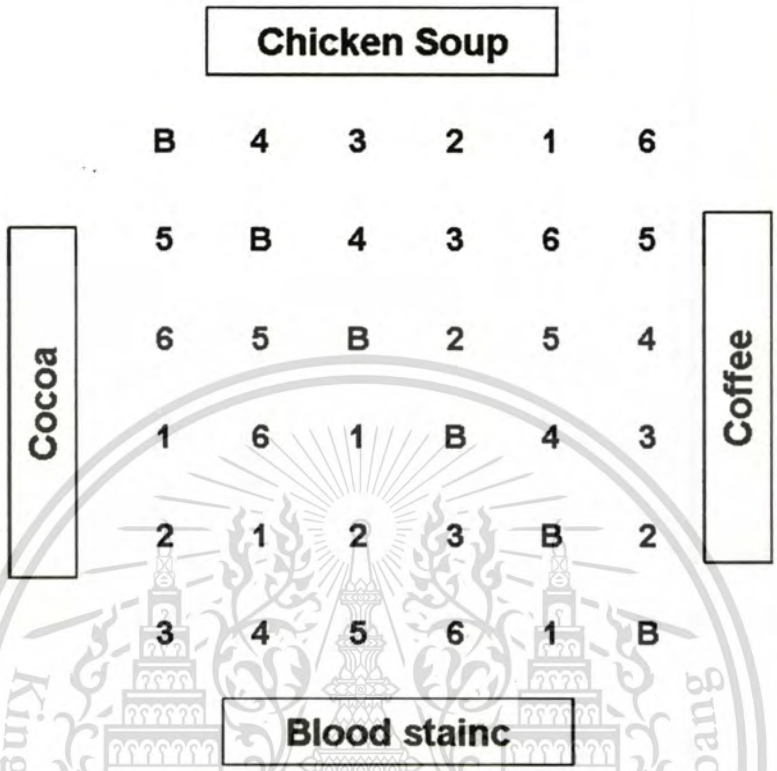

Figure 5.2 The arrangement of stains on all substrates is shown. The letter B represents the blood stain and the numbers represent stains as follows: 1. coffee, 2. rust, 3. cocoa, 4. dirt, 5. tea, and 6. chicken essence soup. Four long stains are also deposited on the rest of the extra areas around the stain spots.

5.3 System calibration

Our multispectral imaging system is calibrated with the white reference calibration method as previously performed in chapter 4. According to the method, reflectance spectrum at any spatial point over the test surface is recovered by comparing camera's digital responses extracted from the spectral image cube of white reference paper with the digital responses at the same spatial point from the spectral image cube of the test surface. The calibration procedure, shown in Figure 5.3 is to be performed for just one time at the beginning of each investigation session to prepare calibration data necessary for use in the blood stain detection procedure.

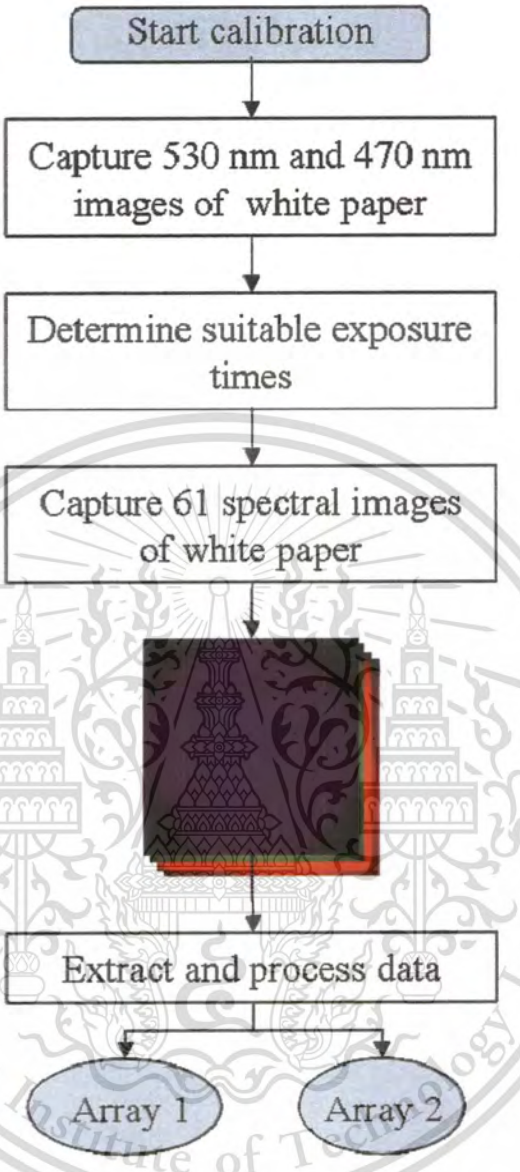

Figure 5.3 Calibration procedure. The calibration process yields calibration data in the form of Array 1 and Array 2.

Once the system is calibrated, it can be used to detect blood stains many times on several substrates without the need for recalibration. In this experiment, for more user convenience, we have designed the system that can automatically perform all necessary calibration tasks, including capturing spectral images with suitably adjusted exposure times, and preparation of the calibration data for use in blood detection stage. The user is just to place a stack of white paper sheets of known reflectance spectrum on the detection zone and starts calibration. The

calibration procedure starts with capturing 530 nm and 470 nm spectral images. Then, the system quickly determines appropriate exposure times for capturing all spectral images. The details about how the system determines the appropriate exposure times will be described separately in section 6. Once the suitable exposure times are determined, the system captures 61 spectral images, one by one, in numerical order of wavelengths starting from 470 nm to 710 nm with a uniform wavelength separation of 4 nm and stores the images in the system. The 530 nm and 470 nm spectral images are also recaptured. Because each opened spectral image requires occupation of space in random access memory (RAM) of the computer system. Opening several spectral images at the same time occupies too much of the RAM, which highly affects the performance and speed of the system. To maximize the speed, our system reserves RAM space for only one spectral image during the image capturing and data processing. After each spectral image is captured, it must be saved in the permanent memory of the system (i.e., the hard disk of the computer) and closed. The next captured spectral image then can reuse the same RAM space.

Since the speed is not quite an issue during calibration, preparation of calibration data is started after all spectral images are captured. According to our proposed calibration method, multispectral image cube is transformed into compact and ready-to-use multispectral data arrays. To prepare the arrays, the system reopens the saved spectral images one by one, extracts digital responses from each spectral image, calculates the calibration numbers ($w(\lambda)$), and arranges them into the arrays shown in Figure 5.4.

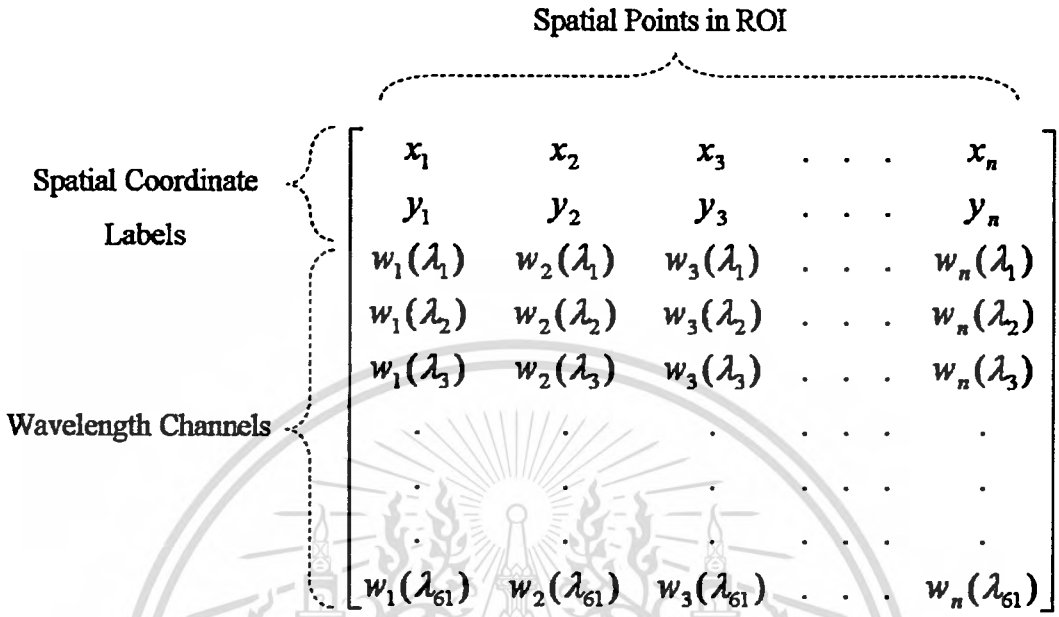

Figure 5.4 Multispectral data array configuration from the calibration stage. This array is stored in text file for the use in blood detection stage.

To save time in the blood detection stage, at each spatial point of each wavelength, all calculations that can possibly be done during calibration are immediately performed so and recorded as a single calibration number as

$$w(\lambda) = \left[\frac{W(\lambda) - D}{\tau_W(\lambda)}\right] \cdot \left[\frac{1}{R_W(\lambda)}\right], \tag{5.1}$$

where $W(\lambda)$ is the spectral camera's digital response from a single spatial point of the spectral image of the white reference (e.g., a white paper), D is the camera's dark response, $\tau_W(\lambda)$ is the wavelength dependent camera's exposure time, and $R_W(\lambda)$ is the known reflectance spectrum of the white paper. The camera's dark response is predetermined by capturing the image while the camera's aperture is covered by slid. There are two kinds of arrays related to multispectral data stored in the system. Both have the same configuration as shown in Figure 5.4, but are intended for different purposes. The first array, namely Array1,

is intended for the purpose of quick sampled substrate position search, substrate reflectance determination, and exposure time adjustment. The second array (Array2) is intended for the purpose of blood stain identification. The rows of both arrays represent spectral dimension while the columns represent the spatial dimension of the multispectral image cube. There are 63 rows in the arrays that are composed of 61 rows representing 61 calibration numbers from 61 wavelength channels, and 2 additional rows at the top of the array for tagging the x-y spatial coordinates of the images. In Array1, $w(\lambda)$ are sampled from every 5×5 pixel all over the image field of view (non-averaged). As a result, only 72×68 = 4,896 pixels are initially sampled to constitute Array 1. In Array2, all pixels in the image are taken into account. Digital responses from a single spatial point are averaged from a group of 3×3 adjacent pixels, and then calculated into a single calibration number $w(\lambda)$. So, there are 120×113 = 13,560 spatial points that represent the physical dimension of the image. The columns of Array2 represent spatial points in the region of interest (ROI). In this work, we define the ROI as all spatial points that still possibly correspond to blood stains. Array2 has bigger number of columns than the Array1 and calculation from all pixels is required, thus taking much longer time to process.

Since our camera's field of view is limited by the circular aperture of the LCTF, the area in the image outside the circular field of view is too dark for the system to effectively determine reflectance and identify blood stain. Processing data from this outside area would waste time and memory reserve of the computer. Therefore, it is preferable to exclude this dark area from the ROI as early as in the calibration stage. Normally, the 530 nm image of white paper is very bright all over the field of view. Our experimental record reveals that the pixels whose $W(530nm) < 40$ correspond to the dim area outside the circular field of view of the LCTF. So, we early exclude those pixels from the arrays just after the firstly taken 530 nm spectral image of the white paper is processed. In our system, the number of spatial points in the ROI are usually reduced to 12,000-13,000 after elimination. However, this step is unnecessary in the system whose field of view is just limited by the field of view of the camera itself, not the LCTF. Therefore, after calibration process, Array2 has 63 rows and n columns, where n is the number of spatial points remaining in the ROI. After those two

initial multispectral data arrays are constructed, they are stored in the system in the form of text files for use in the blood detection stage. According to our experimental record, the initial multispectral data arrays are still valid for the blood stain detection even if the lamps and the computers are turned off and turned back on again many times as long as the physical setup is unaltered. So, the users do not have to recalibrate the system even when the computer is turned off and turned back on. The entire calibration process takes between 55 and 68 seconds.

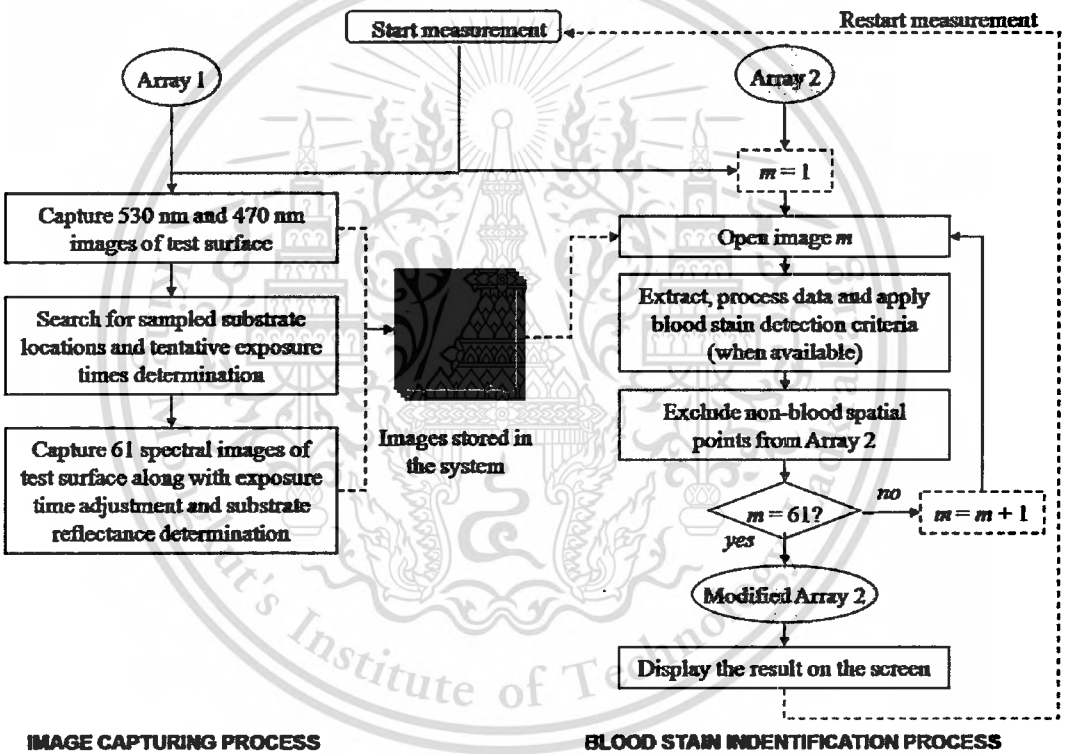

Figure 5.5 Propose Procedure for Rapid Blood Stain Detection.

5.4 Proposed rapid blood stain detection procedure

At the beginning of our blood detection stage, the initial multispectral arrays from calibration stage are quickly extracted from the aforementioned text files to get ready for blood stain detection. Then, the user can place the test surface on the detection zone and start

blood detection right away. The proposed rapid blood stain detection procedure is shown in Figure 5.5.

Because of the need for speed in the blood stain detection, the multispectral image capturing process and the blood stain identification process are run simultaneously in parallel. Immediately after the first image (530 nm) is captured and saved, blood stain identification process starts. Therefore, during blood stain detection, the system has to reserve RAM space for 2 images, one for image capturing process and the other for blood stain identification process.

5.4.1 Image capturing process

Before capturing each spectral image, the system sends the command to the LCTF to tune to a designated wavelength and then wait 200 ms for the LCTF to physically respond and tune to the wavelength before the exposure begins. In fact, the response time for this LCTF model given by the manufacturer is about 50 ms. However, since the response time depends on a number of factors such as ambient temperature, we decide to wait longer (i.e., 200 ms) to ensure that the LCTF gives the desired stable filtering wavelength window. In blood stain detection stage, spectral images of the test surface are not captured and processed in numerical order of wavelengths. Since our system works by gradually eliminating spatial points proved to be not corresponding to blood stain, the image capturing order and criterion order are arranged according to its tentative ability to exclude other stains (its specificity) in order to identify stains of blood as quickly as possible. The first two spectral images to be captured are 530 nm and 470 nm spectral images. These two spectral images are used in preliminary processing, including quick sampled substrate position searching (will be described in section 5) and fast determination of tentative camera's exposure times for the rest of the images (will be described in section 6). The system then captures another 7 spectral images to be tested by preliminary criteria. In this work, preliminary criteria are defined as the criteria that use reflectance or absorbance values as only spectral parameters to distinguish blood from other surfaces. After each spectral image is captured, the system can quickly determine substrate reflectance and save the spectral image in the system before

capturing the next spectral images (also depicted in section 6). The capturing order for preliminary spectral images is 530 nm, 470 nm 546 nm, 518 nm, 502 nm, 710 nm, 586 nm, 642 nm, and 622 nm, respectively. Then, the system captures the remaining spectral images in numerical order of wavelength to be used for polynomial coefficient criteria but skips the already captured spectral images. Performing spectral image capturing and blood stain identification processing in parallel has the advantage of reducing time for blood detection. During the 200 ms waiting for the LCTF to respond and during the exposure of the camera (50 – 125 ms), the computer waits idly for the wavelength tuning and the camera to return the image. At these waiting periods, the measured CPU usage is very low (about 2-3%), providing us an opportunity to efficiently extract, process multispectral data, and apply the blood stain detection criteria for the already captured spectral images.

5.4.2 Blood stain identification process

The blood stain identification processing order is the same as that of image capturing order. To identify blood stain, the system reopens and processes one spectral image at a time. For each opened spectral image, the system extracts digital responses, takes the average value, and processes data, one spatial point at a time, in the ROI. For each spatial point, test surface reflectance value ($R(\lambda)$) is calculated. Note that the reflectance value of both substrate and spatial point on the surface can be recovered by the following expression.

$$R(\lambda) = \frac{1}{w(\lambda)} \cdot \frac{T(\lambda) - D}{\tau_T(\lambda)}, \tag{5.2}$$

where is the digital response on the test surface image and $\tau_T(\lambda)$ is the exposure time of the camera at the corresponding wavelength channel. The value of $T(\lambda)$ is extracted from the calibration array. Eqn.2 is valid only if the incident light on the white reference surface and the substrates is almost identical. This suggests that the would-be in-situ blood stain detection device is possible but must be equipped with built-in light sources and shade covers. Once the reflectance values are determined, the KM absorption at each spatial point on the test surface can be obtained immediately using

$$\frac{R_T(\lambda)}{R_S(\lambda)} = 1 - \frac{K(\lambda)}{S(\lambda)}\left(\sqrt{1+\frac{2K(\lambda)}{S(\lambda)}}+1\right), \tag{5.3}$$

where is the scattering at any spatial point on the surface. Here, for simplicity, we assume Lorentz-Mie scattering as and we take = 450 nm and = 1 for all points on the test surface. Remind that the average substrate reflectance value ( ) has already determined during image capturing process.

5.4.3 Application of blood stain discrimination criteria

Once the reflectance and KM absorption values of the currently processed spectral image are determined, the system immediately applies the assigned blood detection criteria if the criteria are available on the wavelength. For the sake of forensic investigation, the spatial points on the surface remain in the ROI until they are identified as not corresponding to blood stains. As soon as any spatial points are identified by each established criterion that they do not correspond to the blood, those spatial points are not to be processed again in the next spectral images. In many interesting scenes, the areas corresponding to substrate are large compared to those areas corresponding to the area corresponding to blood. As mentioned in chapter 4, it is advantageous to eliminate the substrate locations on the test surface from ROI as early as possible. The 530 nm and 470 nm spectral images are employed to eliminate substrate locations using the selection criteria. $R_T(530nm)/R_S(530nm) \le 0.97$ and $R_T(470nm)/R_S(470nm) \le 0.98$. The spatial points that do not satisfy these conditions usually correspond to the substrate or very thin stains. This results in reduction of spatial points to be processed for the rest of the spectral images, especially in case where the stain area on the image is small relative to the substrate area. After the processing and criteria application on each spectral image are finished, the multispectral data array (Figure 5.4) is modified by removing the columns identified as non-blood from the array and also replacing in the row corresponding to the wavelength channels by . As a result, the size of the blood detection array becomes smaller or at least

remains the same after any image is processed. Another 13 preliminary criteria, such as those exemplified in Figure 4.6 (a)-(c) of chapter 4 are then applied during the processing of the next 7 spectral images. Preliminary criteria are relatively quick to process since they make use of only a few spectral images. After that the system processes the rest of the spectral images. During the time, the system extracts absorption values from spectral images to perform polynomial fitting and applies another 11 criteria to the polynomial coefficient when appropriate. Examples of the criteria based on polynomial fits are shown in Figure 4.6 (d)-(f) of chapter 4. After all 61 spectral images are processed and all 26 criteria are applied, the remaining spatial points in the two-dimensional (2-D) array are the final spatial points identified by the system as possibly corresponding to blood stains. Those spatial points are then masked with 2×2 red pixels on the result screen. After the blood detection process is finished, the user can place another test surface on the detection zone and restart the blood stain detection process. The blood stain detection can indefinitely reuse the multispectral data array obtained during calibration without recalibration. The result images show of spatial points remaining in the ROI on gypsum and artificial wood board test surfaces after the first two wavelengths are processed (Figure 5.6 (a)), and after all the preliminary criteria are applied as shown in Figure 5.6(b). The arrangement of the images based on substrates is similar to the arrangement of the photo images in Figure 5.2 (a)-(e). The arrangement of stains in any single result image is already provided in Figure 5.3. The red diagonal rectangular frame on each image encompasses 6 blood stain spots. The long horizontal stain at the bottom of each image also corresponds to blood. The two result images in Figure 5.6(a) clearly indicate that most substrate areas are eliminated after the first two spectral images are processed. In most cases for all test surfaces, the spatial points are reduced from about 12,000 points at the beginning of blood stain detection stage to about 1,000-2,100 points after just the first 2 images are applied, and are decreased further as more spectral images are processed. This is good in terms of increasing the speed of the system. Normally, these result images are not shown to the user during blood detection on the screen in the real setup to save time for processing.

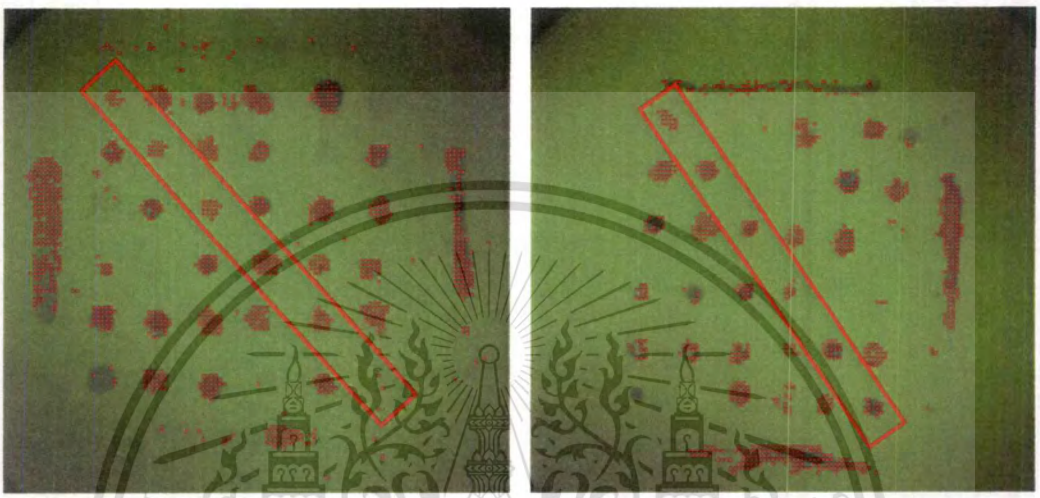

(a)

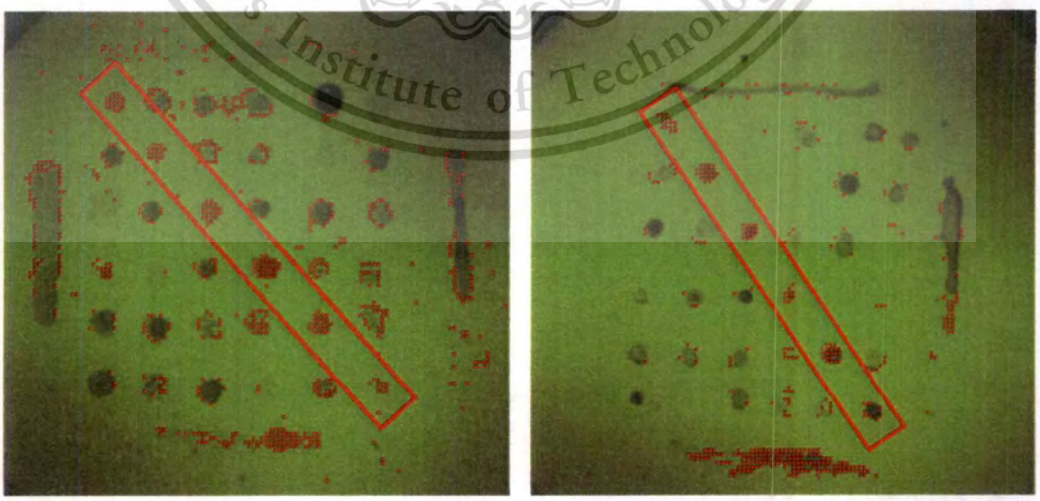

(b)

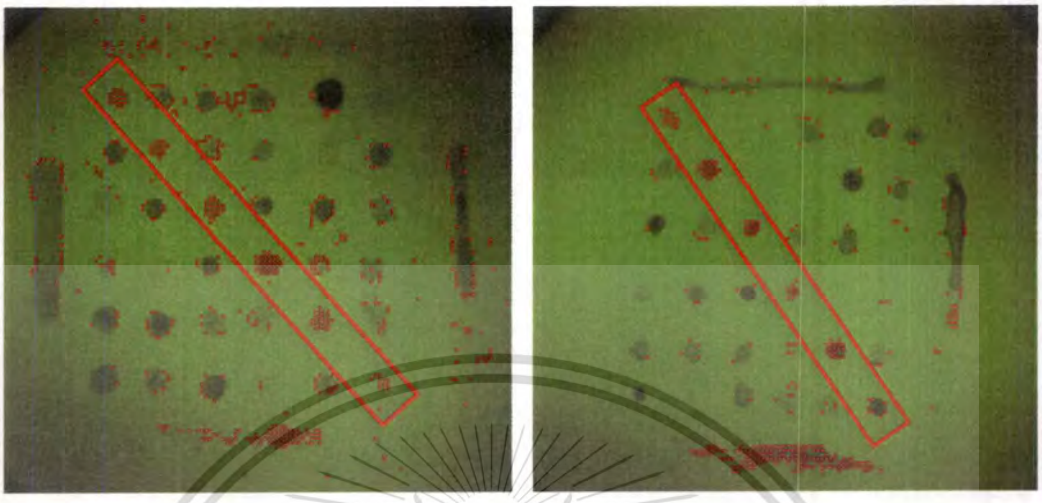

(c)

Figure 5.6 Result images of gypsum (left), and artificial wood (right) test surfaces show spatial points (masked with red) remaining in region of interest (ROI), after (a) first two spectral images, (b) 9 spectral images associated with preliminary criteria, and (c) all spectral images with all criteria are processed. The red diagonal frame on each image highlights the real blood stains spots on the substrate.

In the real system, only the final result images would be shown to the user at the end of the process. Figure 5.6(b) shows the spatial point left in ROI after all 9 preliminary images are processed. Normally, for our stain configuration presented in this experiment, 100-400 spatial points remains in the ROI after preliminary images. The final result images on gypsum and artificial wood test surfaces, corresponding to Figure .6(a) and (b), are shown in Figure 5.6(c). It is evident that final result images are improved just a little from those using just preliminary criteria. However, for the interest of forensic investigation, this little improvement might be of important values.

5.5 Substrate reflectance determination

In our blood stain detection method, the recovery of substrate reflectance spectrum ($R_s(\lambda)$) is a requirement in finding the KM absorption spectra on the test surface (see Eqn.3). The substrate reflectance spectrum could be obtained by having the users capture separate multispectral images of the clean substrate area and then having the system extract the spectrum from those images just before performing blood stain detection, as we did in chapter 4. However, the method would be inconvenient and time consuming. Furthermore, stains may be scattered over the test surface, and in some scenes, the large clean substrate area may be difficult to manually find. Therefore, the best way to obtain $R_s(\lambda)$ is to have the system automatically search for the sampled unstained substrate locations in the images of the test surface, and then determine the reflectance spectrum from those locations by itself during detection. It is also preferred that substrate locations must be determined as early as the first few spectral images are captured and so that the substrate reflectance can be quickly extracted from each following spectral image. To economize the time for substrate reflection search and determination, just every 5 × 5 pixels are uniformly sampled all over the image field of view using Array1. From the calibration stage, Array1 contains the calibration numbers from those sampled pixels. Spatial sampling of the pixels has the advantage of lessening calculation, hence increasing the speed of finding substrate reflectance. In addition, it allows the system to quickly collect the substrate reflectance even if stains are scattered all over the spectral images of the test surface. The search for the substrate positions makes use of the first two captured spectral images (530 nm and 470 nm wavelength) in the blood detection stage. The wavelengths are selected because typical absorption of stains is relatively large at such low wavelengths. Therefore, the difference between the reflectance values of stains and the substrate are usually high and it is easy to distinguish between the stains and substrate locations from these spectral wavelengths. The system determines reflectance values at all sampled pixels from these two spectral images. Recall from section 3 that the dim pixels outside field of view of the circular aperture are eliminated from consideration during calibration. Hence, it is very likely that correct reflectance spectra can be recovered from all sampled pixels in consideration. For each

wavelength, the reflectance values of all sampled pixels are then sorted into 21 class intervals ranging from 0.20 to 1.00, with the class interval size of 0.04. Note that the first class has $0.20 < R(\lambda) \leq 0.24$ while the last one has $0.96 < R(\lambda) \leq 1.00$.

The assumption is made that the substrate area would cover a majority of the area in the image. Even if the stain area is larger than that of the substrate, it is rare that the stain concentrations, hence reflectance values, are equal over the test surface. Presumably, the reflectance values that are most frequently found on the surface belong to the substrate. Accordingly, we take that the class interval that contains the largest number of observations (the modal class) corresponds to the substrate area. This modal class is statistically easy to determine. For more accuracy, the pixels deemed as the substrate locations must have the reflectance values fall within the modal classes in both 530 nm and 470 nm spectral images. Those pixels whose reflectance values fall outside the modal class in both images or fall within the modal class of only one of the two spectral images are excluded from substrate locations by removing the corresponding columns from Array1. After substrate location determination, the modified Array1 then represents the sampled substrate locations in the images. Figure 5.7 shows examples of the resultant substrate locations highlighted in red pixels on gypsum and blue tile. It looks clear that the sampled locations determined by our method correspond to the true locations of the pure substrates. The time for substrate position search using 530 nm and 470 nm spectral images ranges from 31 to 78 ms.

(a)

(b)

Figure 5.7 Determined sampled substrate positions (masked with red) by our substrate position search method on (a) gypsum and (b) artificial wood.

Once the sampled substrate pixels are determined, after each spectral image is captured, the system can quickly determine the average calibration number and the average digital response ($T_{AVG}(\lambda)$) from those pixels in the modified Array1. The average substrate reflectance values $R_S(\lambda)$ at any spectral image can then be readily determined using Eqn.2. Figure 5.8 shows comparison between reflectance spectra of substrates determined by our method and by manual extraction from a large clean substrate area. The result of substrate reflectance recovery is however sufficiently accurate, with accuracy of > 95%. The substrate reflectance determination takes as quickly as 4-22 ms for each spectra image. Also, the average digital responses ($T_{AVG}(\lambda)$) are used to adjust exposure times of the later captured image to obtain appropriate image brightness. The process of exposure time adjustment will be explained in the next section.

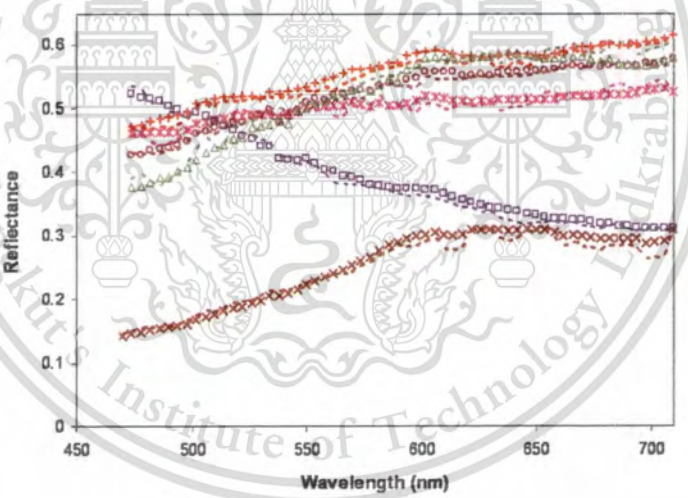

Figure 5.8 Comparison between our substrate reflectance spectra determined by our substrate searching method (dotted lines), and by spectral recovery from the clean substrate area (different markers).

Recovery of substrate reflectance spectrum ($R_s(\lambda)$) is required in the application of the KM theory to find the absorption spectra of the stains. During blood detection, the substrate spectrum could be obtained by having the user capture separate spectral images of the clean substrate area, before performing blood stain detection on the same substrate. However, the method is inconvenient and time consuming, since the users must find the clean substrate area by themselves. Furthermore, stains may be scattered over the image and the large clean substrate area may be difficult to find manually in some scenes. The best way to obtain $R_s(\lambda)$ is to have the system automatically seach for the substrate locations and then extract the reflectance spectrum from unstained substrate locations in the images of test surface by itself during the blood stain detection period.

5.6 Rapid exposure time adjustment

Although the white reference calibration and spectral reconstruction method can automatically correct for the spatial non-uniformity of illumination incident on the image surface, the raw camera's digital responses for all spectral images must lie within linear response range of the CCD pixel array for ease of analysis. Either saturated or too dark pixels would lead to incorrect blood detection. From our experimental observation, the acceptable linear response zone of our 8-bit camera ranges from 30 to 230. Moreover, to accomplish high signal to noise ratio (SNR), the digital responses not only must be kept within the linear zone but should also be kept as high as possible within the linear response zone. Small digital responses are more subjected to low signal to quantization noise ratio [76]. Figure 5.9 (a) shows the calculated normalized camera digital responses while capturing spectral images of the white reference paper and all other 6 substrates if spectral images were captured at constant exposure time for all wavelength channels.

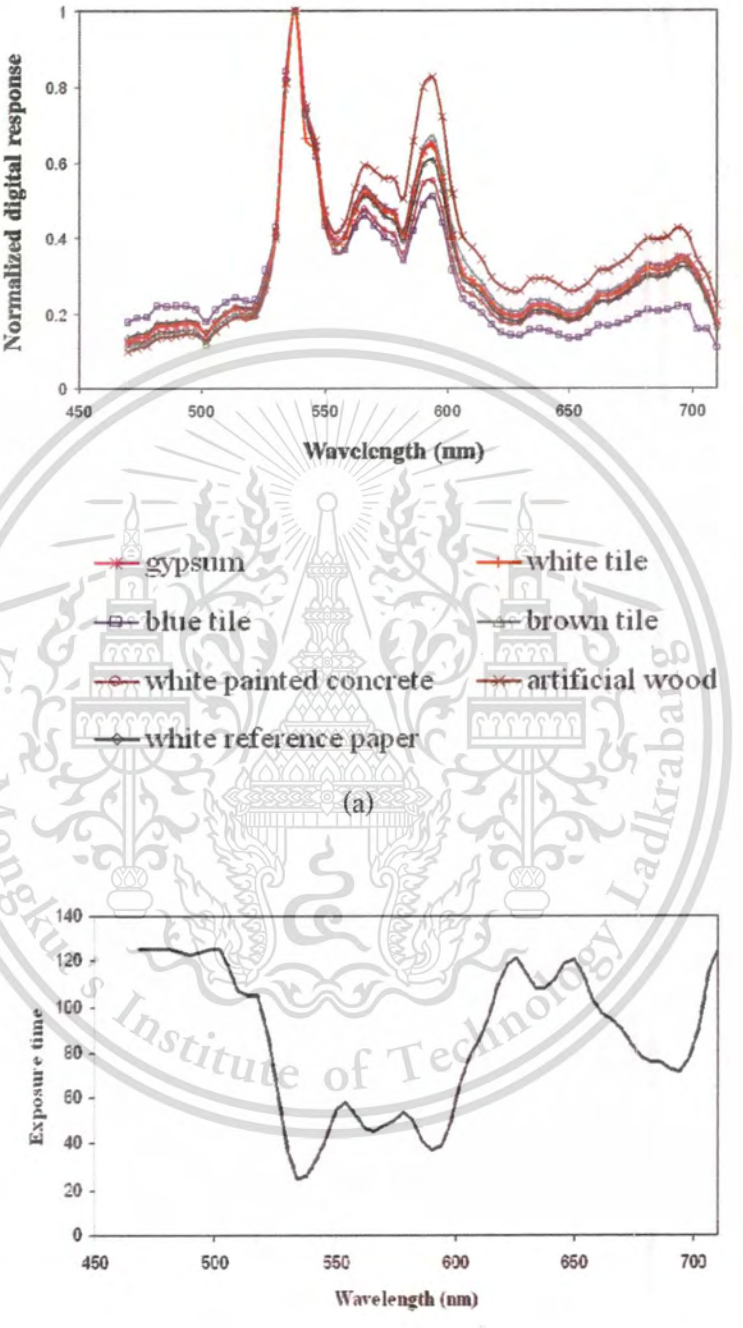

Figure 5.9 (a) Normalized digital responses when spectral images of the white paper and other 6 substrates are captured. (b) The exposure time base used for luminance adaptation in this system.

The spectral shapes of the camera's digital responses are not uniform, but spiky due to the non-uniform spectral shape of the combined multispectral imaging instruments, especially the metal halide lamps. As a result, it is almost impossible to keep digital responses of all spectral images within the linear response zone if all spectral images are captured with constant exposure time. Our system's camera can controllably capture images at different exposure times. In establishment of the criteria in chapter 4, for each scene, we captured several sets of multispectral images, each with a certain exposure time. Then, we manually selected the images whose exposure time yielded suitable brightness. The method was, however, very time consuming. In this part of our work, we intend to build the detection system that can automatically adapt its image capturing to any kind of surfaces by dynamically varying exposure times with wavelength channels. According to Figure 5.9(a), the spectral shapes of the digital responses are not much different among different surfaces. This suggests that the spectral shape is dominated by the spectral shape of the combined imaging instruments. Our key idea is to establish exposure time basis function, in which the relative exposure times are inversely proportional to the normalized digital responses of the images in order to counteract the non-uniform spectral response of the imaging instruments. Since the images of the white paper reference surface and the images of the test surfaces are different by nature, we consider the exposure time adjustment in the two stages separately in the two following subsections.

5.6.1 Exposure time adjustment during calibration

Since the white paper surface is spatially uniform and its reflectance spectrum is constant, the digital responses of the spectral images of the white paper are more predictable than those of the test surfaces. To achieve high SNR, we prefer that the average digital responses in the field of view for all spectral images should be roughly 180. At this average level, the brightest areas in the field of view tend not to be saturated while dimmest areas still have high enough digital responses. With the relative spectral responses of the spectral images of the white paper shown in Figure 5.9(a), and a little modification of Eqn.1, the exposure time basis for capturing spectral images of white paper $\tau_B(\lambda_k)$ shown in Figure 5.9 (b) are derived from $\tau_B(\lambda_k) = (180 - D)\tau_W(\lambda_k)/(W_{AVG}(\lambda_k) - D)$, where $W_{AVG}(\lambda_k)$

is the average digital responses from the sampled pixels of the captured white paper images, when the images are captured with corresponding exposure times of $\tau_W(\lambda_k)$. The acquired exposure time basis is kept in the permanent memory of the system. It is valid for a relatively long time since the spectral shape of the combined instruments change very slowly through the aging of the instruments.

During the calibration, the system capture the 530 nm spectral image first, extracts digital responses of pixels from Array1, and take the average into a single value $W_{AVG}(\lambda_k)$. The exposure times that will give the average digital response around 180, $\tau_{W180}(\lambda_k)$, for all wavelength channels can be readily determined by

$$\tau_{W180}(\lambda_k) = c_W \cdot \tau_B(\lambda_k). \tag{5.4}$$

Here, c_W is given by $c_W = (180 - D)/(W_{AVG}(530nm) - D)$.

5.6.2 Exposure time adjustment during blood stain detection

Adjustment of the exposure time during blood stain detection is more complicated due to several reasons. Firstly, the test surface is not spatially uniform, but may contain pale and dark spots that possibly correspond to blood stains. It is important to keep the digital responses on all of these spots high enough to achieve adequate SNR. Due to high absorption of blood stain, it is likely that the blood stain spots are dimmer than the substrate area. Our key idea is to keep the average digital responses at substrate locations at 180 at all wavelengths. At this average digital responses values, the dimmer stain spots still have the digital responses within the linear range of the camera. It is also unharmed to let the spots brighter than the substrate saturated since those brighter spots do not, anyways, correspond to blood stains. After the sampled substrate locations are determined using 530 nm and 470 nm spectral images (see section 5), we take the average digital response from the sampled substrate locations of the 530 nm spectral image $T_{AVG}(530nm)$. As mentioned earlier, the spectral shapes of digital responses are dominated by the spectral shape of the responses of the combined multispectral imaging instruments. Looking closely into Figure 5.9 (a), we find that the normalized responses of the white reference paper are approximately the

average normalized digital values of all substrates. So, we also use the same exposure time basis $\tau_B(\lambda_k)$ for all test surfaces. The exposure times which give average digital value of 180 ($\tau_{T180}(\lambda_k)$) for the rest of the spectral images can be determined the same way as during calibration.

$$\tau_{T180}(\lambda_k) = c_T \cdot \tau_B(\lambda_k), \tag{5.5}$$

where $c_T = (180 - D)/(T_{AVG}(530nm) - D)$.

The second issue is that the substrates to be detected can be of any types or colors, so their reflectance spectra are unpredictable. Unmonitored image capturing with the above exposure times can cause the image digital responses to fall out of the desired linear responses zone of the camera at any time. To alleviate the problems, we recheck the digital responses during capturing the spectral images of the test surface. During capturing of the preliminary spectral images, wavelength channels are far apart. This indicates that the relationship in reflectance values among these images is unknown. The images may fall out of linear range any time. So, we dynamically keep monitoring the average digital response of the images by measuring the average digital values on the substrate locations in all spectral images and allowing only the values within the acceptable range (i.e., $150 < T_{AVG}(\lambda_k) < 210$). If the average digital value of any spectral image falls out of this desired range, the stage has to recapture the spectral image with the new exposure time of $\tau_{NEWT180}(\lambda_k) = [180 / T_{AVG}(\lambda_k)]\tau_{T180}(\lambda_k)$, except that the image is already captured at the maximum exposure time of the camera (125 ms). After finish capturing all the preliminary spectral images, the remaining spectral images are captured in numerical order of wavelengths. Since the reflectance curves of most construction materials are usually slowly varying, the reflectance values at the adjacent wavelength channels do not vary much. In addition, recapturing the spectral images take longer times than dynamically determining the right exposure times during capturing. Hence, we adjust the exposure time based on the previously captured wavelength during spectral image capturing as

$$\tau_{T180}(\lambda_k) = \left[\frac{180}{T_{AVG}(\lambda_{k-1})} \cdot \frac{\tau_B(\lambda_k)}{\tau_B(\lambda_{k-1})}\right] \cdot \tau_B(\lambda_k), \tag{5.6}$$

where subscript (*k-1*) signifies the previous wavelength which is 4 nm less than the present capturing wavelength. With the above mentioned capturing method, we obtain smooth determination of blood stain detection. Since averaging the digital responses of the captured image ($T_{AVG}(\lambda_{k-1})$) is a prerequisite for the determination of substrate reflectance as described in section 5, Eqn.6 takes just a little extra calculation to determine the exposure time of the subsequent image $\tau_{T180}(\lambda_k)$.

5.7 Experimental results and discussions

The final result images for blood identification on 6 different substrates shown in Figure 5.10. Different trials of the result images on gypsum and artificial wood board test surfaces (Figure 5.10 (a) and (b)) are also shown for comparison with Figure 5.6. As mentioned in chapter 4, we evaluate the performance of our blood stain detection system by its true positive rate (TPR) or sensitivity, true negative rate (TNR) or specificity, and speed. TPR and TNR have already been evaluated then and are not quantitatively evaluated here again. Qualitatively, from visual evaluation, the results show comparable TPR and TNR to the results described in part 1 of this work. It is plainly seen from Figure 5.10 that the proposed detection system can be efficiently used to distinguish blood from all 6 stains on different substrates, though false positives are usually seen at the edges of the stains. This is because the criteria are designed to select all the undetermined spatial points in the ROI and deselect the areas sure as not blood stains. Criteria may not be made specific enough to exclude the areas at the edge of other stains where spectral mixing between stains and substrates occurs. This can be improved by adjusting the criteria to eliminate more of those areas but may sacrifice the specificity of the system. False positives on substrate areas are most noticed in brown tile substrate due to spatial non-uniformity of the substrate's spatial profile.

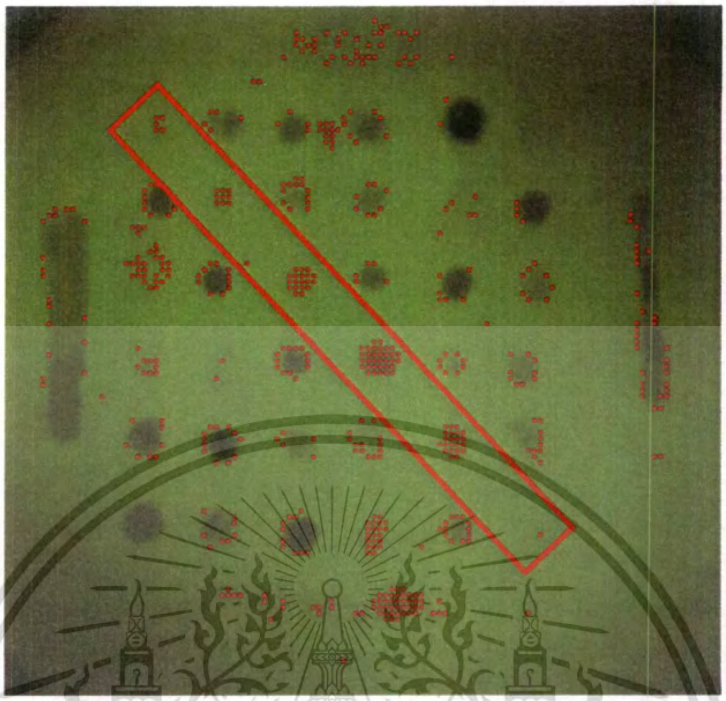

(a)

(b)

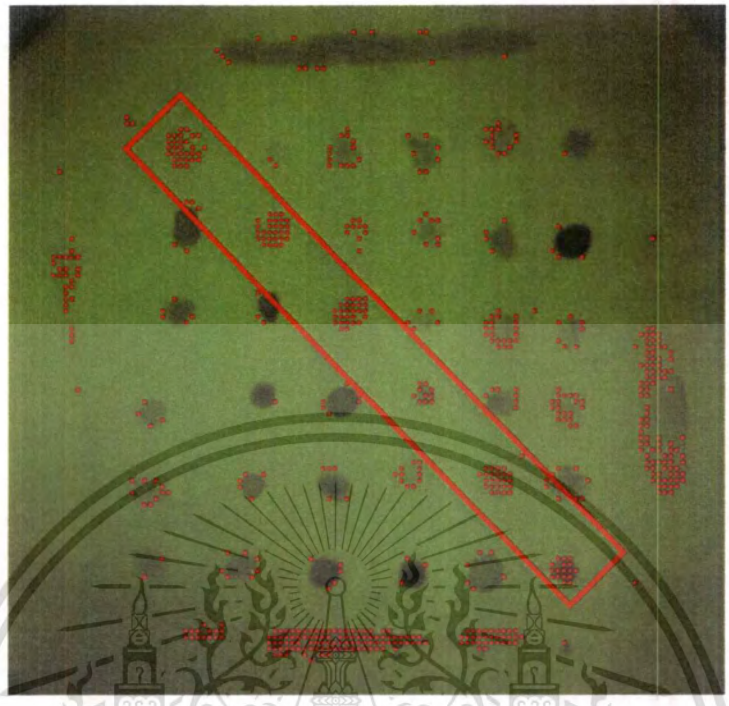

(c)

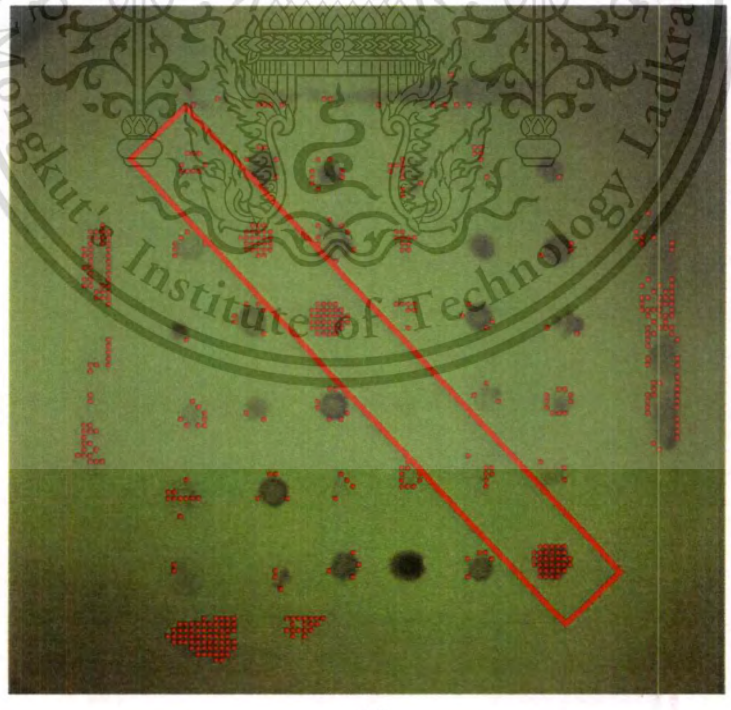

(d)

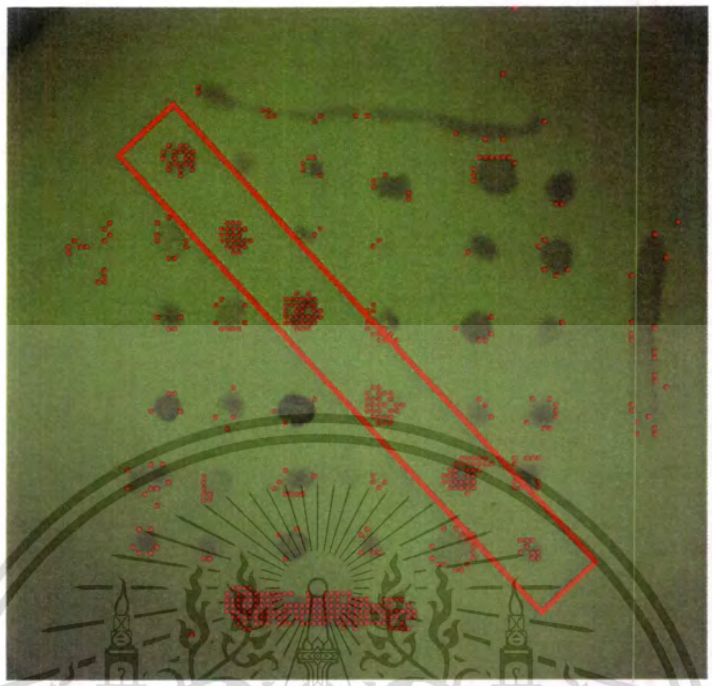

(e)

(f)

Figure 5.10 Final result images of blood identification on (a) gypsum, (b) brown artificial wood, (c) white painted concrete, (d) white tile, (e) blue tile, and (f) rough brown tile.

In this section, we focus on evaluating the speed of our proposed rapid blood stain detection system. The times taken for any task steps can be easily measured by using the LabVIEW program. The average total image capturing times and total blood stain identification times for all six test surfaces are shown in Table 5.1. As mentioned earlier, our parallel procedures between spectral image capturing and data processing processes allow the two processes to run simultaneously. The spectral image capturing time for each test surface, shown on the right side of Table 1, ranges between 22.4 and 26.3 seconds, while the entire identification times (on the left side) range between 23.3 and 28.7 seconds. The times taken for capturing all 64 spectral images are just about 1-2 seconds shorter than the times for the entire identification process.

Test Surface	Average Image Capturing Time (seconds)	Average Total Detection Time (seconds)
Gypsum	23.6	25.7
Artificial wood	26.9	27.6
White painted concrete	22.4	23.3
White tile	24.0	25.2
Blue tile	22.8	23.4
Brown tile	26.3	28.7

Table 5.1 The average times taken to capture all 61 spectral images and to identify the blood stain.

The total image capturing time depends on brightness of the test surfaces. The brighter test surfaces results in lower capturing time, hence identification times, than the dark images since the exposure times are lower. The white painted concrete and the blue tile surfaces have the fastest image capturing times, since they are among the brightest surface. In addition to the image capturing time, the total blood stain identification time also depends on

the stain profiles. Basically, the larger the stain area on the image, the more time needed to process the images. However, the key to rapid detection is to eliminate the spatial points identified as non-blood as early as possible. Table 5.2 shows the measured time ranges taken to process some specific images and data processing steps. The time taken for data processing of the first two images (530nm and 470nm) alone ranges from 1,300 to 2,500 ms (the average of 650-1,250 ms per spectral image). Recall that these two images are processed together in search for substrate location, extracting digital responses, applying criteria and array manipulation.

Image or Process	Measured Processing Time (ms)
First 2 images (530 nm and 470 nm)	1300-1500
3rd image (470 nm)	123-166
9th image (622 nm)	23 – 55
61st image (706 nm)	20-55
Application of polynomial fitting	32-74

Table 5.2 The range of time taken for processing some spectral images or some data processing tasks.

This relatively long processing time results from a large number of spatial points in ROI. The time taken for data processing of the third images (470 nm spectral image), however, is reduced significantly to 123 - 166 ms since the spatial points to be processed reduces from about 12,000 down to 1,000-2100 in the second images and the substrate searching has already been done. Thank to our planed ordering of criteria, discussed in section 4.3, a number of spatial points can be eliminated as early spectral images are processed, and the processing times decrease as further images are processed. The processing time for the ninth image (622 nm spectral image), which is the last preliminary images, drops to 23-55 ms. Remind that all the blood stain identifications are taken while the all stains are covered in the

images according to configuration in Figure 5.3. So, all stains spots are included in the images. For the images with less stain spots, spatial points in ROI are even less and the identification should be even faster. In later spectral images, the processing time is slightly shorter. And there are another 11 blood discrimination criteria that make use of polynomial fits applied after specific images are processed. Application of each polynomial fitting criterion takes additional 32-74 ms. Despite a relatively long process of polynomial fitting criteria, they can eliminate only a small additional number of spatial points in ROI. Most of the polynomial fitting criterion efforts are redundant to the previous criteria. Optimistically, this may be beneficial in that we can improve in the future by having more preliminary criteria and removing polynomial fitting criteria.

Though varied due to the exposure time adjustment, image capturing times are relatively constant compared to data processing. They are not getting faster as more images are processed. The capturing time for a single image ranges from 300-400 ms depending on wavelengths and test surface's brightness. At early stage of blood stain identification process, data processing takes longer than image capturing since there are a lot of spatial points in ROI. Data processing very much lags behind the image capturing. However, as more and more spatial points are excluded from consideration, blood identification process is performed faster. Yet, blood stain detection criteria must await the capturing of the needed spectral images. The speed of the system is limited mostly by the image capturing time.

Chapter 6

Conclusions

6.1 Summary

In this thesis, we have developed the multispectral imaging system for detection of blood stains for forensic investigation. Through many development steps, we can invent the methods of detection of blood stains that is less independent of substrate, types, color and textures. We have performed literature review of exist methods and found that no existing methods have been able to distinguish blood independently of substrates. The following steps, we experimentally collected the reflectance spectra of several stains on different substrates and found that the reflectance spectra of over the stains are to a large degree dependent on the spectra of the substrates due mainly to spectral mixing. In the first part of the experiment, which is described in chapter 4, we have developed a multispectral imaging-based forensic blood stain detection method on construction material surfaces and established blood discrimination criteria. According to the method, multispectral image cubes are transformed into arrays, and then the reflectance spectra at each point in the captured spectral images are transformed into the less independent KM absorbance spectra using KM theory. From those spectra of the collected samples, we instinctively find several spectral parameters that can be used to separate blood from other stains. Blood stain identification is done mathematically via Boolean logics. Up to 26 blood selection criteria have been established. The criteria are proved to be able to distinguish blood stains from other reddish brown stain with high sensitivity ($0.60<TPR<0.95$) depending on blood stain concentration and substrate type as well as high specificity ($0.55<TNR<0.96$). In the second part of the experiment, which is illustrated in chapter 5, we have demonstrated a rapid multispectral-imaging based blood stain detection system, based upon our blood stain detection criteria established in chapter 4. Necessary tasks are sequentially and programmatically performed by the system in order to achieve the fastest and most reliable detection and make the user convenient. All calibration data, obtained from the captured spectral images are stored and readily processed

in the form of arrays. Substrate reflectance is determined by our substrate searching and determination method. The well-planned image capturing order and the blood detection criteria application order are intended for the fastest elimination of unnecessary data. Parallel procedures between image capturing and blood stain detection process allow for fast detection. The exposure time monitoring and adaptation keep all spectral images to have suitable brightness for detection. The system can automatically detect blood against several other stains on several substrates. The speed of the system has also been evaluated. Our proposed system takes averagely 23.3-28.7 seconds to detect blood stain depending on the test surfaces. The time results suggest that the detection process is limited by the image capturing time, not the time for the blood stain detection process. All the framework and methods developed in this thesis will hopefully pave the way for the unprecedented portable substrate-independent multispectral image based blood stain detection device in the near future. Using of multispectral imaging for blood detection method has the advantage over using of spectrophotometer large area can be inspected at once instead of measuring it point by point. So, the investigators do not have to guess on the point where blood stains are located. This can save considerable amount of time for the investigators. Our system also has the advantage that it is to a large extent substrate independent, so the system can be used to detect blood on a wide range of substrates. The system adjusts image capturing by itself to prevent false determination.

6.2 Future work

Although this thesis has not yet solved the problem of Kunying Pornthip Rojanasunand's team, the future realization of in-situ device is promising. Our research focus in the near future is still on improvement of criteria, extending the spectral range to the entire visible spectrum and into near infrared region as well as reducing spectral channel sampling frequency. Alternatively, this method may be combined with other existing methods to obliterate the limitations from each method in order to make a very efficient device. The Future work will also be focused on using permanent filters or different light source for multispectral scan instead of an expensive LCTF device, and building in-situ devices. With

further improvement this method can even also potentially be extended to identify other substances or stains on any substrates, which is not limited to forensic science.

References

1. A. C. Ponce, and A. C. Pascual, Forensic Sci. Comm. 1 (1991) 1-15.
2. M. Cox, J. Forensic Sci. 36 (1991) 1503–1511.
3. A. M. Gross, K. A. Harris, and G. L. Kaldun, J. Forensic Sci. 44 (1999) 837–840.
4. F. Carlysle, Glasglow Insight into Sci. and Tech. (2011) [online] available: http://the-gist.org/2011/03/seeing-red-%E2%80%93-presumptive-tests-for-blood/
5. N. Vandenberg, and R. A. van Oorschot, J. Forensic Sci. 51 (2006) 361-370.
6. W. C. Lee, and B. E. Khoo, Malaysian J. Forensic Sci. 1 (2010) 17-28.
7. A. C. Lin, H. M. Hsieh, L. C. Tsai, A. Linacre, and J. C. Lee, J. Forensic Sci. 52 (2007) 1148-1150.
8. M. Perkins, J. Forensic Id. 55 (2005) 1-9.
9. H. Brooke, M. R. Baranowski, J. N. McCutcheon, S. L. Morgan, and M. L. Myrick, Anal. Chem. 82 (2010) 8412-8420.
10. H. Brooke, M. R. Baranowski, J. N. McCutcheon, S. L. Morgan, and M. L. Myrick, Anal. Chem. 82 (2010) 8421-8426.
11. H. Brooke, M. R. Baranowski, J. N. McCutcheon, S. L. Morgan, and M. L. Myrick, Anal. Chem. 82 (2010) 8427-8431.
12. T. Haraguchi, T. Shimi, T. Koujin, N. Hashiguchi, and Y. Hiraoka, Genes Cells 7 (2002) 881–887.
13. Y. Hiraoka, T. Shimi and T. Haraguchi, Cell Struct. Funct. 27 (2002) 367-374.
14. L. Fauch, E. Nippolainen, V. Teplov, and A. A. "Kamshilin, Opt. Exp. 18 (2010). 23394-23405.
15. P. Latorre-Carmona, E. Sánchez-Ortiga, X. Xiao, F. Pla, M. Martínez-Corral, H. Navarro, G. Saavedra, and B. Javidi, Opt. Exp. 20 (2012) 25960-25969.
16. J. Y. Hardeberg, F. Schmitt, and H. Brettel, Proc. SPIE 3963 (2000) 77-88.
17. L. J. Cheng, T. H. Chao, M. Dowdy, C. LaBaw, C. Mahoney, G. Reyes, and K. Bergman, Proc. SPIE 1874 (1993) 224-231

18. L. J. Cheng, T. H. Chao, and G. Reyes. AIAA Space Programs and Technologies Conf. (1992) paper no. 92-1439.

19. J. Brauers, N. Schulte, and T. Aach, IEEE Transact. Image Process. 17 (2008) 2368-2380.

20. J. Park, M. Lee, M. D. Grossberg, and S. K. Nayar, Proc. IEEE ICCV (2007) 1-8.

21. E. John, D. Lau, and S. Leung, unpublished, (2008) [online] available http://scien.stanford.edu/pages/labsite/2008/psych221/projects/08/DavidLau/Psych_221_Report.pdf

22. C. Chi, H. Yoo, and M. Ben-Ezra, Int. J. Comput. Vis. 86 (2010) 140–151.

23. J. Spigulis, D. Jakovels, and U. Rubins, Proc. SPIE 7557 (2010) 75570M-1-9

24. F. Vagni, RTO Technical Report, NATO, (2007) TR-SET-065-P3

25. H. L. Shen, P. Q. Cai, S. J. Shao, and J. H. Xin, Opt. Exp. 15 (2007) 15545-15554.

26. G. Sharma and H. J. Trussell, IEEE Trans. Image Process. 6 (1997) 990–1001.

27. Y. Zhao, and R. S. Berns. Color Res. and Appli. 32 (2007) 343-351.

28. C. van Trigt, J. Opt. Soc. Am. A 7 (1990) 2208-2222.

29. R. Jolivot, P. Vabres, and F. Marzani, Compu Med. Imag. Grap. 25 (2011) 85-88.

30. A. Mansouri, F. S. Marzani, and P. Gouton, Proc. IEEE ICIP (2005) 718-721.

31. N. Keshava, and J. F. Mustard, IEEE Signal Process. Mag. 19 (2002) 44–57.

32. N. Shimano, IEEE Trans. Image Process. 15 (2006) 1848-1856.

33. A. Ribes, and F. Schmitt, Pattern Recogn. Lett. 24 (2003) 1691-1701.

34. P. A. Mayes, D. Dicker, Y. Liu, and W. S. El-Deiry, Bio. Tech. 45 (2008) 459-464.

35. I. Kuzmina, I. Diebele, L. Asare, A. Kempele, A. Abelite, D. Jakovels, and J. Spigulis Proc. SPIE 7376 (2010); 73760J-1-6

36. C. L. Jones, N. O. Maness, M. L. Stone, and R. Jayasekara, Proc. ASAE 043081 (2004) 043081-1-12.

37. C. Payes, J. A. Rodriguez, S. Friend, and G. Helguera Open Access Medical Text Book: Cell Interaction (2012) [online] available http://medicaltextboks.blogspot.com/2013/02/textbook-cell-interaction.html

38. J. C. Noordam, W. van den Broek, and L. Buydens. J. Sci. Food Agri. 85 (2005) 2249-2259

39. S. Sumriddetchkajorn, K. Suwansukho, and P. Buranasiri, Proc. SPIE 7715, (2010) 771501

40. K. Suwansukho, S. Sumriddetchkajorn and P. Buranasiri, Appl Opt. 50 (2011) 4024-4030.

41. Y. Intaravanne, S. Sumriddetchkajorn, and J. Nukeaw, Sensors Acuta. B 168 (2012) 390-394.

42. B. Park, K. C. Lawrence, W. R. Smith, and D. P. Smith, J. Food Process. Eng. 27 (2004) 311-327

43. D. Landgrebe, Photogramm. Eng. Rem. S. 7 (1997) 859–867.

44. G. P. Asner, and K. B. Heidebrecht, Int. J. Remote Sens. 23 (2002) 3939-3958.

45. G.Andreoli, B.Bulgarelli, B.Hosgood, D.Tarchi, Joint Research Center, EU (2007) [online] available http://publications.jrc.ec.europa.eu/repository/bitstream/111111111/5106/1/6875%20-%20EUR%2022739%20-%20hyperspectral_23-05-2007_rev2.pdf

46. J.B. Dalton, R. R. McDougal, and C.A. Gent, J. Geophys. Res. 108 (2003) 1-44

47. Y. Huang, S. J. Thomson, Y. Lan, and S. J. Maas, Int. J. Agric. Biol. Eng. 3 (2010) 50-62.

48. J. H. Wagner, Ph.D. Dissertation, U. Auckland (2008).

49. G. M. Miskelly and J. H. Wagner, Forensic Sci Int. 155 (2005) 112–118.

50. ChemImage product sheet PSREV005 (2010) [online] available http://www.chemimage.com/docs/product.../CI-productsheet-CONDOR.pdf,

51. Application note, ANREV002 (2010) [online] available https://www.chemimage.com/docs/application-notes/forensics/CI-appnote-Visualization-of-Bloodstains.pdf,

52. Forensic Focus E-Newsletter 11, (2010) [online] available http://www.chemimage.com/news/newsletter/forensic_focus/november2010.aspx, Forensic Focus E-Newsletter 11, (2010).

53. ChemImage product sheet PSREV001 (2012) [available online] http://www.chemimage.com/products/instrumentation/examiner/

54. R. H. Bremmer, A. Nadort, T. G. van Leeuwen, M. J. van Gemert, and M. C. Aalders, Forensic Sci. Int. 206 (2011) 166–171.

55. T. Asakura, K. Minakata, K. Adachi, M. O. Russell, and E. Schwartz, J. Clin. Invest. 59 (1977) 633–640.

56. W. G. Zijlstra, A. Buursma, and W. P. Meeuwsen-Vanderroest, Clin. Chem. 37 (1991) 1633–1638.

57. P. Kubelka, J. Opt. Soc. Am. 38 (1948) 448-457.

58. M. J. C. van Gemert, S. L. Jacques, H. J. C. M. Sterenborg, and W. M. Star, IEEE Trans. Biomed. Eng. 36 (1989) 1146-1154.

59. M. J. C. van Gemert, and W. M. Star, Lasers Life Sci. 1 (1987) 287-298.

60. F. W. Billmeyer and R. L. Abrams , J. Paint Tech. 45 (1973) 23-30.

61. R. S. Berns, and M. Mohammadi, Color Res. Appl. 32 (2006) 201-207.

62. L. N. M. Duysens, Biochim. Biophys. Acta. 19 (1956) 1–12.

63. J. C. Finlay, and T. H. Foster, Opt. Lett. 29 (2004) 965–967.

64. N. Rajaram, A. Gopal, X. Zhang, and J. W. Tunnell, Laser Surg. Med. 42 (2010) 680-688.

65. W. Hergert, and T. Wriedt, The Mie Theory Basic and Applications, Springer (2012)

66. Philips' compact HID lamp and gear manual (2009) [online] available http://www.manualslib.com/download/126732/Philips-Compact-Hid-Lamp-And-Gear.html

67. R. W. Slawson, Z. Ninkov, and E. P. Horch, Astron. Soc. Pac. 759 (1999) 621-626

68. User's manual for Varispec (2010) [online] available http://www.perkinelmer.com/CMSResources/Images/44140159MAN_LST_Q112_VarispecUserManual1107-9252.pdf

69. User's manual for GigE Vision Cameras (2007) [online] available http://www.bnl.gov/atf/systems/diagnostics/scout-g_users_manual.pdf

70. E. Pirard, Mineral Mag. 68 (2004) 323-333

71. R. Shogenji, Y. Kitamura, K. Yamada, S. Miyatake, and J. Tanida, Opt. Exp. 12 (2004) 1643-1655.

72. J. M. Medina, L. M. Pereira, H. T. Correia, and S. Nascimento, J Biomed Opt. 16, (2011) 076001-076001-12.

73. H. T. Sencar, and N. D. Memon, Digital Image Forensic, New York, Springer Science & Business Media (2013).

74. W.G. Zijlstra, and A. Buursma, Comp. Biochem. Physiol. B 118 (1997) 743-749.

75. http://en.wikipedia.org/wiki/Sensitivity_and_specificity, March 2012.

76. P. R. Perez-Alcazar, and A. Santos, Proc. IEEE ICDSP 2 (2002) 807-810.

Appendices

A. The list of blood stain discrimination criteria used in this thesis.

No.	Parameter	Criterion
1.	$x = R_T(530nm)/R_S(530nm)$	$x \leq 0.97$
2.	$x = R_T(470nm)/R_S(470nm)$	$x \leq 0.98$
3.	x = K(530nm), y = K(470nm)	If $x \leq 1.5$ then $y < 6$, if $1.5 < x \leq 29$ then $y < 1.87x + 8.2$, if $29 < x \leq 80$ then $y < 1.1x + 31.6$, if $x > 35$, then $y < 1..07x + 13.8$
4.	x = K(530nm), y = K(546nm)-K(530nm)	$y > 0.19x - 0.32$
5.	x = K(518nm), y = K(546nm)	If $x \leq 1.1$ then true, if $x > 1.1$ then $y < 1.4x - 1.2$, and if $1.1 < x \leq 20$, then $y > 0.68x - 0.7$, if $20 < x \leq 30$, then $y > 0.90x - 5.2$ if $x > 30$, then $y > 1.9x - 38.0$
6.	x = K(470nm), y = K(502nm)	If $x \leq 16$ then $y > 2.3x - 3.3$, if $x > 16$, then $y > 1.76x - 3.8$
7.	x = K(546nm), y = K(502nm)	$y < 1.34x + 1.6$
8.	x = K(710nm)	$x < 1$
9.	x = K(546nm), y = K(586nm)	if $x < 36$ then $y < 0.18x + 1$, and if $36 < x \leq 280$, then $y < 0.042x + 5.9$, if x>280, then $y < 0.071x - 1.9$
10.	x = K(546nm)-K(586nm), y = K(530nm)- K(546nm)	If $x \leq 3$ then $y > -1.4$, if $x > 3$, then $y > -0.29x - 0.5$

No.	Parameter	Criterion
11.	x = K(622nm), y = K(642nm)	If $x \le 1$ then $y < .0.20x + 0.5$, and if $1 < x \le 11.5$ then $y < 0.51x + 0.2$, if $x > 11.5$, then $y < 0.27x + 2.9$
12.	x = K(622nm), y = K(710nm)	If $x \le 0.6$ then $y > 2..2x - 0.39$, if $x > 0.6$, then $y > 10.5x - 6.9$
13.	x = K(622nm), y = K(586nm)	$y > 1.4x - 0.68$
14.	x = K(586nm)- K(622nm), y = K(546nm)-K(586nm)	If $x \le 10$ then all true, if $x > 10$, then $y > 0.99x - 3.2$
15.	x = K(530nm)- K(518nm), y = K(530nm)-K(586nm)	If $x \le 5$, then $y > -0.3$, if $x > 5$, then $y > 1.4x - 6.2$
16.	x = K(482nm) y = 1st order polynomial coeff. of K(470nm) – K(502nm), centered at 482nm	If $x \le 40$ then $y < 1.75x + 12$, if $x > 40$, then $y < 24x - 370$
17.	x = K(482nm) y = 2nd order polynomial coeff. of K(470nm) – K(502nm), centered at 482nm	$y > 655x - 2650$
18.	x = K(514nm) y = 1st order polynomial coeff. of K(482nm) – K(534nm), centered at 514nm	If $x \le 16$ then $y < -13.8x - 30$, if $1 < x \le 10.5$ then $y < -8.4x + 51$, if $x > 10.5$, then $y < -89x + 1080$,
19.	x = K(546nm) y = 2nd order polynomial coeff. of K(498nm) – K(574nm), centered at 546nm	If $x \le 120$, then $y < -3.2x + 540$, if $x > 10.4$, then $y < -75x + 9000$,

No.	Parameter	Criterion
20.	x = K(546nm) y = 3rd order polynomial coeff. of K(498nm) – K(574nm), centered at 546nm	If $x \leq 16$, then all true, if $x > 16$, then $y < -244x + 23{,}900$, and $y < -540x + 11{,}300$
21.	x = K(554nm) y = 2nd order polynomial coeff. of K(526nm) – K(582nm), centered at 554 nm	If $x \leq 20$, then $y < 80$, if $x > 20$, then $y < -32x + 590$
22.	x = K(554nm) y = 2nd order polynomial coeff. of K(526nm) – K(582nm), centered at 554 nm	If $x \leq 42$, then $y < 80$, if $x > 42$, then $y < -6.5x + 270$
23.	x = K(518nm) y = 2nd order polynomial coeff. of K(514nm) – K(598nm), centered at 546nm	If $x \leq 1$ then $y < 50$, if $1 < x \leq 10.5$ then $y < -8.4x + 51$, if $x > 10.5$, then $y < -89x + 1080$
24.	x = K(630nm) y = 2nd order polynomial coeff. of K(602nm) – K(662nm), centered at 630nm	$y > 33x - 206$
25.	x = K(686nm) y = 1st order polynomial coeff. of K(662nm) – K(694nm), centered at 686nm	If $x \leq 1.5$, then $y < 2$, if $1.5 < x \leq 10.4$, then $y < -5.6x + 10.4$, if $x > 10.4$, then $y < -14x + 102$
26.	x = K(678nm) y = 2nd order polynomial coeff. of K(658nm) – K(706nm), centered at 678 nm	If $x \leq 0.4$, then $y > -50$, if $x > 0.4$, then $y > 78x - 82$

B. Publications in international journals

B.1 S. Janchaysang, S. Sumriddetchkajorn, and P. Buranasiri, Appl Opt, 51, (2012) 6984-6996.

B.2 S. Janchaysang, S. Sumriddetchkajorn, and P. Buranasiri, Appl Opt, 52, (2013) 4898-4910.

Tunable filter-based multispectral imaging for detection of blood stains on construction material substrates. Part 1. Developing blood stain discrimination criteria

Suwatwong Janchaysang,[1] Sarun Sumriddetchkajorn,[2,*] and Prathan Buranasiri[1]

[1]Physics Department, Faculty of Science, King Mongkut's Institute of Technology Ladkrabang, Bangkok, Thailand

[2]Intelligent Devices and Systems Research Unit, National Electronics and Computer Technology Center, National Science and Technology Development Agency, Ministry of Science and Technology, 112 Thailand Science Park, Phahonyothin Rd, Klong 1, Klong Luang, Pathumthani 12120, Thailand

*Corresponding author: sarun.sumriddetchkajorn@nectec.or.th

Received 22 May 2012; revised 9 August 2012; accepted 10 August 2012; posted 13 August 2012 (Doc. ID 168919); published 5 October 2012

In this article, we establish blood stain detection criteria that are less substrate dependent for use in a liquid crystal tunable filter-based multispectral-imaging system. Kubelka–Munk (KM) theory is applied to transform the acquired stains' reflectance spectra into the less substrate dependent spectra. Chosen spectral parameters are extracted from the KM absorbance spectra of several stain samples on several substrates. Blood discrimination criteria based upon those spectral parameters are then established from empirical data, tested, and refined. In our newly invented method, instead of introducing conventional contrast enhancement on the blood stain image, blood stain determination is executed mathematically via Boolean logic, resulting in more discriminative blood stain identification. This proposed approach allows for nondestructive, quick, discriminative, and easy-to-improve presumptive blood stain detection. Experimental results confirm that our blood stain discrimination criteria can be used to locate blood stains on several construction materials with high precision. True positive rates (sensitivity) from 0.60 to 0.95 are achieved depending on blood stain faintness and substrate types. Also, true negative rates (specificity) between 0.55 and 0.96 and identification time of 4–5 min are accomplished, respectively. The established blood stain discrimination criteria will be incorporated in a real blood stain detection system in part 2 of this article, where system design and considerations as well as speed issues are discussed.

OCIS codes: 110.4234, 120.0120, 120.4630, 100.2960, 150.1488.

1. Introduction

Efficient presumptive blood stain detection is crucial to crime scene investigation. In chemical-based tests, visible traces occur as a result of chemical reactions between heme proteins in red blood cells (RBCs) and active reagents [1–3]. However, nonspecificity of the reactions usually brings high false-positive rates. Moreover, the application of chemicals can potentially wash away scarce evidence and produce chemical wastes. To alleviate these issues, noncontact detection approaches via imaging technology are preferred. In the simplest nonimaging method, forensic light sources make use of ultraviolet (UV) light to detect fluorescent traces of body fluids, such as semen, urine, and saliva [4,5]. However, fluorescence emission of blood is not observed over the spectrum

1559-128X/12/296984-13$15.00/0

ranging from UV to near-infrared regions. The use of UV light sources is therefore limited to making visible the blood spatters on some fluorescent substrates such as clothes, papers, and some painted surfaces. Moreover, UV light can possibly damage DNA evidence in blood.

Other noncontact approaches rely on spectral imaging. Due to nonfluorescence of blood stains, all the existing imaging-based blood stain detection methods are based on reflection. Unlike reflection-based imaging of plain surfaces, several complications occur when the substance of interest is just a blood stain deposited on a substrate. The main problem of using the reflection-based spectral imaging method to identify blood stains is that the reflectance on the blood stain surface is substrate dependent. The granular nature of blood stains, deposited on the substrates, inevitably causes spectral mixing between light reflected from blood stains and substrates. Given infinite possibility of substrate spectra and blood stain concentrations, blood stain detection criteria, universal to all substrates, have not been established. Current imaging methods still have considerable limitations in types of substrates and specificity in detecting blood against other stains. For example, infrared photography can enhance the visibility of blood spatters on dark-colored clothes since blood strongly absorbs near-infrared radiation (700–1000 nm), while most fabrics reflect it [6,7]. Nevertheless, those reports have been focused simply on the detection of blood stains on cloth, but the blood stain detection on other substrates has not yet been demonstrated. Recently, Brooke *et al.* [8–10] have combined the measurement of infrared reflectance, thermal emission, and thermal diffusion rates in multimode imaging to successfully enhance the contrast of faint blood stains and detect blood against four other stains. Nonetheless, the approach has been demonstrated only for the detection of blood stains on black acrylic fabric.

Multispectral imaging and hyperspectral imaging (HIS) are the promising technologies. They have been employed for several applications including data nonintrusive credit card verification [11,12], Thai jasmine rice identification [13,14], and two-dimensional (2D) banana ripeness level indication [15]. In the blood stain detection scenario, Wagner [16] and Miskelly and Wagner [17] took advantage of the distinct narrow high-absorption band (i.e., Soret band) of heme proteins, centered around 415 nm. The arithmetic image divisions are performed between 415 and 440 nm spectral images, where blood exhibits steep spectral absorbance characteristics, in order to enhance the visibility of blood stains on wood. Since a number of substances in the real world exhibit high absorption around 400 nm wavelength, the proposed technique is impractical for other substrates. In addition, camera response around Soret band is usually too low to overcome noise and distinguish one stain from another. Furthermore, spectra of RBCs are mostly flat around the Soret band since the region is subject mostly to the packing effect [18]. The commercially available CONDOR wide field HIS system [19–21] and its newest version HIS examiner systems [22] from ChemImage make use of HIS in forensic investigations, including visualization of fingerprints, questioned documents, inks, gun powder residue, and blood stains. However, for blood stain detection, the main focus of the systems is on visualization of the blood stain on dark fabrics using visible to near-infrared contrast enhancement techniques. To our knowledge, no existing multispectral imaging-based blood stain detection methods have thoroughly investigated the effect of substrate reflectance spectra. In addition, no imaging based blood stain detection systems have been demonstrated to distinguish blood from several stains on various substrates.

In addition, all the aforementioned spectral methods make use of traditional contrast enhancement through the predesigned image operations, such as image subtraction, addition, and division among spectral images. Contrast enhancement has several limitations. For example, some substances may have different reflectance values from blood at one small part of the electromagnetic spectrum, and the other substances may at the other parts of the spectrum. It is, therefore, very difficult to enhance contrast for blood and eliminate contrast for all other stains at the same time. Another limiting issue is that image operations are sensitive to saturation and undesired loss of information.

Hence, this paper proposes the new blood stain detection methodology and criteria for use in a multispectral-imaging system. Key features include substrate contribution reduction through Kubelka–Munk (KM) theory and criteria establishment based upon empirical data and blood discrimination criteria, which identify the blood stains using mathematical inequalities and Boolean logic. Mathematical determination of blood stains through Boolean logic based upon chosen spectral parameters allows for concatenation of blood stain detection criteria. After each stain is determined as not corresponding to blood by any criterion, the stain can be immediately excluded from interest. This method allows for more discriminative and fast detection.

In Sections 2–4, we discuss the experimental details and the procedure for establishment of blood stain criteria. In Section 5, we demonstrate that the strain reflectance spectra really depend on substrate spectra, and Section 6 shows that KM theory can reduce the dependence of stain reflectance spectra on substrates. Then, in Sections 7 and 8, we describe in detail how the blood detection criteria can be established and evaluated.

2. Multispectral-Imaging System

A. Hardware

Our multispectral-imaging system for blood stain detection is based on a typical liquid crystal tunable

filter (LCTF) shown in Fig. 1. Illumination is achieved using two metal halide lamps (Philips CDM–R 70W/942), which yield desired full spectral range over the visible region. The nonuniformity of the illumination on the image surface is kept to less than 25%. An 8 bit multispectral-grade color camera (Basler Scout scA750-60gc) is coupled with an LCTF (VariSpec, VIS 7-HC-20). The surface to be imaged is placed on the optical table just below the camera. A personal computer, equipped with LabVIEW program, is connected, so as to control image capturing of the camera and spectral scanning of the LCTF. The LCTF has a full-width half-maximum (FWHM) bandwidth of 7 nm, a wavelength scanning range from 400 to 720 nm, and a 20 mm circular aperture. The 2D image sensor of the camera contains 750 × 480 pixels and it is set to operate in RGB mode. However, the camera's field of view is limited by the LCTF's circular aperture to ±7°. Since the camera is placed 30 cm above the sample surface, the image visibility is limited to a circular area of 10.5 cm in diameter (see Fig. 2). To lessen our calculation, we set the camera's area of interest (AOI) to 360 × 339 pixels, a rectangular area just to cover the visible circular field of the images.

B. Image Capturing

To capture desired multispectral images, the LCTF is programmatically tuned to uniformly sample 64 wavelength images, ranging from 458 to 710 nm, with the tuning step of 4 nm wavelength. For each captured scene, the camera catches 64 images, one image for each tuning wavelength, to form a three-dimensional (3D) image cube that contains information in two spatial dimensions and one spectral dimension. The 3D image cube therefore has the size of 360 × 339 × 58 pixels. Since the spectral response of our multispectral-imaging system is spiky and the surfaces on which we look for blood stains can be of any type or reflectance spectra, the spectral images can easily be saturated or too dark to recover their true spectra. To solve the problem, while capturing one spectral image, we propose to capture several 3D image cubes of the same scene with different exposure times ranging from 10,000 to 120,000 μs.

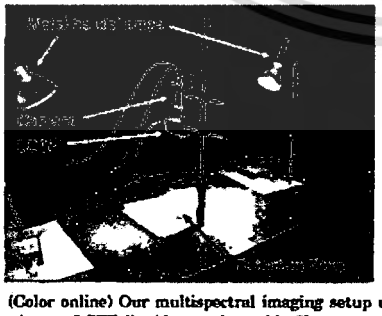

Fig. 1. (Color online) Our multispectral imaging setup used in this experiment. LCTF, liquid crystal tunable filter.

Then the set of spectral images whose exposure times give suitable bright image, but not saturated or not too dark, are selected so that true reflectance spectra of the surface are obtained. To manually select suitable exposure times for spectral images, we first extract the spectral digital responses on the substrate areas on the images and realize that the spectral digital responses are dominated mostly by the spectral responses of the multispectral imaging instruments. Then, we can manually select the exposure times that yield high but unsaturated and still linear digital response zone. This is a slow and pains-taking process. However, this is the process to be performed exclusively by the system developer to establish blood detection criteria not by the expected end users. In the second part of this article [23], we will make the system automatically adjust the exposure times so that the captured images will fall within linear response range.

3. Procedure for Establishing Blood Stain Discrimination Criteria

Intuitively, the reflectance spectra of the stains (especially the faint stains) depend on the spectrum of the substrates. This will be verified later in Section 5 of this article. Since absorbance of the substance is substrate independent, it is likely that absorbance could be the base for detection of a blood stain. Unfortunately, we cannot physically measure the absorbance spectra from the reflection-based multispectral-imaging system. However, KM theory allows transformation of the measured reflectance into the values that are less substrate independent. To develop blood stain discrimination criteria, the procedure in Fig. 2 is proposed and performed. First, we collect many sets of multispectral images of blood and other stain samples on different substrates. Then, we use our proposed calibration and spectral recovery method, and later apply KM theory to estimate the KM absorbance spectra of each stain. Since KM is not perfect theory in yielding absorbance spectra, the blood detection criteria are established based upon the KM absorbance spectra, empirically obtained from the known blood and other stains. Then the criteria are tested and refined. In the following sections, we describe in detail the step-by-step developments of blood detection methodology according to our proposed idea.

4. Sample Preparation

To establish efficient blood stain detection criteria, we must collect enough sample spectra of blood and other stains on a variety of substrate materials to be certain that true spectral characteristics of blood stains are appreciated. In this work, several common construction materials including gypsum boards, concrete boards, green tiles, white tiles, and wood planks are used as substrates. We also use bovine blood instead of human blood as it possesses absorption spectra comparable to human blood [24]. Other stains under our study include coffee, cocoa drink,

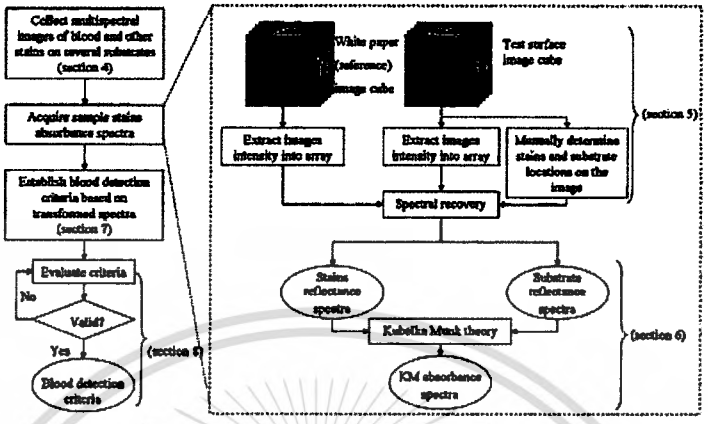

Fig. 2. (Color online) Proposed procedure in development of blood detection criteria. The section numbers in this figure correspond to the section numbers of this article.

ketchup, soy sauce, mud, soil, and oyster sauce. For the purpose of spectra collection, each stain substance is intentionally spread out on the substrates so that different concentrations of each substance are deposited on the substrates. Figure 3 shows some of our sample surfaces, including gypsum board, wood plank, green tile, white tile, concrete, and orange-painted concrete. Several multispectral images of these surfaces are captured with our aforementioned multispectral system.

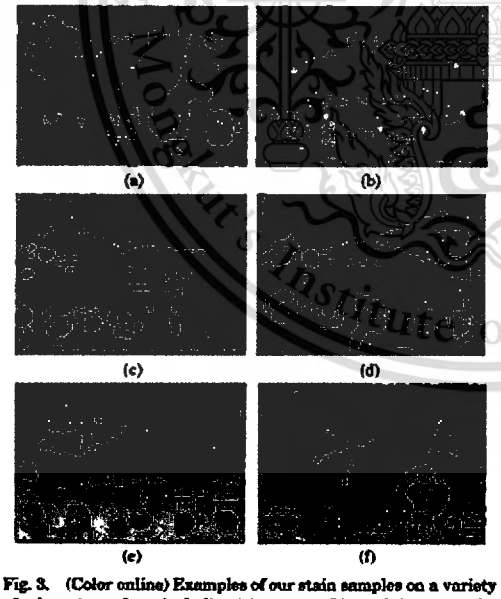

Fig. 3. (Color online) Examples of our stain samples on a variety of substrate surfaces including (a) gypsum, (b) wood, (c) green tile, (d) white tile, (e) concrete, and (f) orange-painted concrete. Each substrate has different concentrations of blood and other stains deposited on them.

5. Calibration and Reflectance Spectra Recovery

To recover diffuse spectral reflectance of the test surface, a widely accepted white reference calibration method [25–27] is performed. By taking into account cost and handling issues in a real world scenario, we propose to use a stack of spatially uniform white bleached paper of known reflectance spectrum, instead of a commercially expensive and careful-handling white reference tile. The white bleached paper used in this research is just the commercial-grade, A4-sized paper, typically used in office work. To calibrate the multispectral images, the white bleached paper is placed on the detection zone in such a way that all pixels in the image field of view can capture the desired spectral images of the white bleached paper ($R_W(\lambda_k)$). After removing the white bleached paper, many sets of spectral images of the test surfaces can be taken as long as all illumination and imaging instruments are kept intact. With the incorporation of exposure time, the spectral reflectance at any pixel on the test surface $R_T(\lambda_k)$ can be expressed as

$$R_T(\lambda_k) = \frac{[(T(\lambda_k) - D)/\tau_T(\lambda_k)]}{[(W(\lambda_k) - D)/\tau_W(\lambda_k)]} \cdot R_W(\lambda_k). \quad (1)$$

where $T(\lambda_k)$ and $W(\lambda_k)$ are the digital responses from the test surface image pixel and the white bleached paper image pixel, respectively. $\tau_T(\lambda_k)$ and $\tau_W(\lambda_k)$ are the camera's exposure times when capturing the test surface and the white bleached paper, respectively, and D is the dark response of the camera. For our 8 bit camera, $T(\lambda_k)$ and $W(\lambda_k)$ range from 0 to 255. They can be taken from either R, G, B, or gray scale digital responses as long as the pixel values are in the linear response range. For our LCTF-based

multispectral-imaging system, it is suitable that the digital responses are extracted from the blue (B) color plane for wavelength channels from 458 to 498 nm and from the green (G) color plane for wavelength channels from 502 to 710 nm. Although blood and most substrates in the real world have high reflectance values at the red end of the visible spectrum (600–700 nm) and the red (R) channel gives high responses in this spectral region, channel R is not chosen. Seemingly, channel R should have been a good channel to select. However, signals from the R channel turn to be noisier due mainly to our camera characteristics. The camera has certain values of exposure times it can capture images. For example, when the camera is programmed to capture the image at the certain exposure time (e.g. 10 000 μs), the camera captures the image at some other exposure times (e.g., 9941 or 10 073 μs). This quantization adds a little more noise to the detection process. For the case of channel R that could have been used around 600–700 nm, the digital responses are very high, so we have to reduce the exposure time. The suitable exposure time values are of the order of 1000 μs. Since this jump in exposure time value (e.g., from 1000 to 960 μs) is relatively high, more noise would have added to the system. So, empirically we have better choice of using less noisy channel G.

Dark response, originating from dark current present in the detector array, can be determined by capturing the image while the camera's slip is covered. There are advantages of using white bleached paper for our calibration method. First, the paper is cheap, replaceable if tarnished, and reusable for other work. Secondly, since the paper is large enough to cover the camera field of view, all pixels in the image are readily calibrated without further correction for spatial nonuniformity of illumination and for the geometrical difference between reference and test surfaces.

As will be evident in later sections of this article, since the detection of blood stains involves complicated mathematical calculations, processing the images directly is not suitable. So, we transform the data in an image cube into an array. To do this, digital responses of 3 by 3 adjacent pixels in any image are extracted and averaged into a single number before becoming a single element of the array, yielding measured spatial resolution of blood stain detection of $0.9 \times .9\,\text{mm}^2$. The 3D image cube of size $360 \times 339 \times 58 = 7,078,320$ elements is therefore compressed and transformed into the 3D array with the corresponding size of $120 \times 113 \times 58 = 786,480$ elements. Two spatial dimensions are further reshaped into 1D, giving the final size of the 2D array of $13,560 \times 58 = 786,480$ elements. From Eq. (1), it can be clearly seen that each element obtained under our white reference array is represented by a calibration number of $w(\lambda_k) = \frac{[(W(\lambda_k) - D)/\tau_W(\lambda_k)]}{K_W(\lambda_k)}$. For the test surface array, each element is represented by $t(\lambda_k) = [(T(\lambda_k) - D)/\tau_T(\lambda_k)]$. In this way, the spectral reflectance of the surface can be calculated directly from $R(\lambda_k) = t(\lambda_k)/w(\lambda_k)$.

There are several pros of transformation of the 3D image cube into an array. First, averaging responses from 3 by 3 pixels into one element before further calculations can reduce noise, and lessen system computational load and memory, thus improving the speed of the detection system. Secondly, calibration data in the form of an array can rapidly be stored and extracted from a single text file. Thirdly, with multispectral data arrays, unnecessary data from spatial points that have been identified as nonblood can immediately be removed from the array without further consideration. This will considerably help reduce computational load in a real blood stain detection system. Lastly, image processing also unnecessarily processes all R, G, and B pixels in the image as our calibration and spectral recovery scheme requires only spectral data in R, G, or B color planes.

Sample reflectance spectra of stains are collected by manually locating the image coordinates where stains are deposited and then, with simple array manipulation, reflectance spectra from those coordinates are extracted. Although this manual collection of the sample stain spectra is a slow process, it is the process for us (as the system developer) only, who wanted to establish the blood stain detection criteria. It is not the process the users have to do. Figure 4(a) shows reflectance spectra of different stain types, deposited on gypsum and wood substrates. Note that more spectral data are actually collected than those appearing in charts in Fig. 4. Only some of the spectral data are shown, so that the tendency of the curve can clearly be seen in the charts and the charts are not flooded with too many spectral lines. It is clear that there are a number of possible reflectance curves for each stain type, depending on stain faintness. The highest reflectance curve (a bold line) in each chart usually belongs to the substrate, while lower curves (thin solid lines) belong to the stain. The higher stains' reflectance curves also indicate thin or faint stains, while the lower curves belong to thick- or high-concentration stains. In addition, differences in curve tendency are also observed among different stain types. When the substrate changes, differences in spectral shape of the blood stains can be observed as shown in Fig. 4(b), pointing out that the shape of blood stain reflectance spectra is much influenced by the reflectance spectra of the substrates. The reason behind this phenomenon is that the granular nature of stains, deposited on the substrates, inevitably causes spectral mixing between light reflected from stains and that from substrates. The fainter the stains are, the larger the contribution of the substrate is to the reflectance spectra. Since substrates in the real world may be anything and may exhibit infinitely possible shape of reflectance spectra, the blood stain reflectance spectra on the substrates can also be of any shapes. A blood stain detection system based upon reflectance spectra is therefore improbable.

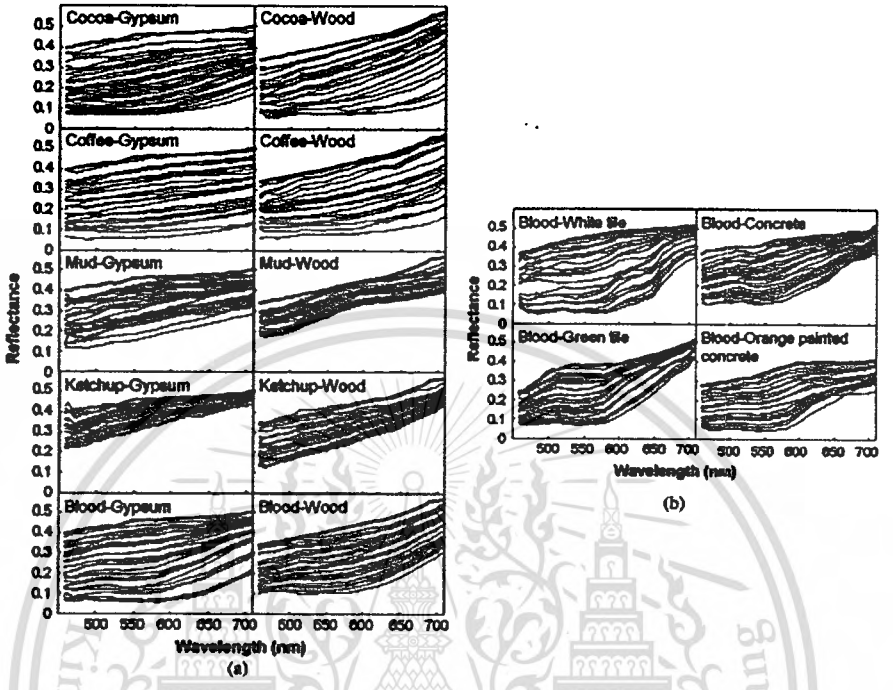

Fig. 4. Recovered reflectance spectra of (a) blood and other stains on gypsum and wood substrates and (b) blood stains on different substrates. Bold lines are reflectance spectra of substrate while solid lines are those of stains.

6. Estimation of Stain Absorbance Spectra

The stains' reflectance spectra obtained from Section 7 depend on the spectrum of the substrate on which the stains are deposited. In order to create the blood stain detection system that is more universal to all substrates, the effect of substrate reflectance must be lessened. Since absorbance is substrate independent, it is likely that spectral absorbance could be the base for blood stain detection. Unfortunately, we cannot physically measure absorbance spectra of blood stains using a multispectral-imaging system. KM theory is one of the methods that can relate the absorption, the reflectance, and the scattering [28]. There have been several versions and modifications of the KM theory through the years. Basically, the theory is only a simplified model, which treats light transmission and scattering as occurring in only forward and backward direction. It also assumes that the medium is isotropic and homogeneous, and ignores discontinuity between reflective indices of air and blood stain. Although the KM model can never give the real absorbance value from reflectance and scattering due to those simplifications and the modeling, the theory is very useful in color prediction and measurement of substances. The examples of applications include the study of optical properties of biological tissues [29–31], modeling for reproduction of natural tooth color for ceramic tooth restoration [32], prediction of nutrients and moisture in soil [33], and color pigment measurement of paints and inks [34–36]. KM formulae have been used by Bremmer *et al.* to estimate blood stain absorption spectra on white cotton substrate to successfully determine the age of the blood [37]. Here, we apply the same formulae as Bremmer *et al.* to the spectral reflectance recovered in the previous section.

$$\frac{R_{ST}(\lambda)}{R_S(\lambda)} = 1 - \frac{K(\lambda)}{S(\lambda)}\left(\sqrt{1+\frac{2K(\lambda)}{S(\lambda)}}+1\right). \quad (2)$$

where $R_{ST}(\lambda)$ and $R_S(\lambda)$ are the reflectance spectra recovered from the stain and pure substrate surface, respectively. $K(\lambda)$ and $S(\lambda)$ relate to stain optical absorption and scattering, respectively. Since the KM theory does not give the real value of absorption, we would refer to $K(\lambda)$ as KM absorption. To find $R_S(\lambda)$, we manually locate the known pure substrate areas in the image, extract reflectance values at all corresponding points, and average them to get the substrate spectrum. For simplicity, the Lorentz–Mie scattering concept is also applied during our estimation of all stains' absorbance spectra.

$$S(\lambda) = S_0\left(\frac{\lambda}{\lambda_0}\right)^{-0.4}. \quad (3)$$

Here, we take $\lambda_0 = 450$ nm and $S_0 = 1$ for all stain samples. Hence, the unit of $K(\lambda)$ becomes arbitrary. Some resultant KM absorbance spectra of the different stains on gypsum and wood substrates are shown in Fig. 5(a) [compare with Fig. 4(a)]. Also, some KM absorbance spectra of blood stain on different substrates are shown in Fig. 5(b) [compare with Fig. 4(b)]. These curves are not necessarily taken from the same stain locations as those reflectance curves in Fig. 4. They are chosen in such a way that the curves are clearly distributed and that the tendency of the curves can be clearly observed on the chart. Higher curves on each chart are associated with thick- or high-concentration stains, while lower absorbance curves belong to faint stains. From the shape of the KM absorbance spectra of blood stain on all six substrates in Fig. 5, more distinguished spectral features can be clearly observed from KM absorbance curves of blood stains than from reflectance curves. It is obvious that KM absorbance spectra of blood stains show similar curve tendency among all six substrates. Prominent spectral features include the steep down-slope at low wavelengths (458–510 nm), the up-slope roughly from 514 to 542 nm wavelength, the down-slope from 546 to 690 nm wavelength, and the very low absorbance at the red end of the visible spectrum. Tendencies in deflection or concavity of the curves are also evident. Inconsistency on KM absorbance curves at low wavelengths (e.g., 458–466 nm) is observed because of low intensity of illumination as well as low response of our multispectral system at this spectral range. Thereby, the criteria that will be established in Section 7 must be based on 2D 470–710 nm spectral data only.

At the time the spectral images are taken, blood stains are a few weeks to several months old. At this time range, the major constituent of blood pigments is hemichrome (50%–70%) and oxyhemoglobin (20%–30%) [37]. The KM absorbance spectra of the two substances taken from [38,39] are shown in Fig. 6. This indicates that our KM absorbance spectra have shape similar to the absorbance spectra of the combined blood stain components, and so the result is in good agreement with Bremmer [37], that RBC pigment at this period of analysis should consist mainly of hemichrome and oxyhemoglobin.

7. Blood Stain Discrimination Criteria

Although the application of KM theory provides the KM absorbance spectra whose shapes are close to the

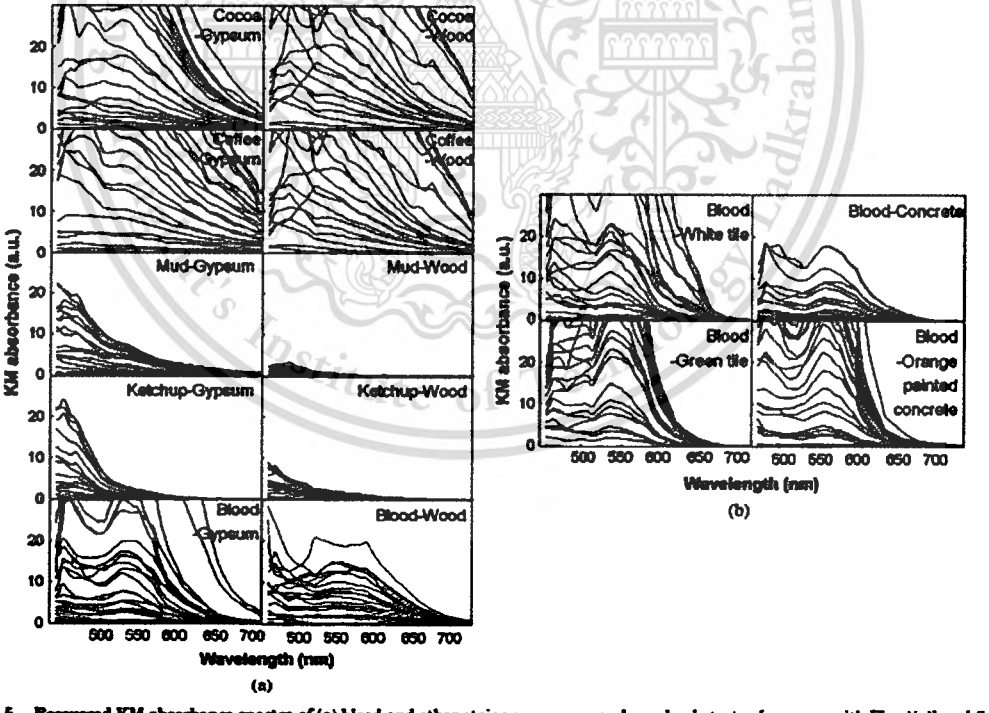

Fig. 5. Recovered KM absorbance spectra of (a) blood and other stains on gypsum and wood substrates [compare with Fig. 4(a)] and (b) blood stains on different substrates [compare with Fig. 4(b)].

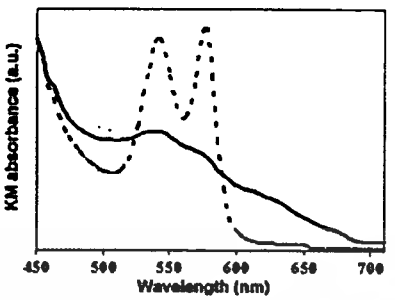

Fig. 6. Absorbance spectra of hemichrome (solid curve) and oxyhemoglobin (dotted curve) are in good agreement with our obtained KM absorbance spectra in Fig. 5.

shape of the real stains' absorbance spectra, these curves, by no means, represent the true absorbance spectra of the stains. Yet, the KM absorbance spectra are shown to be less dependent on the substrate. Therefore, to establish blood stain detection criteria, we base our criteria on the KM absorbance spectra, empirically collected from the real samples on several substrates instead of using the true absorbance curves of blood. Our blood stain detection methodology is that the blood stain identification is determined mathematically through a series of blood stain detection criteria and the results are to be expressed in pseudo-color on the image pixels. The advantage is that the method produces a more discriminative result than the contrast enhancement method. In the contrast enhancement method, it is hard to distinguish blood from all other stains since stains may possess different reflectance values from blood at one part of the spectrum, and the other stains may at the other parts of the spectrum. In addition, image operations may distort the image information through saturation and quantization. Mathematical determination of blood stains through Boolean logic based upon chosen spectral parameters allows for concatenation of blood stain detection criteria.

In our real fully developed detection system, predetermined spectral parameters from all spatial points on images of a test surface will be programmatically extracted and tested by a series of our blood stain detection criteria. The criteria are simply the mathematical inequalities involving the spectral parameters purposely made in the way that they would pass the spatial points in the image that possibly correspond to the blood stain and at the same time prevent the points ascertained as definitely not corresponding to blood. Spectral parameters include reflectance values, KM absorbance values, arithmetic operations of these values, and polynomial coefficients of KM absorbance spectra. The spatial locations on the test surface that pass all of our criteria will be finally identified as the blood stain. Criteria are established based on empirically collected data from blood and other stain samples. To establish the criteria, we first choose spectral parameters that can intuitively reflect the distinct spectral characteristics of blood stain reflectance and KM absorbance curves as well as can simultaneously eliminate other stains. The simplest criteria make use of only a single spectral parameter. For example, since we observe that blood stain KM absorbance is very small at the red end of the visible spectrum, we make a criterion that the KM absorbance at 710 nm wavelength must be less than 1 (i.e., $K(710\ \text{nm}) < 1$; see KM absorption values at 710 nm wavelength shown in Fig. 5). In this way, we can exclude many spatial points corresponding to coffee and cocoa stains. In another criterion example, we exclude spatial points whose reflectance values are close to the reflectance of the substrate in order to eliminate the substrate locations, $(R_{ST}(470\ \text{nm})/R_S(470\ \text{nm}) \le 0.98$; consider reflectance values at 470 nm wavelength on the charts in Fig. 4). In a more complex criterion, two extracted spectral parameters are plotted on the x and y axes of a scatter chart. For conciseness, only six examples of these charts are shown in Fig. 7. Each data point on the charts corresponds to the stain type indicated by the shape of the marker. The substrate type is indicated by the color of the marker. For clarity, the separate charts on the right side show data points corresponding only to the blood stain whose trend can clearly observed. Criterion boundaries are manually selected to loosely encompass the blood stain region. Each boundary is drawn, based on the observed empirical data, with joining straight line segments (red line segments in Fig. 7), so that criteria expressed in simple linear inequalities (i.e., $y > mx + c$ or $y < mx + c$) can be applied, where x and y are the extracted spectral parameters on the horizontal and vertical axes of the chart, respectively, m is the slope, and c is the y intercept of the line segment. The correct marks indicate the interesting region to be selected and cross marks indicate the regions to be deselected by our proposed criteria. During the real detection stage. which will be performed in Section 8, any spatial points on the images whose spectral parameter coordinates fall outside the interesting region on the chart will be immediately excluded from the our interest. We normally make slightly loose criteria to spare for noise in the system. However, the data points from blood stains that considerably deviate from the trend possibly due to large noise or impurity have to be excluded. Otherwise, specificity of the system must be sacrificed. Although spectral parameters made from reflectance and KM absorbance values of a few wavelengths [Figs. 7(a)–7(c)] are quick to process and useful to preliminarily exclude some stains, they are not discriminative enough to exclude all other stains. More discriminative spectral parameters take advantage of polynomial coefficients [Figs. 7(d)–7(f)] since they are established from more wavelengths and hence less subject to the system's noise. To make the criteria, we apply polynomial fits (up to the third order) to selected portions of the KM absorbance spectra. For

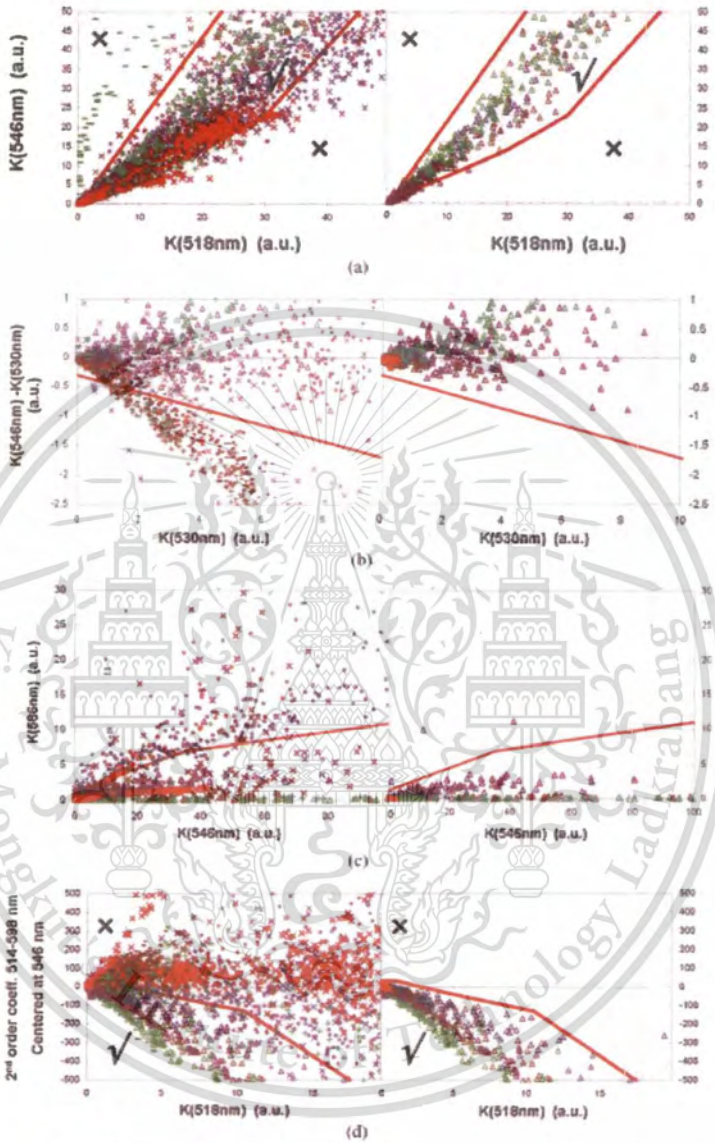

Fig. 7. Six examples of our established blood detection criteria (*figure continued on next page*). (a)–(c) are preliminary criteria, and (d)–(f) are more complex criteria with different order of polynomial coefficients on different curve segments versus KM absorbance values at selected wavelengths. Charts on the left side show data points from all stains, while those on the right side show only those from blood stains. Criterion boundaries are drawn with red straight line segments to cover the blood stain region.

instance, since blood stain KM absorbance curves have prominent concave downward shape along 514–586 nm and centered around 550 nm wavelength, we estimate that the second-order coefficients of this curve section for the blood stain must be some negative values. Accordingly, we apply polynomial fit to this curve section, for which we let the center be at 550 nm and adjust the x scale so that the distribution of data points is clearly observed. Then, we plot the second-order coefficients against the zeroth-order coefficients [Fig. 7(d)]. The distribution of data points on many scattering charts

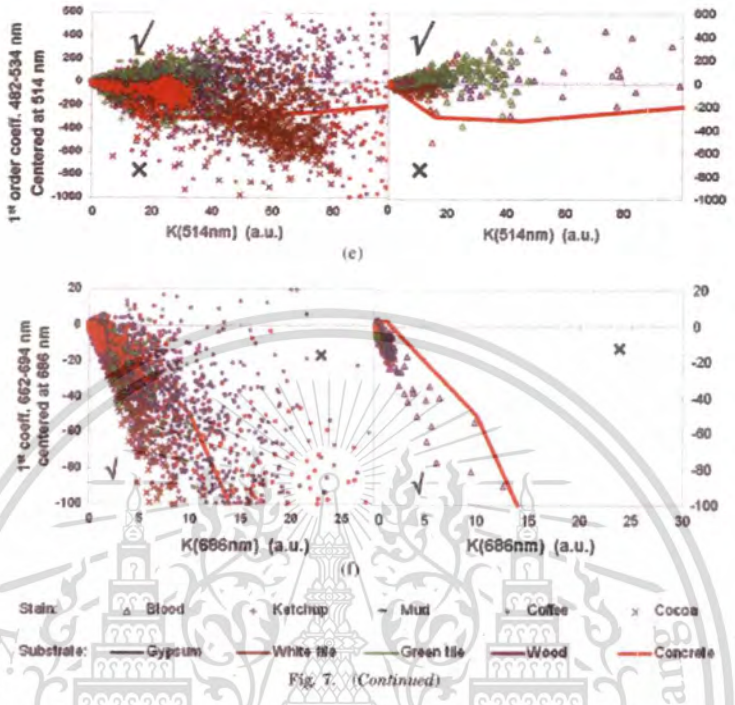

Fig. 7. (Continued)

for each stain usually has imperfect trianglelike shape with one tip at the origin. The points closer to the origin belong to thin stains. One criterion may be able to exclude only some stains or some concentrations of stains. Taken into account the interest of forensic investigation and based on 2D spectral data in the 470–710 nm wavelength range, we currently make as many as 26 criteria in order to take out as many different stain points as possible. Although several criteria may exclude many same spatial points in the image, we rely on the fact that if some spatial points of other stains are misidentified by a criterion, there may be another criterion that can exclude the points. Having many criteria may not hurt the speed of the system much, because criteria can be cascaded so that the excluded spatial points will not be calculated again in the later criteria. One advantage of this detection system is that the system specificity can always be improved by finding more criteria, refining existing criteria, or even removing some redundant criteria.

8. Experimental Test of the Established Criteria

To evaluate our detection criteria for the blood stain, we capture several other multispectral image cubes of stain samples and perform blood stain detection with our established criteria on those new image cubes. The image cubes are transformed into arrays and calibrated by the method described in Sections 5 and 6. The detection program operating under LabVIEW 2011 is designed such that the required spectral parameters for every spatial point are extracted. Then, all spatial points are sequentially tested by all 26 criteria established in Section 7. Only the spatial points that pass all criteria are identified as possible blood stains. Although this is not a computationally efficient method of detecting blood, the purpose of this part of this article is to establish and refine our detection criteria for the blood stain. In part 2 of this article [23], we will propose and experimentally show the method to eliminate unnecessary calculation steps in the real blood detection system. Figure 8 shows result images after they pass through our blood detection criteria. The points identified as blood stains are masked with 2 × 2-pixels pseudo-red color on the original 530 nm images.

Performance of the detection system is appraised by its sensitivity, specificity, and speed [40]. Since we know the true locations of our blood stain samples on the result images, we can appraise the performance of the system in terms of true positive rate (TPR). Note that TPR is often referred to sensitivity and true negative rate (TNR) is also frequently referred to specificity [41–45]. Because the TPR of blood stain detection depends on stain faintness, plotting the TPR versus stain concentration is appropriate. As discussed earlier, in order to see the data trend, the stains are purposely spread out such that

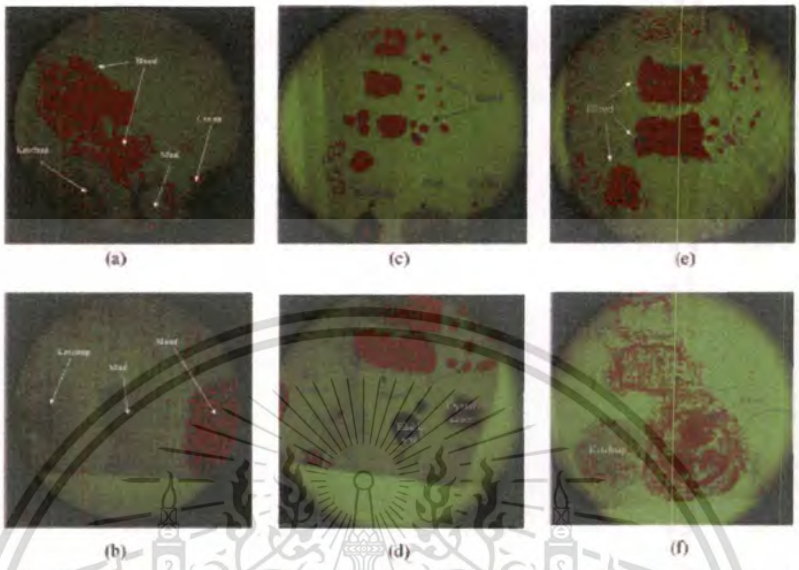

Fig. 8. (Color online) Examples result images for blood stain detection on (a) gypsum, (b) wood, (c) green tile, (d) white tile, (e) concrete, and (f) orange-painted concrete. Spatial points identified as blood are masked with 2×2-pixel pseudo-red color on the original 530 nm spectral images.

there are several concentrations of each stain deposited on the substrates. The height of the stain reflectance curves (Section 5) and KM absorbance curves (Section 6) can indicate how similar the stain appears to the substrate. The reflectance curve separations between substrates and strains are typically larger at low wavelengths and the lowest available wavelength that gives consistent measurement in our system is 470 nm (see Fig. 4). So, we use the value of $R_{ST}(470\text{ nm})/R_S(470\text{ nm})$ to represent the faintness of the stains. The closer the value is to 1, the closer the stain looks to the substrate, and hence the more difficult the stain is to be seen by naked eyes. For most reddish brown stains, the stains are darker than the substrates and the value of $R_{ST}(470\text{ nm})/R_S(470\text{ nm})$ usually ranges from 0 to 1. Though this value is not the measurement of concentration that is used by most chemists and forensic scientists, it does really indicate how similar the surface looks to the substrate. In this experiment, the value is even better than concentration because high-concentration stains do not necessarily mean that the stains look more different from the substrates. In fact, the appearance also depends on types and colors of stains and substrates.

So, we plot TPR versus $R_{ST}(470\text{ nm})/R_S(470\text{ nm})$ [see Fig. 9(a)]. According to Fig. 9, the values of $R_{ST}(470\text{ nm})/R_S(470\text{ nm})$ are grouped into class intervals just like in histograms, with the interval size of 0.1. The markers represent the middle value of their classes. For example, markers at 0.9 represent $R_{ST}(470\text{ nm})/R_S(470\text{ nm})$ values between 0.85 and 0.95. TPR is determined for each class. For all substrates, high sensitivity ($0.7 < \text{TPR} < 0.95$) is achieved at slightly thick blood stain ($0.3 < R_{ST}(470\text{ nm})/R_S(470\text{ nm}) < 0.7$). These slightly thick stains have high SNR levels and are the easiest to identify. The highest sensitivity for blood station detection is observed on gypsum substrate ($0.8 < \text{TPR} < 0.95$), while the lowest is on wood ($0.6 < \text{TPR} < 0.79$), because of the high local variation of the wood substrate profile. For thin blood stains ($0.8 < R_{ST}(470\text{ nm})/R_S(470\text{ nm}) < 0.9$), sensitivity is lower ($0.55 < \text{TPR} < 0.84$) with the average of 0.74 because small spectral signals from thin blood stains' KM absorbance spectra are embedded in larger signals from the substrate spectra resulting in lower SNR values. For thick blood stains [$(0.1 < R_{ST}(470\text{ nm})/R_S(470\text{ nm}) < 0.2)$], sensitivity is also low ($0.60 < \text{TPR} < 0.81$) with the average of 0.73, because original digital response values are very low, especially at low wavelength ($\lambda < 500$ nm), which also causes lower SNR values. Furthermore, thick stains are more subject to the packing effect of pigment particles in stains [18], which distorts the high absorbance parts of the spectra far more than lower parts.

The TNR (i.e., specificity) are also plotted against $R_{ST}(470\text{ nm})/R_S(470\text{ nm})$ by the same method as above. For our system, TNR measures the ability to exclude other stains from blood. For each stain type, we determine TNR for each substrate and take average of TNR values from all substrates. The TNR values as a function of $R_{ST}(470\text{ nm})/R_S(470\text{ nm})$ are

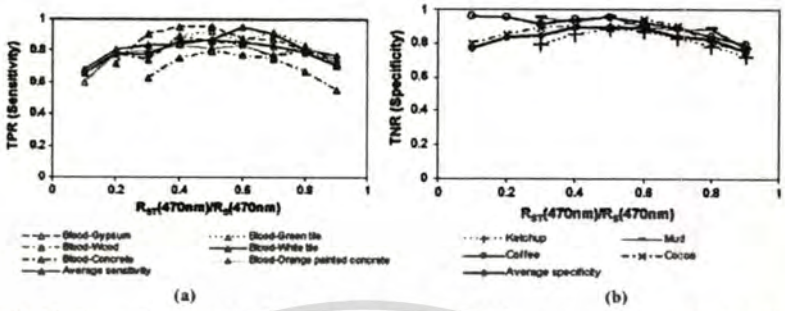

(a) (b)

Fig. 9. (Color online) System performance of our blood stain detection described in (a) true positive rate (sensitivity) and (b) and true negative rate (specificity).

shown in Fig. 9(b). High specificity ($0.8 < \text{TNR} < 0.96$) is achieved at medium and thick stains. Highest specificity is obtained in mud stains ($0.86 < \text{TNR} < 0.96$) and lowest in ketchup stains ($0.78 < \text{TNR} < 0.88$). For the same reasons as sensitivity measurement, at faint and thick stain, TNR for all stains reduces. The average TNR for thin stain ($0.8 < R_{ST}(470\,\text{nm})/R_S(470\,\text{nm}) < 0.9$) is 0.75, and for thick stain ($0.1 < R_{ST}(470\,\text{nm})/R_S(470\,\text{nm}) < 0.2$) is 0.77.

In this part of the paper, the identification process take 4–5 minutes for each image cube, because at all spatial points, all required parameters are extracted and tested by all criteria. In part 2 of this article, we will take into account the speed issues and evaluate speed when we employ the criteria established in this part of the article to make a rapid blood stain detection system.

9. Conclusion

We have developed a multispectral imaging-based forensic blood stain detection method on construction material surfaces and established blood discrimination criteria. According to the method, multispectral image cubes are transformed into arrays, and then the reflectance spectra at each point in the captured spectral images are transformed into the less independent spectra using KM theory. From those spectra of the collected samples, we instinctively find several spectral parameters that can be used to separate blood from other stains. Blood stain identification is done mathematically via blood detection criteria. At present, 26 blood selection criteria have been established. The criteria are proved to be distinguishable blood stains from other reddish brown stains with high sensitivity ($0.60 < \text{TPR} < 0.95$) depending on blood stain concentration and substrate type as well as high specificity ($0.55 < \text{TNR} < 0.96$). Our research focus in the near future is still on improvement of criteria, extending the spectral range to the entire visible spectrum and into near-infrared region, as well as reducing the spectral channel sampling frequency. With further improvement, this method can even potentially be extended to identify other substances or stains on any substrates, which is not limited to forensic science. In addition, in the second part of this article [23], we will discuss how to use these established criteria to achieve a rapid blood stain detection system.

S. Janchaysang would like to thank the Thailand Graduate Institute of Science and Technology for scholarship support (Grant No. TG-44-22-50-081D).

References

1. A. C. Ponce and A. C. Pascual, "Critical revision of presumptive tests bloodstains," Forensic Sci. Commun. 1, 1–15 (1999).
2. M. A. Cox, "A study of the sensitivity and specificity of four presumptive tests for blood," J. Forensic Sci. 36, 1503–1511 (1991).
3. A. M. Gross, K. A. Harris, and G. L. Kaldun, "The effect of luminol on presumptive tests and DNA analysis using the polymerase chain reaction," J. Forensic Sci. 44, 837–840 (1999).
4. N. Vandenberg and R. A. van Oorschot, "The use of Polilight in the detection of seminal fluid, saliva, and bloodstains and comparison with conventional chemical-based screening tests," J. Forensic Sci. 51, 361–370 (2006).
5. W. C. Lee and B. E. Khoo, "Forensic light sources for detection of biological evidences in crime scene investigation: a review," Malays. J. Forensic Sci. 1, 17–28 (2010).
6. A. C. Lin, H. M. Hsieh, L. C. Tsai, A. Linacre, and J. C. Lee, "Forensic applications of infrared imaging for the detection and recording of latent evidence," J. Forensic Sci. 52, 1148–1150 (2007).
7. M. Perkins, "The application of infrared photography in bloodstain pattern documentation of clothing," J. Forensic Sci. 55, 1–9 (2005).
8. H. Brooke, M. R. Baranowski, J. N. McCutcheon, S. L. Morgan, and M. L. Myrick, "Multimode imaging in the thermal infrared for chemical contrast enhancement. Part 1: methodology," Anal. Chem. 82, 8412–8420 (2010).
9. H. Brooke, M. R. Baranowski, J. N. McCutcheon, S. L. Morgan, and M. L. Myrick, "Multimode imaging in the thermal infrared for chemical contrast enhancement. Part 2: simulation driven design," Anal. Chem. 82, 8421–8426 (2010).
10. H. Brooke, M. R. Baranowski, J. N. McCutcheon, S. L. Morgan, and M. L. Myrick, "Multimode imaging in the thermal infrared for chemical contrast enhancement. Part 3: visualizing blood on fabrics," Anal. Chem. 82, 8427–8431 (2010).
11. S. Sumriddetchkajorn and Y. Intaravanne, "A hyperspectral imaging-based credit card verifier structure with adaptive learning," Appl. Opt. 47, 6594–6600 (2008).
12. S. Sumriddetchkajorn and Y. Intaravanne, "Data-nonintrusive photonics-based credit card verifier with a low noise rejection rate," Appl. Opt. 49, 764–771 (2010).

13. S. Sumriddetchkajorn, K. Suwansukho, and P. Buranasiri, "Two-wavelength spectral image-based Thai rice breed identification," Proc. SPIE **7715**, 771501 (2010).
14. K. Suwansukho, S. Sumriddetchkajorn, and P. Buranasiri, "Demonstration of a single-wavelength spectral-imaging-based Thai jasmine rice identification," Appl. Opt. **50**, 4024–4030 (2011).
15. Y. Intaravanne, S. Sumriddetchkajorn, and J. Nukeaw, "Cell phone-based two-dimensional spectral analysis for banana ripeness estimation," Sens. Actuators B **168**, 390–394 (2012).
16. J. H. Wagner, "Applications of UV-visible spectral imaging in forensic science," Ph.D. dissertation (University Of Auckland, 2008).
17. G. M. Miskelly and J. H. Wagner, "Using spectral information in forensic imaging," Forensic Sci. Int. **155**, 112–118 (2005).
18. N. Rajaram, A. Gopal, X. J. Zhang, and J. W. Tunnell, "Experimental validation of the effects of microvasculature pigment packaging on in vivo diffuse reflectance spectroscopy," Lasers Surg Med. **42**, 680–688 (2010).
19. http://www.chemimage.com/docs/product.../CI-productsheet-CONDOR.pdf, "Condor Wide-field hyperspectral imaging system," ChemImage product sheet PSREV005 (2010).
20. https://www.chemimage.com/docs/application-notes/forensics/CI-appnote-Visualization-of-Bloodstains.pdf, "Hyperspectral imaging enables straightforward visualization of bloodstains," ChemImage Application note, ANREV002 (2010).
21. http://www.chemimage.com/news/newsletter/forensic_focus/november2010.aspx, "Hypserspectral imaging: a high-contrast alternative to visualizing blood spatter and stains," Forensic Focus E-Newsletter 11 (2010).
22. http://www.chemimage.com/products/instrumentation/examiner/, "HSI Examiner 1000," ChemImage product sheet PSREV001 (2012).
23. S. Janchaysang, S. Sumriddetchkajorn, and P. Buranasiri, "Tunable filter-based multispectral imaging for detection of blood stains on construction material substrates. Part 2. Realization of rapid blood stain detection," Appl. Opt. **51**, xx–xx (2012).
24. W. G. Zijlstra and A. Buursma, "Spectrophotometry of hemoglobin: absorption spectra of bovine oxyhemoglobin, deoxyhemoglobin, carboxyhemoglobin, and methemoglobin," Comp. Biochem. Physiol. B **118**, 743–749 (1997).
25. E. Pirard, "Multispectral imaging of ore minerals in optical microscopy," Mineral. Mag. **68**, 323–333 (2004).
26. R. Shogenji, Y. Kitamura, K. Yamada, S. Miyatake, and J. Tanida, "Multispectral imaging using compact compound optics," Opt. Express **12**, 1643–1655 (2004).
27. J. M. Medina, L. M. Pereira, H. T. Correia, and S. Nascimento, "Hyperspectral optical imaging of human iris in vivo: characteristics of reflectance spectra," J. Biomed. Opt. **16**, 076001 (2011).
28. P. Kubelka, "New contributions to the optics of intensely light scattering materials. Part I," J. Opt. Soc. Am. **38**, 448–457 (1948).
29. M. J. C. van Gemert, S. L. Jacques, H. J. C. M. Sterenborg, and W. M. Star, "Skin optics," IEEE Trans Biomed. Eng. **36**, 1146–1154 (1989).
30. W. F. Cheong, S. A. Prahl, and A. J. Welch, "A review of the optical properties of biological tissues," IEEE J. Quantum Electron. **26**, 2166–2185 (1990).
31. M. M. Lana, M. Hogenkamp, and R. B. M. Koehorst, "Application of Kubelka–Munk analysis to the study of translucency in fresh-cut tomato," Innov. Food Sci. Emerg. Technol. **7**, 302–308 (2006).
32. L. M. Schabbach, F. Bondioli, and M. C. Fredel, "Colouring of opaque ceramic glaze with zircon pigments: formulation with simplified Kubelka–Munk model," J. Eur. Ceram. Soc. **31**, 659–664 (2011).
33. S. Shibusawa, "On-line real time soil sensor," in *Proceedings 2003 IEEE/ASME International Conference on Advanced Intelligent Mechatronics* (2003), pp. 1061–1066.
34. L. Yang, "Characterization of inks and ink application for ink-jet printing: model and simulation," J. Opt. Soc Am. A **20**, 1149–1154 (2003).
35. R. Berns, J. Kreuger, and M. Swicklik, "Multiple pigment selection for in painting using visible reflectance spectrophotometry," Stud. Conserv. **47**, 46 (2002).
36. R. S. Berns, "Spectral modeling of a dye diffusion thermal transfer printer," J. Electron. Imaging **2**, 359–369 (1993).
37. R. H. Bremmer, A. Nadort, T. G. van Leeuwen, M. J. van Gemert, and M. C. Aalders, "Age estimation of blood stains by hemoglobin derivative determination using reflectance spectroscopy," Forensic Sci. Int. **206**, 166–171 (2011).
38. W. G. Zijlstra, A. Buursma, and W. P. Meeuwsen-Van der Roest, "Absorption spectra of human fetal and adult oxyhemoglobin, de-oxyhemoglobin, carboxyhemoglobin, and methemoglobin," Clin. Chem. **37**, 1633–1638 (1991).
39. T. Asakura, K. Minakata, K. Adachi, M. O. Russell, and E. Schwartz, "Denatured hemo-globin in sickle erythrocytes," J. Clin. Invest. **59**, 633–640 (1977).
40. http://en.wikipedia.org/wiki/Sensitivity_and_specificity (March 2012).
41. D. R. Busch, W. Guo, R. Choe, T. Durduran, M. D. Feldman, C. Mies, M. A. Rosen, M. D. Schnall, B. J. Czerniecki, J. Tchou, A. DeMichele, M. E. Putt, and A. G. Yodh, "Computer aided automatic detection of malignant lesions in diffuse optical mammography," Med. Phys. **37**, 1840–1849 (2010).
42. M. U. Akram, A. Tariq, M. A. Anjum, and M. Y. Javed, "Automated detection of exudates in colored retinal images for diagnosis of diabetic retinopathy," Appl. Opt. **51**, 4858–4866 (2012).
43. M. D. Adamson and S. J. Rehse, "Detection of trace Al in model biological tissue with laser-induced breakdown spectroscopy," Appl. Opt. **46**, 5844–5852 (2007).
44. I. Leonard, A. Alfalou, and C. Brosseau, "Spectral optimized asymmetric segmented phase-only correlation filter," Appl. Opt. **51**, 2638–2650 (2012).
45. M. Amini, "Novel design of an optical probe for detecting perfusion changes in Buccal tissue," IEEE Sens. J. **12**, 1861–1867 (2012).

Tunable filter-based multispectral imaging for detection of blood stains on construction material substrates part 2: realization of rapid blood stain detection

Suwatwong Janchaysang,[1] Sarun Sumriddetchkajorn,[2,*] and Prathan Buranasiri[1]

[1]Physics Department, Faculty of Science, King Mongkut's Institute of Technology Ladkrabang, Bangkok, Thailand

[2]Intelligent Devices and Systems Research Unit, National Electronics and Computer Technology Center, National Science and Technology Development Agency, Ministry of Science and Technology, 112 Thailand Science Park, Phahonyothin Road, Klong 1, Klong Luang Pathumthani 12120, Thailand

*Corresponding author: sarun.sumriddetchkajorn@nectec.or.th

Received 15 January 2013; revised 22 May 2013; accepted 3 June 2013; posted 4 June 2013 (Doc. ID 183538); published 5 July 2013

Based on the blood stain detection method and criteria established in part 1 of this article, we combine and organize all necessary tasks to realize the multispectral imaging-based rapid blood stain detection system. To rapidly detect blood stains on the test surface, the developed system automatically captures the spectral images, extracts their spectral data, determines the positions of blood stains, and accurately highlights the positions of blood stains on the display. To achieve such a system, several tasks are newly introduced, including adjustment of camera exposure times to prevent image saturation or excessive darkness, the search for the sampled clean positions of the substrate to determine the substrate reflectance spectrum, and suitable detection procedures and proper arrangement of criteria to eliminate unnecessary calculations. Parallel processes between image capturing and blood stain identification help shorten the time for blood stain identifications despite a large amount of spectral data to be processed. The developed system can identify blood against several other reddish brown stains on several substrates. The measured average identification times on different test surfaces range from only 23.3 to 28.7 s, including the image capturing process. © 2013 Optical Society of America

OCIS codes: (110.4234) Multispectral and hyperspectral imaging; (120.0120) Instrumentation, measurement, and metrology; (120.4630) Optical inspection; (100.0100) Image processing; (100.2960) Image analysis; (150.1488) Calibration.

http://dx.doi.org/10.1364/AO.52.004898

1. Introduction

Crime scene investigation often involves presumptive blood stain detection. Several approaches have been used or proposed as presumptive blood stain detection methods. Chemical methods produce visible traces due to chemical reactions between heme groups in red blood cells (RBCs) and active reagents [1–3]. Nevertheless, the methods usually bring high false-positive rates due to nonspecificity of the reactions, wash away evidence, and produce chemical wastes. Several noncontact approaches are used to correct the problems. For example, ultraviolet (UV) light sources can make visible the blood spatters on fluorescent substrates, such as some clothes and papers, because blood does not exhibit fluorescent trace all over the visible spectrum [4,5]. Unfortunately, UV

1559-128X/13/204898-13$15.00/0

light can possibly destroy DNA in blood. Infrared imaging can also make visible faint blood stains on dark-colored clothes, because blood absorbs near infrared radiation (700–1000 nm) while most fabrics reflect it [6,7]. Another proposed method is multimode infrared imaging, which combines the measurement of infrared reflectance, thermal emission, and thermal diffusion rates to detect faint blood against other stains [8–10]. However, the approach has been demonstrated only for the detection of blood stain on fabric substrates. Differential spectral imaging between 415 and 440 nm wavelengths was proposed to highlight blood stain areas, but with only two wavelengths, the system specificity is low [11,12]. In addition, due to the granular nature of RBCs in blood stains, to the best of our knowledge, there are no noncontact reflective approaches that have been proved to be able to detect blood stain on a variety of substrates. The commercially available CONDOR wide field hyperspectral imaging (HIS) system [13–15] and its newest version HIS examiner systems [16] from ChemImage are designed for several tasks of forensic investigations, including visualization of fingerprints, questioned documents, inks, gun-powder residue, and blood stains. However, their blood stain detection makes use of visible to near-infrared contrast enhancement techniques, which have been focused on visualization of the blood stain on dark fabrics.

In part 1 of this work [17], we have established the multispectral imaging based blood stain detection criteria and method that can be used to detect blood stains on several kinds of substrates. To establish the criteria, we first capture several multispectral images of blood and other different types of reddish–brown stains, such as coffee, cocoa drink, soy sauce, mud, and ketchup on substrates, such as gypsum, wood, concrete boards, and tiles. Then, with the white reference calibration method, we collect a number of sampled reflectance spectra of those stains, which are found to be extremely substrate independent. To lessen the dependency of the substrate on the spectra, we apply Kubelka–Munk (KM) theory to the collected stain reflectance spectra. The blood stain detection criteria are then established based upon the less substrate-dependent KM absorbance spectra. We validate the criteria by using them to identify blood on different spectral images of the stain surfaces and evaluate sensitivity and specificity of the system.

Yet, the established method is far from a real-world application. In realization of a blood stain detection system, several issues arise in making the technique practical. First, since our blood stain detection method is operated by sequentially eliminating spatial points (a group of 3×3 adjacent pixels) in the spectral images, mathematically identified as not corresponding to blood using a series of criteria, the system must involve several processing steps and have a large amount of multispectral data to be accounted for. In part 1 of this article [17], we did not demonstrate the real-time detection, but instead detected blood stains from the already-captured multispectral images of the test surfaces. Even so, the process took a few minutes. To make the blood stain detection system as fast and automatic as possible, all the procedures, including image capturing, criteria application and so on, must be well planned. Second, our blood detection process requires determination of the substrate reflectance spectrum. In part 1 of this article [17], we manually located the clean substrate area on the surface to find the substrate reflectance spectra. Instead, the system should automatically search for locations of the clean substrate and determine its reflectance spectrum. Third, crime scene investigation may cover large search areas and a wide variety of colors and textures of substrates. Given usually spiky spectral shapes of the combined response of the multispectral imaging instruments, the captured spectral image can be easily saturated or darkened, which therefore can deteriorate the performance of the system, implying that obtaining suitable multispectral data is nontrivial. Moreover, the image test surface may contain faint and dark stain spots that could potentially correspond to blood. In the first part of this article [17], we captured spectral images with several exposure times and manually selected the spectral images that are usable. In fact, forensic investigators should not waste much of their valuable time setting up or adjusting lighting conditions to suit each scene by themselves. The ideal blood stain detection system should be automatically adjusted itself for any kinds of substrates and environmental conditions. Detection systems should also adapt its image capturing to collect usable spectral data from all those faint and dark spots in the field-of-view. All the above problems are evidently unique for our established blood stain detection method. As of our knowledge, no application needs to deal with these integrated problems to make the near real-time blood stain detection system.

In this part of the article, we demonstrate the system that can correct the above problems and realize the rapid blood stain detection based on our blood detection criteria established in part 1 of this work [17]. In this discussion, we explain how the above problems are dealt with. In Section 2 we briefly review the physical system and describe the sample materials used in the experiment. The key features are included in Sections 3–6. Section 3 describes the automatic calibration procedure, in which special data manipulation in the form of multispectral data arrays is proposed. The arrays can be easily modified during the blood stain detection to exclude the spatial points, already identified as not corresponding to blood, and can effectively handle a large amount of multispectral data. Section 4 illustrates the arrangement of all tasks combined to realize the rapid and automatic blood stain detection system. In this section, we propose the parallel procedures between the image capturing process and blood stain identification process. This configuration can make use of

the CPU and memory efficiently to save time for detection. In Section 5, we discuss the automatic search for sample substrate positions on the test surface images and automatic determination of substrate reflectance, so that the users do not have to waste time to do that by themselves. Section 6 depicts the automatic adjustment of camera exposure times to obtain the usable spectral images. All of the tasks introduced in Sections 3–6 are performed automatically by the system. Section 7 gives the results in terms of blood stain position identification and time taken, and Section 8 concludes the article. It is recommended that the reader first read part 1 of this work [17] before and along with this part because many issues discussed here require knowledge from the first part.

2. Multispectral Imaging Hardware and Materials

A. Multispectral Imaging Setup

The multispectral imaging setup used in this part of the article is shown in Fig. 1. Physically, it is the same liquid-crystal-tunable filter (LCTF)-based multispectral imaging system as described in the first part of this work [17]. In the setup, two metal halide lamps (Philips CDM–R 70W/942) are used to illuminate a 10.5 cm × 10.5 cm detection zone. These two lamps yield full spectral range over the entire visible region. They illuminate the whole test surface with a measured uniformity of greater than 75%. The sample surface is placed 30 cm right below the camera (Basler Scout scA750-60gc) of our LCTF-based multispectral imaging system. The camera allows programmatic control of exposure time, ranging between 0.12 and 125 ms. A personal laptop computer equipped with our LabVIEW-based program is used for both controlling the image capturing process of the camera and the spectral scanning process of the LCTF. The computer is Acer, model Aspire 4736Z, with the CPU speed of 1.18 GHz and 956 MB of random access memory (RAM). The LCTF (Varispec, VIS-HC-20) has a 20 mm circular aperture and its specified bandwidth is 7 nm with a wavelength scanning range from 400 to 720 nm. The camera's area of interest is set to 360 × 339 pixels, a rectangular area just to cover 10.5 cm visible circular field of the image. The difference from part 1 of this work [17] is the new procedure for real-world blood stain detection that takes into account all aforementioned issues. This new procedure will be described in Section 5.

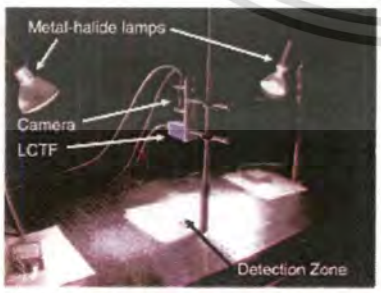

Fig. 1. Multispectral imaging setup used to demonstrate rapid blood stain detection.

B. Sample Materials

In this work, new sets of substrates and stain samples, shown in Figs. 2(a)–2(f), are prepared show that the criteria, established in part 1 of this work [17], can be applied to different samples and substrates. The stains include bovine blood, coffee, rust, cocoa drink, dirt, tea, and chicken essence soup. The substrates used in the experiment are chosen to have a variety of colors and textures, including a gypsum board, tiles (white, blue, and brown), white-painted concrete, and an artificial wood board. The sample arrangement [Fig. 2(g)] is similar for all substrates. Thirty-six stain spots are arranged in a 6 *cm* × 6 *cm* rectangular area so that they can be seen at the same time in one image. The size of the stain spots varies between 0.2 and 0.5 cm in diameter. The horizontal and vertical distances between each pair of stain spots are about 1.2 cm apart. Each substance is stained with different, but unspecified, concentration values. We also put four extra long stains from blood, coffee, cocoa, and chicken essence soup outside the above area.

3. System Calibration

Our multispectral imaging system is calibrated with the white reference calibration method as previously performed in part 1 of this work [17]. According to the method, reflectance spectrum at any spatial point over the test surface is recovered by comparing a camera's digital responses extracted from the spectral image cube of white reference paper with the digital responses at the same spatial point from the spectral image cube of the test surface. The calibration procedure, shown in Fig. 3, is to be performed for just one time at the beginning of each investigation session to prepare calibration data necessary for use in the blood stain detection procedure. Once the system is calibrated, it can be used to detect blood stains many times on several substrates without the need for recalibration. In this part of the article, for more user convenience, we have designed a system that can automatically perform all necessary calibration tasks, including capturing spectral images with suitably adjusted exposure times and preparation of the calibration data for use in blood detection stage. The user simply has to place a stack of white paper sheets of known reflectance spectrum on the detection zone and start calibration. The calibration procedure starts with capturing 530 and 470 nm spectral images. Then, the system quickly determines appropriate exposure times for capturing all spectral images. The details about how the system determines the appropriate exposure times will be described separately in Section 6. Once suitable exposure times

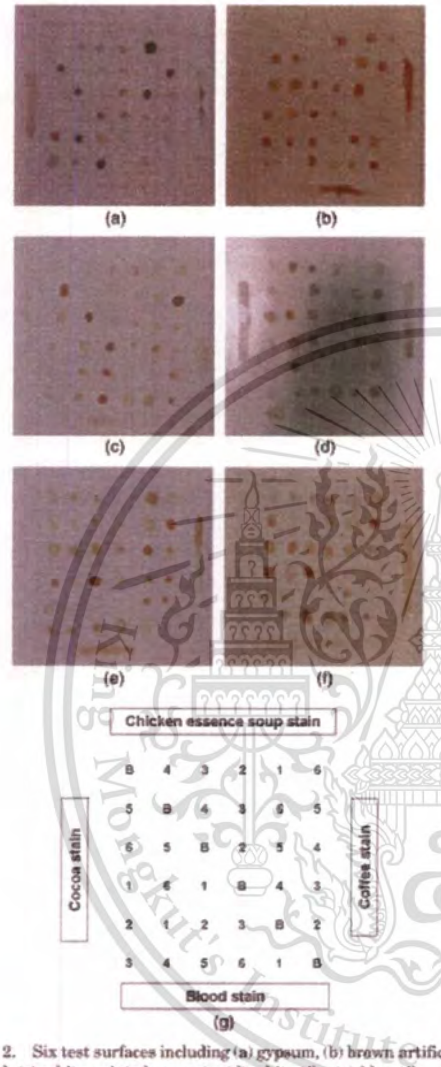

Fig. 2. Six test surfaces including (a) gypsum, (b) brown artificial wood, (c) white-painted concrete, (d) white tile, (e) blue tile, and (f) rough brown tile. Each substrate is stained with blood and six other substances. The arrangement of stains on all substrates is shown in (g), in which B represents the blood stain and the numbers represent stains as follows: 1. coffee, 2. rust, 3. cocoa, 4. dirt, 5. tea, and 6. chicken essence soup. Four long stains are also deposited on the rest of the extra areas around the stain spots.

are determined, the system captures 61 spectral images, one by one, in numerical order of wavelengths starting from 470 to 710 nm with a uniform wavelength separation of 4 nm and stores the images in the system. The 530 and 470 nm spectral images are also recaptured. Because each opened spectral image requires occupation of space in the RAM of

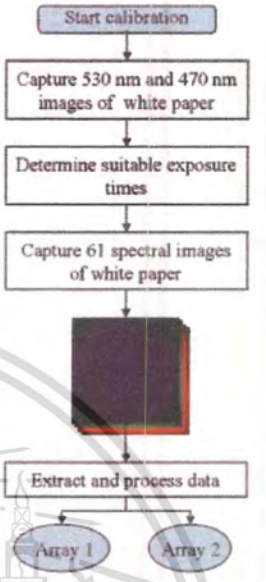

Fig. 3. Calibration procedure. The calibration process yields calibration data in the form of Array 1 and Array 2.

the computer system, opening several spectral images at the same time occupies too much of the RAM, which highly affects the performance and speed of the system. To maximize the speed, our system reserves RAM space for only one spectral image during the image capturing and data processing. After each spectral image is captured, it must be saved in the permanent memory of the system (i.e., the hard disk of the computer) and closed. The next captured spectral image then can reuse the same RAM space.

Since the speed is not quite an issue during calibration, preparation of calibration data is started after all spectral images are captured. According to our proposed calibration method [17], a multispectral image cube is transformed into compact and ready-to-use multispectral data arrays. To prepare the arrays, the system reopens the saved spectral images one by one, extracts digital responses from each spectral image, prepares the calibration data, and arranges them into the arrays shown in Fig. 4. To save time in the blood detection stage, at each spatial point of each wavelength channel, all calculations that can possibly be done during calibration are immediately performed and recorded as a single calibration number as

$$w(\lambda_k) = \frac{[W(\lambda_k) - D]/\tau_W(\lambda_k)}{R_W(\lambda_k)}. \quad (1)$$

where $W(\lambda_k)$ is the spectral camera's digital response from a single spatial point of the spectral image of the white reference (e.g., a white paper), D is the

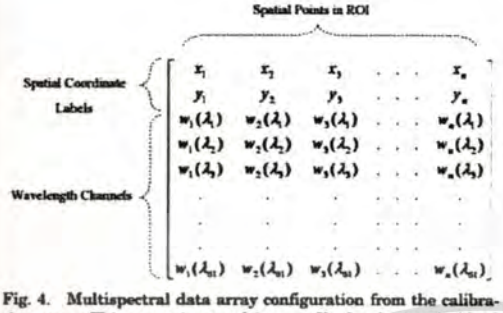

Fig. 4. Multispectral data array configuration from the calibration stage. This array is stored in text file for the use in blood detection stage.

camera's dark response, $r_W(\lambda_k)$ is the wavelength dependent camera's exposure time, and $R_W(\lambda_k)$ is the known reflectance spectrum of the white paper [17]. The subscript k of the variable λ represents the number of the sampled wavelength channel. In this part of the article, the channel number k is an integer ranging from 1 to 61, where $\lambda_1 = 470$ nm, $\lambda_2 = 474$ nm,..., and $\lambda_{61} = 710$ nm, respectively.

The camera's dark response is predetermined by capturing the image while the camera's aperture is covered by slid. There are two kinds of arrays related to multispectral data stored in the system. Both have the same configuration as shown in Fig. 4, but are intended for different purposes. The first array, namely Array 1, is intended for the purpose of quick sampled substrate position search, substrate reflectance determination, and exposure time adjustment. The second array (Array 2) is intended for the purpose of blood stain identification. The rows of both arrays represent spectral dimension while the columns represent the spatial dimension of the multispectral image cube. There are 63 rows in the arrays that are composed of 61 rows representing 61 calibration numbers from 61 wavelength channels, and 2 additional rows at the top of the array for tagging the x–y spatial coordinates of the images. In Array 1, $w(\lambda_k)$ are sampled from every 5×5 pixel all over the image field-of-view (nonaveraged). As a result, only $72 \times 68 = 4896$ pixels are initially sampled to constitute Array 1. In Array 2, all pixels in the image are taken into account. Digital responses from a single spatial point are averaged from a group of 3×3 adjacent pixels, and then calculated into a single calibration number $w(\lambda_k)$. So, there are $120 \times 113 = 13,560$ spatial points that represent the physical dimension of the image. The columns of Array 2 represent spatial points in the region of interest (ROI). In this work, we define the ROI as all spatial points that still possibly correspond to blood stains. Array 2 has a larger number of columns than the Array 1 and calculation from all pixels is required, thus taking a much longer time to process.

Since our camera's field-of-view is limited by the circular aperture of the LCTF, the area in the image outside the circular field-of-view is too dark for the system to effectively determine reflectance and identify blood stain. Processing data from this outside area would waste time and memory reserve of the computer. Therefore, it is preferable to exclude this dark area from the ROI as early as in the calibration stage. Normally, the 530 nm image of white paper is very bright all over the field-of-view. Our experimental record reveals that the pixels whose $W(530\text{ nm}) < 40$ correspond to the dim area outside the circular field-of-view of the LCTF. So, we exclude those pixels early from the arrays just after the first taken 530 nm spectral image of the white paper is processed. In our system, the number of spatial points in the ROI is usually reduced to 12,000–13,000 after elimination. However, this step is unnecessary in the system whose field-of-view is just limited by the field-of-view of the camera itself, not the LCTF. Therefore, after calibration process, Array 2 has 63 rows and n columns, where n is the number of spatial points remaining in the ROI. After those two initial multispectral data arrays are constructed, they are stored in the system in the form of text files for use in the blood detection stage. According to our experimental record, the initial multispectral data arrays are still valid for blood stain detection even if the lamps and the computers are turned off and turned back on again many times, as long as the physical setup is unaltered. This is preferable because the users do not have to recalibrate the system even when the computer is turned off and turned back on. The entire calibration process, including spectral image capturing of white reference paper and data processing, takes between 55 and 68 s.

4. Proposed Rapid Blood Stain Detection Procedure

At the beginning of our blood detection stage, the initial multispectral arrays from the calibration stage are quickly extracted from the aforementioned text files to get ready for blood stain detection. Then, the user can place the test surface on the detection zone and start blood detection right away. The proposed rapid blood stain detection procedure is shown in Fig. 5.

Because of the need for speed in the blood stain detection, the multispectral image capturing process and the blood stain identification process are run simultaneously in parallel. Immediately after the first image (530 nm) is captured and saved, the blood stain identification process starts. Therefore, during blood stain detection, the system has to reserve RAM space for two images, one for the image capturing process and the other for the blood stain identification process.

A. Image Capturing Process

Before capturing each spectral image, the system sends the command to the LCTF to tune to a designated wavelength and then waits 200 ms for the LCTF to physically respond and tune to the wavelength before the exposure begins. In fact, the

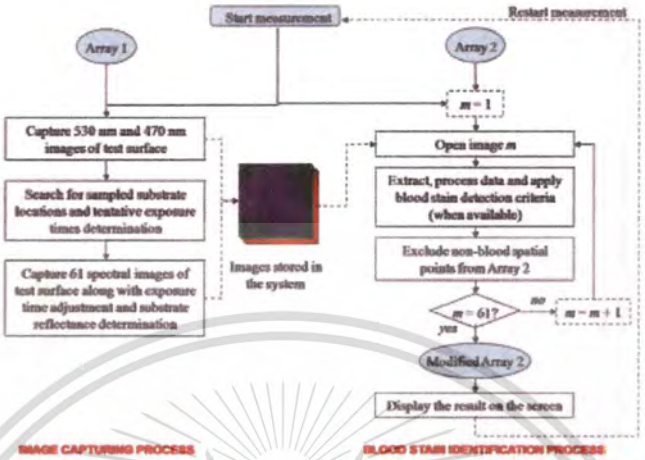

Fig. 5. Proposed blood stain detection procedure. Parallel process between spectral image capturing and blood stain identification allows for fast detection.

response time for this LCTF model given by the manufacturer is about 50 ms. However, since the response time depends on a number of factors, such as ambient temperature, we decide to wait longer (i.e., 200 ms) to ensure that the LCTF gives the desired stable filtering wavelength window. In the blood stain detection stage, spectral images of the test surface are not captured and processed in numerical order of wavelengths. Since our system works by gradually eliminating spatial points proven to be not corresponding to blood stain, the image capturing order and criterion order are arranged according to its tentative ability to exclude other stains (its specificity) to identify stains of blood as quickly as possible. The first two spectral images to be captured are 530 and 470 nm spectral images. These two spectral images are used in preliminary processing, including quick sampled substrate position searching (will be described in Section 5) and fast determination of the tentative camera's exposure times for the rest of the images (which will be described in Section 6). The system then captures another seven spectral images to be tested by preliminary criteria. In this work, preliminary criteria are defined as the criteria that use reflectance or absorbance values as only spectral parameters to distinguish blood from other surfaces. After each spectral image is captured, the system can quickly determine substrate reflectance and save the spectral image in the system before capturing the next spectral images (also depicted in Section 6). The capturing order for preliminary spectral images is 530, 470, 546, 518, 502, 710, 586, 642, and 622 nm, respectively. Then, the system captures the remaining spectral images in numerical order of wavelength to be used for polynomial coefficient criteria but skips the already captured spectral images.

Performing spectral image capturing and blood stain identification processing in parallel has the advantage of reducing time for blood detection. During the 200 ms waiting for the LCTF to respond, and during the exposure of the camera (50–125 ms), the computer waits idly for the wavelength tuning and the camera to return the image. At these waiting periods, the measured CPU usage is very low (about 2%–3%), providing us with an opportunity to efficiently extract, process multispectral data, and apply the blood stain detection criteria for the already captured spectral images.

B. Blood Stain Identification Process

The blood stain identification processing order is the same as that of image capturing order. To identify blood stain, the system reopens and processes one spectral image at a time. For each opened spectral image, the system extracts digital responses, takes the average value, and processes data, one spatial point at a time, in the ROI. For each spatial point, the test surface reflectance value $[R_T(\lambda_k)]$ is calculated. Note that the reflectance value of both the substrate and any spatial point on the surface can be recovered by the following expression:

$$R(\lambda_k) = \frac{t(\lambda_k)}{w(\lambda_k)}, \tag{2}$$

where $t(\lambda_k) = [T(\lambda_k) - D]/\tau_T(\lambda_k)$ can be easily determined during the blood stain identification process [17]. The values $T(\lambda_k)$ and $\tau_T(\lambda_k)$ are the digital response on the test surface image and the exposure time of the camera at the corresponding wavelength channel, k, respectively. The calibration number $w(\lambda_k)$ is extracted from the calibration array. Equation 2 is valid only if the incident light on the

white reference surface and the substrates are almost identical. This suggests that the would be *in situ* blood stain detection device is possible but must be equipped with built-in light sources and shade covers. Once the reflectance values are determined, the (KM) absorbance at each spatial point on the test surface can be obtained immediately using

$$\frac{R_T(\lambda_k)}{R_S(\lambda_k)} = 1 - \frac{K(\lambda_k)}{S(\lambda_k)}\left(\sqrt{1+\frac{2K(\lambda_k)}{S(\lambda_k)}}+1\right). \quad (3)$$

where $R_T(\lambda_k)$ is the reflectance value of any point on the test surface, $R_S(\lambda_k)$ is the reflectance value of the substrate, and $S(\lambda_k)$ is the scattering at any spatial point on the surface [17,18]. Here, for simplicity, we assume Lorentz–Mie scattering as $S(\lambda_k) = S_0(\lambda_k/\lambda_0)^{-0.4}$ and we take $\lambda_0 = 450$ nm and $S_0 = 1$ for all points on the test surface. Remember that the average substrate reflectance value $[R_S(\lambda_k)]$ is quickly determined during image capturing by the process to be discussed in Section 5 of this part of the article. The introduction of Eqs. 1–3 to our blood stain detection method can be found in part 1 of this article [17].

C. Application of Blood Stain Detection Criteria

Once the reflectance and KM absorption values of the currently processed spectral image are determined, the system immediately applies the assigned blood detection criteria if the criteria are available on the wavelength. For the sake of forensic investigation, the spatial points on the surface remain in the ROI until they are identified as not corresponding to blood stains. As soon as any spatial points are identified by each established criterion so they do not correspond to the blood, those spatial points are not to be processed again in the next spectral images. In many interesting scenes, the areas corresponding to substrate are large compared to those areas corresponding to the area corresponding to blood. As mentioned in part 1 of this work [17], it is advantageous to eliminate the substrate locations on the test surface from ROI as early as possible. The 530 and 470 nm spectral images are employed to eliminate substrate locations using the selection criteria $R_T(530\text{ nm})/R_S(530\text{ nm}) \le 0.97$ and $R_T(470\text{ nm})/R_S(470\text{ nm}) \le 0.98$. The spatial points that do not satisfy these conditions usually correspond to the substrate or very thin stains. This results in reduction of spatial points to be processed for the rest of the spectral images, especially in cases where the stain area on the image is small relative to the substrate area. After the processing and criteria application on each spectral image are finished, the multispectral data array (Fig. 4) is modified by removing the columns identified as nonblood from the array and also replacing $w(\lambda_k)$ in the row corresponding to the wavelength channels by $K(\lambda_k)$. As a result, the size of the blood detection array becomes smaller or at least remains the same after any image is processed. Another 13 preliminary criteria, such as those exemplified in Figs. 7(a)–7(c) of part 1 of this work [17], are then applied during the processing of the next seven spectral images. Preliminary criteria are relatively quick to process because they make use of only a few spectral images. After that, the system processes the rest of the spectral images. During this time, the system extracts absorption values from spectral images to perform polynomial fitting and applies another 11 criteria to the polynomial coefficient when appropriate. Examples of the criteria based on polynomial fits are shown in Figs. 7(d)–7(f) of part 1 of this work [17]. After all 61 spectral images are processed and all 26 criteria are applied, the remaining spatial points in the two-dimensional array are the final spatial points identified by the system as possibly corresponding to blood stains. Those spatial points are then masked with 2×2 red pixels on the result screen. After the blood detection process is finished, the user can place another test surface on the detection zone and restart the blood stain detection process. The blood stain detection can indefinitely reuse the multispectral data array obtained during calibration without recalibration. The result images show spatial points remaining in the ROI on gypsum and artificial wood board test surfaces just after the first two wavelengths are processed [Fig. 6(a)], and after all the preliminary criteria are applied [Fig. 6(b)]. The arrangement of the images based on substrates is similar to the arrangement of the photo images in Figs. 2(a)–2(f). The arrangement of stains in any single result image is already provided in Fig. 2(g). The red diagonal rectangular frame on each image encompasses six blood stain spots. The long horizontal stain at the bottom of each image also corresponds to blood. The two result images in Fig. 6(a) clearly indicate that most substrate areas are eliminated from ROI after the first two spectral images are processed. In most cases for all test surfaces, the spatial points are reduced from about 12,000 points at the beginning of blood stain detection stage to about 1000–2100 points after just the first two images are applied and are decreased further as more spectral images are processed. This is good in terms of increasing the speed of the system so that a small number of spatial points are to be processed in the latter images. Normally, these result images are not shown to the user during blood detection on the screen in the real setup to save time for processing. In the real system, only the final result images would be shown to the user at the end of the process. Figure 6(b) shows the spatial point left in ROI after all nine preliminary images are processed. Normally, for our stain configuration presented in this experiment, 100–400 spatial points remain in the ROI after preliminary images. The final result images on gypsum and artificial wood test surfaces, corresponding to Figs. 6(a) and 6(b), are shown in Fig. 6(c). It is evident that final result images are improved just a little from those using just preliminary criteria. However,

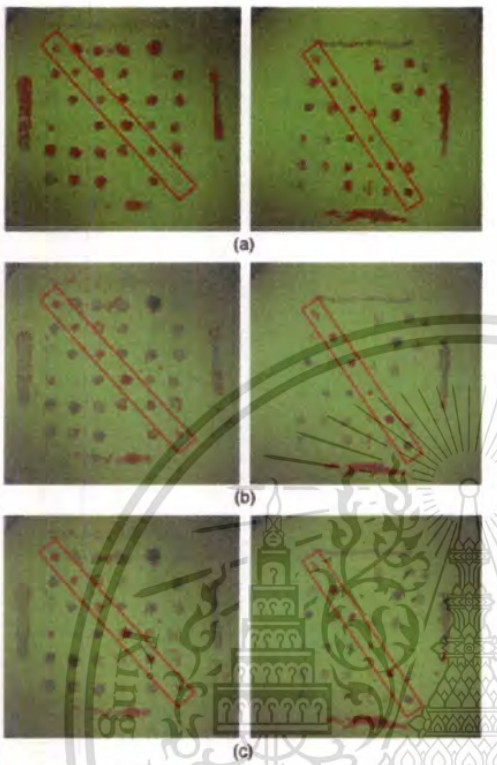

Fig. 6. Result images of gypsum (left), and artificial wood (right) test surfaces show spatial points (masked with red) remaining in ROI, after (a) first two spectral images, (b) nine spectral images associated with preliminary criteria, and (c) all spectral images with all criteria are processed. The red diagonal frame on each image highlights the real blood stains spots on the substrate.

for the interest of forensic investigation, this little improvement might be of important values.

5. Substrate Reflection Determination

In our blood stain detection method, the recovery of substrate reflectance spectrum $[R_S(\lambda_k)]$ is a requirement in finding the KM absorption spectra on the test surface (see Eq. 3). The substrate reflectance spectrum could be obtained by having the users capture separate multispectral images of the clean substrate area and then having the system extract the spectrum from those images just before performing blood stain detection, as we did in part 1 of this work [17]. However, the method would be inconvenient and time consuming. Furthermore, stains may be scattered over the test surface, and in some scenes, the large clean substrate area may be difficult to manually find. Therefore, the best way to obtain $R_S(\lambda_k)$ is to have the system automatically search for the sampled unstained substrate locations in the images of the test surface, and then determine

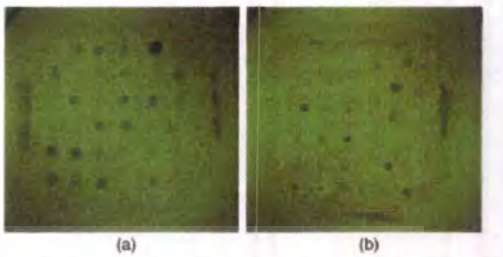

Fig. 7. Determined sampled substrate positions (masked with red) by our substrate position search method on (a) gypsum and (b) artificial wood.

the reflectance spectrum from those locations by itself during detection. It is also preferred that substrate locations must be determined as early as the first few spectral images are captured so that the substrate reflectance can be quickly extracted from each following spectral image. To economize the time for substrate reflection search and determination, just every 5×5 pixels are uniformly sampled all over the image field-of-view using Array 1. From the calibration stage, Array 1 contains the calibration numbers from those sampled pixels. Spatial sampling of the pixels has the advantage of lessening calculation, hence increasing the speed of finding substrate reflectance. In addition, it allows the system to quickly collect the substrate reflectance even if stains are scattered all over the spectral images of the test surface. The search for the substrate positions makes use of the first two captured spectral images (530 and 470 nm wavelength) in the blood detection stage. The wavelengths are selected because typical absorption of stains is relatively large at such low wavelengths. Therefore, the difference between the reflectance values of stains and the substrate are usually high and it is easy to distinguish between the stains and substrate locations from these spectral wavelengths. The system determines reflectance values at all sampled pixels from these two spectral images. Recall from Section 3 that the dim pixels outside field-of-view of the circular aperture are eliminated from consideration during calibration. Hence, it is very likely that correct reflectance spectra can be recovered from all sampled pixels in consideration. For each wavelength, (530 and 470 nm), the reflectance values of all sampled pixels are then sorted into 21 class intervals ranging from 0.20 to 1.00, with the class interval size of 0.04. Note that the first class has $0.20 < R(\lambda_k) \leq 0.24$, while the last one has $0.96 < R(\lambda_k) \leq 1.00$.

The assumption was made that the substrate area would cover a majority of the area in the image. Even if the stain area is larger than that of the substrate, it is rare that the stain concentrations, hence reflectance values, are equal over the test surface. Presumably, the reflectance values that are most frequently found on the surface belong to the substrate. Accordingly, we take that the class interval that contains

the largest number of observations (the modal class) corresponds to the substrate area. This modal class is statistically easy to determine. For more accuracy, the pixels deemed as the substrate locations must have the reflectance values fall within the modal classes in both 530 and 470 nm spectral images. Those pixels whose reflectance values fall outside the modal class in both images, or fall within the modal class of only one of the two spectral images, are excluded from substrate locations by removing the corresponding columns from Array 1. After substrate location determination, the modified Array 1 then represents the sampled substrate locations in the images. Figure 7 shows examples of the resultant substrate locations highlighted in red pixels on gypsum and blue tile. It looks clear that the sampled locations determined by our method correspond to the true locations of the pure substrates. The time for substrate position search using 530 and 470 nm spectral images ranges from 31 to 78 ms. Once the sampled substrate pixels are determined, after each spectral image is captured, the system can quickly determine the average calibration number and the average digital response ($T_{AVG}(\lambda_k)$) from those pixels in the modified Array 1. The average substrate reflectance values $R_S(\lambda_k)$ at any spectral image can then be readily determined using Eq. (2). Figure 8 shows comparison between reflectance spectra of substrates determined by our method and by manual extraction from a large clean substrate area. The result of substrate reflectance recovery is, however sufficiently accurate, with accuracy of >95%. This indicates that the number of sample pixels is large enough, and the method is suitable to find the reflectance of the substrate. Also, the average digital responses $[T_{AVG}(\lambda_k)]$ obtained during substrate reflection determination are used to adjust exposure times of the later captured image to obtain appropriate image brightness. This process of exposure time adjustment will be explained in the Section 6. The substrate reflectance determination takes as quickly as 4–22 ms for each spectra image. This short range of time is preferred because substrate reflection determination and exposure time adjustment must be finished before the system can capture the next spectral image.

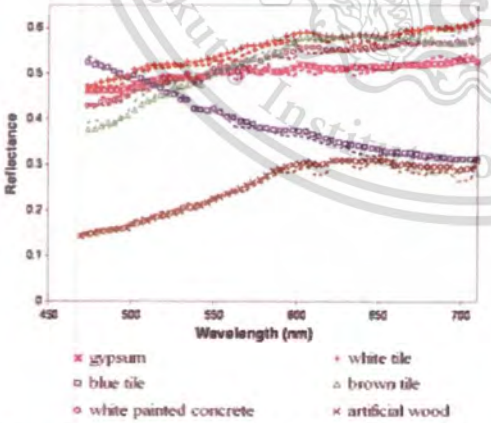

Fig. 8. Comparison between our substrate reflectance spectra determined by our substrate searching method (dotted lines) and by spectral recovery from the clean substrate area (different markers).

6. Rapid Exposure Time Adjustment

Although the white reference calibration and spectral reconstruction method can automatically correct for the spatial nonuniformity of illumination incident on the image surface, the raw camera's digital responses for all spectral images must lie within linear response range of the CCD pixel array for ease of analysis. Either saturated or too dark pixels would lead to incorrect blood detection. From our experimental observation, the acceptable linear response zone of our 8-bit camera ranges from 30 to 230. Moreover, to accomplish high signal to noise ratio (SNR), the digital responses not only must be kept within the linear zone but should also be kept as high as possible within the linear response zone. Small digital responses are more subjected to low signal to quantization noise ratio [19]. Figure 9(a) shows the calculated normalized camera digital responses while capturing spectral images of the white reference paper and all other six substrates if spectral images were captured at constant exposure time for all wavelength channels. The spectral shapes of the camera's digital responses are not uniform, but spiky due to the nonuniform spectral shape of the combined multispectral imaging instruments, especially the metal halide lamps. As a result, it is almost impossible to keep digital responses of all spectral images within the linear response zone if all spectral images are captured with constant exposure time. Our system's camera can controllably capture images at different exposure times. In part 1 of this work [17], for each scene, we captured several sets of multispectral images, each with a certain exposure time. Then, we manually selected the images whose exposure time yielded suitable brightness. The method was, however, very time consuming. In this part of our work, we intend to build the detection system that can automatically adapt its image capturing to any kind of surfaces by dynamically varying exposure times with wavelength channels. According to Fig. 9(a), the spectral shapes of the digital responses are not much different among different surfaces. This suggests that the spectral shape is dominated by the spectral shape of the combined imaging instruments. Our key idea is to establish exposure time basis function, in which the relative exposure times are inversely proportional to the normalized digital responses of the images to counteract the nonuniform spectral response of the imaging instruments. Since the images of the white paper reference surface and the images of the test surfaces are

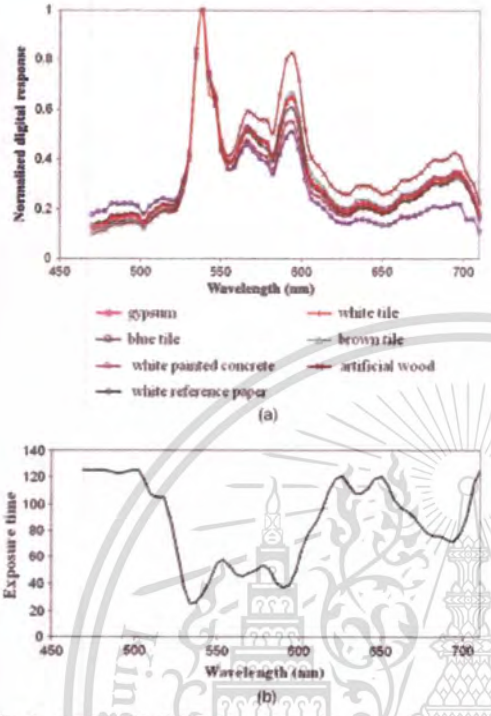

Fig. 9. (a) Normalized digital responses when spectral images of the white paper and six other substrates are captured. (b) Exposure time base used for luminance adaptation in this system.

different by nature, we consider the exposure time adjustment in the two stages separately in the two following subsections.

A. Exposure Time Adjustment during Calibration

Since the white paper surface is spatially uniform and its reflectance spectrum is constant, the digital responses of the spectral images of the white paper are more predictable than those of the test surfaces. To achieve high SNR, we prefer that the average digital responses in the field-of-view for all spectral images should be roughly 180. At this average level, the brightest areas in the field-of-view tend not to be saturated while dimmest areas still have high enough digital responses. With the relative spectral responses of the spectral images of the white paper shown in Fig. 9(a), and a little modification of Eq. (1), the exposure time basis for capturing spectral images of white paper $\tau_B(\lambda_k)$ shown in Fig. 9(b) are derived from $\tau_B(\lambda_k) = (180 - D)\tau_W(\lambda_k)/(W_{AVG}(\lambda_k) - D)$, where $W_{AVG}(\lambda_k)$ is the average digital responses from the sampled pixels of the captured white paper images, when the images are captured with corresponding exposure times of $\tau_W(\lambda_k)$. The acquired exposure time basis is kept in the permanent memory of the system. It is valid for a relatively long time since the spectral shape of the combined instruments change very slowly through the aging of the instruments.

During the calibration, the system captures the 530 nm spectral image first, extracts digital responses of pixels from Array 1, and takes the average into a single value $W_{AVG}(\lambda_k)$. The exposure times that will give the average digital response around 180, $\tau_{W180}(\lambda_k)$, for all wavelength channels can be readily determined by

$$\tau_{W180}(\lambda_k) = c_W \cdot \tau_B(\lambda_k). \quad (4)$$

Here, c_W is given by $c_W = (180 - D)/(W_{AVG}(530\ \text{nm}) - D)$.

B. Exposure Time Adjustment during Blood Stain Detection

Adjustment of the exposure time during blood stain detection is more complicated due to several reasons. First, the test surface is not spatially uniform, but may contain pale and dark spots that possibly correspond to blood stains. It is important to keep the digital responses on all of these spots high enough to achieve adequate SNR. Due to high absorption of blood stain, it is likely that the blood stain spots are dimmer than the substrate area. Our key idea is to keep the average digital responses at substrate locations at 180 at all wavelengths. At these average digital responses values, the dimmer stain spots still have the digital responses within the linear range of the camera. It is also does no harmed to let the spots brighter than the substrate saturate since they do not correspond to blood stains.

After the sampled substrate locations are determined using 530 and 470 nm spectral images (see Section 5), we take the average digital response from the sampled substrate locations of the 530 nm spectral image $T_{AVG}(530\ \text{nm})$. As mentioned earlier, the spectral shapes of digital responses are dominated by the spectral shape of the responses of the combined multispectral imaging instruments. Looking closely into Fig. 9(a), we find that the normalized responses of the white reference paper are approximately the average normalized digital values of all substrates. So, we also use the same exposure time basis $\tau_B(\lambda_k)$ for all test surfaces. The exposure times which give average digital value of 180 $[\tau_{T180}(\lambda_k)]$ for the rest of the spectral images can be determined the same way as during calibration:

$$\tau_{T180}(\lambda_k) = c_T \cdot \tau_B(\lambda_k). \quad (5)$$

where the constant $c_T = (180 - D)/(T_{AVG}(530\ \text{nm}) - D)$.

The second issue is that the substrates to be detected can be of any type or color, so their reflectance spectra are unpredictable. Unmonitored image capturing with the above exposure times can cause the image digital responses to fall out of the desired linear responses zone of the camera at any time. To

alleviate the problems, we recheck the digital responses during capturing the spectral images of the test surface. During capturing of the preliminary spectral images, wavelength channels are far apart. This indicates that the relationship in reflectance values among these images is unknown. The images may fall out of linear range any time. So, we dynamically keep monitoring the average digital response of the images by measuring the average digital values on the substrate locations in all spectral images and allowing only the values within the acceptable range [i.e., $150 < T_{AVG}(\lambda_k) < 210$]. If the average digital value of any spectral image falls out of this desired range, the stage has to recapture the spectral image with the new exposure time of $\tau_{NEWT180}(\lambda_k) = [180/T_{AVG}(\lambda_k)]\tau_{T180}(\lambda_k)$, except that the image is already captured at the maximum exposure time of the camera (125 ms). After capturing all the preliminary spectral images, the remaining spectral images are captured in numerical order of wavelengths. Since the reflectance curves of most construction materials are usually slowly varying, the reflectance values at the adjacent wavelength channels do not vary much. In addition, recapturing the spectral images takes a longer time than dynamically determining the right exposure times during capturing. Hence, we adjust the exposure time based on the previously captured wavelength during spectral image capturing as

$$\tau_{T180}(\lambda_k) = \left[\frac{180}{T_{AVG}(\lambda_{k-1})} \cdot \frac{\tau_B(\lambda_k)}{\tau_B(\lambda_{k-1})}\right] \cdot \tau_B(\lambda_k). \quad (6)$$

where subscript $k-1$ signifies the previously taken wavelength channel, which is 4 nm less than the present capturing wavelength channel (k). With the abovementioned exposure time adjustment and image capturing method, we obtain smooth calibration and blood stain detection. Since averaging the digital responses of the captured image [$T_{AVG}(\lambda_{k-1})$] is a prerequisite for the determination of substrate reflectance as described in Section 5, Eq. (6) takes just a little extra calculation and time from the process in Section 5 to determine the exposure time of the subsequent image $\tau_{T180}(\lambda_k)$.

7. Results and Discussion

The final result images for blood identification on six different substrates are shown in Fig. 10. Different trials of the result images on gypsum and artificial wood-board test surfaces [Figs. 10(a) and 10(b)] are also shown for comparison with Fig. 6. As mentioned in part 1 of this work [17], we evaluate the performance of our blood stain detection system by its true positive rate (TPR) or sensitivity, true negative rate (TNR) or specificity, and speed. TPR and TNR have already been evaluated then and are not quantitatively evaluated here again. Qualitatively, from visual evaluation, the results show comparable TPR and TNR to the results described in part 1 of this work. It is plainly seen from Fig. 10 that the proposed detection system can be efficiently used to distinguish blood from all six stains on different substrates, though false positives are usually seen at the edges of the stains. This is because the criteria are designed to select all the undetermined spatial points in the ROI and deselect the areas sure as not blood stains. Criteria may not be made specific enough to exclude the areas at the edge of other stains where spectral mixing between stains and substrates occurs. This can be improved by adjusting the criteria to eliminate more of those areas but may sacrifice the specificity of the system. False positives on substrate areas are most noticed in brown tile substrate due to spatial nonuniformity of the substrate's spatial profile.

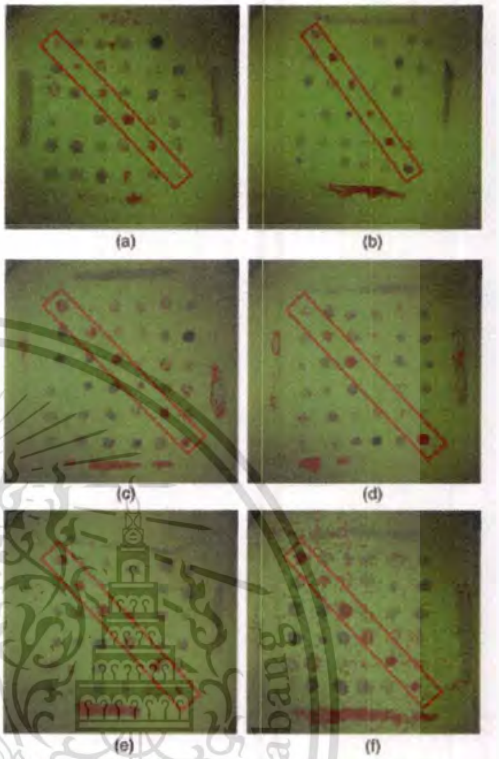

Fig. 10. Final result images of blood identification on (a) gypsum, (b) brown artificial wood, (c) white painted concrete, (d) white tile, (e) blue tile, and (f) rough brown tile.

In this section, we focus on evaluating the speed of our proposed rapid blood stain detection system. The times taken for any task steps can be easily measured by using the LabVIEW program. The average total image capturing times and total blood stain identification times for all six test surfaces are shown in Table 1. As mentioned earlier, our parallel procedures between spectral image capturing and data processing processes allow the two processes to

Table 1. Average Times Taken to Capture All 61 Spectral Images and to Identify the Blood Stain

Test Surface	Average Image Capturing Time (seconds)	Average Total Detection Time (seconds)
Gypsum	23.6	25.7
Artificial wood	26.9	27.6
White painted concrete	22.4	23.3
White tile	24.0	25.2
Blue tile	22.8	23.4
Brown tile	26.3	28.7

run simultaneously. The spectral image capturing time for each test surface, shown on the right side of Table 1, ranges between 22.4 and 26.3 s, while the entire identification times (on the left side) range between 23.3 and 28.7 s. The times taken for capturing all 61 spectral images are just about 1–2 s shorter than the times for the entire identification process. This means that most of the calculations, data extraction, and processing are completed before the image capturing process is finished. During the blood stain detection, the CPU usage sways between 30% and 90%, which indicates efficient spending of the computer resources. The total image capturing time also depends on brightness of the test surfaces. The brighter test surfaces result in lower capturing time, hence identification times, than the dark images since the exposure times are lower. The white painted concrete and the blue tile surfaces have the fastest image capturing times, since they are among the brightest surface. In addition to the image capturing time, the total blood stain identification time also depends on the stain profiles. Basically, the larger the stain area on the image, the more time needed to process the images. However, the key to rapid detection is to eliminate the spatial points identified as nonblood as early as possible. Table 2 shows the measured time ranges taken to process some specific images and data processing steps. The time taken for data processing of the first two images (530 and 470 nm) alone ranges from 1300 to 2500 ms (the average of 650–1250 ms per spectral image). Recall that these two images are processed together in search of the substrate location, extracting digital responses, applying criteria and array manipulation. This relatively long processing time results from a large number of spatial points in ROI. The time taken for data processing of the third images (470 nm spectral image), however, is reduced significantly to 123–166 ms since the spatial points to be processed reduce from about 12,000 down to 1000–2100 after the second images and the substrate searching has already been done. Thanks to our planed ordering of criteria, discussed in Section 4.C, a number of spatial points can be eliminated as early spectral images are processed, and the processing times decrease as further images are processed. The processing time for the ninth image (622 nm spectral image), which is the last preliminary image, drops to 23–55 ms. Remember that all the blood stain identifications are taken while the all stain spots are covered in the images according to configuration in Fig. 2(g). For the images with fewer stain spots, spatial points in ROI should have been less and the identification could be even faster. In later spectral images, the processing time is slightly shorter. There are another 11 blood discrimination criteria that make use of polynomial fits applied after specific images are processed. Application of each polynomial fitting criterion takes an additional 32–74 ms. Despite a relatively long process of polynomial fitting criteria, they can eliminate only a small additional number of spatial points in ROI. Most of the polynomial fitting criterion efforts are redundant to the previous criteria. Optimistically, this may be beneficial in that we can improve in the future by having more preliminary criteria and removing polynomial fitting criteria.

Table 2. Range of Time Taken for Processing Some Spectral Images or Some Data Processing Tasks

Image or Process	Measured Processing Time (ms)
First 2 images (530 and 470 nm)	1300–1500
Image 3 (470 nm)	123–166
Image 9 (622 nm)	23–55
Image 61 (706 nm)	20–55
Application of polynomial fitting	32–74

Though varied due to the exposure time adjustment, image capturing times are relatively constant compared to data processing. They are not getting faster as more images are processed. The capturing time for a single image ranges from 300 to 400 ms depending on wavelengths and test surface's brightness. At early stage of the blood stain identification process, data processing takes longer than image capturing since there are a lot of spatial points in ROI. Data processing lags greatly behind the image capturing. However, as more and more spatial points are excluded from consideration, the blood identification process has become faster. Yet, blood stain detection criteria must wait for the capturing of the needed spectral images. The speed of the system is limited mostly by the image capturing time.

8. Conclusions

We have demonstrated a rapid multispectral-imaging-based blood stain detection system, based upon our blood stain detection criteria established in part 1 of this article [17]. Our system automatically captures multispectral images of the test surface, extracts necessary spectral data, determines the positions of blood stains, and highlights the positions of blood stains on the screen. Several key features are introduced to the system to achieve the fastest and most reliable detection and make the user convenient. First, all procedures and data are organized in the most effective way. Multispectral data are readily stored and processed in the form of array. The well-planned image capturing order

and the blood detection criteria application order permit the system to efficiently eliminate unnecessary data as rapid as possible. Parallel procedures between the image capturing and the blood stain detection process allow for fast detection and efficient usage of the computer resources. Second, the prerequisite substrate reflectance is accurately determined by our automatic substrate searching and determination method. Third, the exposure time monitoring and adaptation keep all bright and dark areas on spectral images brightness enough for blood stain detection for different test surface profiles. The system can automatically detect blood against several other stains on several substrates. The speed of the system has also been evaluated. Our proposed system takes 23.3–28.7 s on average to detect blood stain depending on the test surfaces. The time results suggest that the detection process is limited by the image capturing time not the time for the blood stain detection process. Future work will be focused on reducing the number of spectral images, extending the spectral range into fully visible and near infrared regions, improving blood detection criteria, using permanent filters or different light source for multispectral scan instead of an expensive LCTF device, and building *in situ* devices.

Mr. Janchaysang would like to thank Thailand Graduate Institute of Science and Technology for scholarship support (Grant No. TG-44–22-50-081D).

References

1. A. C. Ponce and A. C. Pascual, "Critical revision of presumptive tests for bloodstains," Forensic Sci. Comm. 1, 1–15 (1991).
2. M. Cox, "A study of the sensitivity and specificity of four presumptive tests for blood," J. Forensic Sci. 36, 1503–1511 (1991).
3. A. M. Gross, K. A. Harris, and G. L. Kaldun, "The effect of luminol on presumptive tests and DNA analysis using the polymerase chain reaction," J. Forensic Sci. 44, 837–840 (1999).
4. N. Vandenberg and R. A. van Oorschot, "The use of Polilight in the detection of seminal fluid, saliva, and bloodstains and comparison with conventional chemical-based screening tests," J. Forensic Sci. 51, 361–370 (2006).
5. W. C. Lee and B. E. Khoo, "Forensic light sources for detection of biological evidences in crime scene investigation: a review," Malaysian J. Forensic Sci. 1, 17–28 (2010).
6. A. C. Lin, H. M. Hsieh, L. C. Tsai, A. Linacre, and J. C. Lee, "Forensic applications of infrared imaging for the detection and recording of latent evidence," J. Forensic Sci. 52, 1148–1150 (2007).
7. M. Perkins, "The application of infrared photography in bloodstain pattern documentation of clothing," J. Forensic Id. 55, 1–9 (2005).
8. H. Brooke, M. R. Baranowski, J. N. McCutcheon, S. L. Morgan, and M. L. Myrick, "Multimode imaging in the thermal infrared for chemical contrast enhancement part 1: methodology," Anal. Chem. 82, 8412–8420 (2010).
9. H. Brooke, M. R. Baranowski, J. N. McCutcheon, S. L. Morgan, and M. L. Myrick, "Multimode imaging in the thermal infrared for chemical contrast enhancement part 2: simulation driven design," Anal. Chem. 82, 8421–8426 (2010).
10. H. Brooke, M. R. Baranowski, J. N. McCutcheon, S. L. Morgan, and M. L. Myrick, "Multimode imaging in the thermal infrared for chemical contrast enhancement part 3: visualizing blood on fabrics," Anal. Chem. 82, 8427–8431 (2010).
11. J. H. Wagner, "Applications of UV-visible spectral imaging in forensic science," Ph.D. dissertation, University of Auckland (2008).
12. G. M. Miskelly and J. H. Wagner, "Using spectral information in forensic imaging," Forensic Sci. Int. 155, 112–118 (2006).
13. http://www.chemimage.com/docs/product.../CI-productsheet-CONDOR.pdf, "Condor Wide-field hyperspectral imaging system," ChemImage product sheet PSREV005 (2010).
14. http://www.chemimage.com/docs/application-notes/forensics/CI-appnote-Visualization-of-Bloodstains.pdf, "Hyperspectral imaging enables straightforward visualization of bloodstains," ChemImage Application note, ANREV002 (2010).
15. http://www.chemimage.com/news/newsletter/forensic_focus/november2010.aspx, "Hypserspectral imaging:a high-contrast alternative to visualizing blood spatter and stains," Forensic Focus E-Newsletter 11, (2010).
16. http://www.chemimage.com/products/instrumentation/examiner/, "HSI Examiner 1000," ChemImage product sheet PSREV001 (2012).
17. S. Janchaysang, S. Sumriddetchkajorn, and P. Buranasiri, "Tunable filter-based multispectral imaging for detection of blood stains on construction material substrates part 1: developing blood stain discrimination criteria," Appl. Opt. 51, 6984–6996 (2012).
18. R. H. Bremmer, A. Nadort, T. G. van Leeuwen, M. J. van Gemert, and M. C. Aalders, "Age estimation of blood stains by hemoglobin derivative determination using reflectance spectroscopy," Forensic Sci Int. 206, 166–171 (2011).
19. B. Widrow and I. Kollar, *Quantization Noise: Roundoff Error in Digital Computation Signal Processing, Control, and Communications.* (Cambridge, 2008).

Author biography

Name	Suwatwong Janchaysang
Date of Birth	16 April 1974

Education

1978-1986	Thanompit Vitdhaya school, Bangkok, Thailand
1986-1992	Sigun Wattananan Uppatham school, Bangkok, Thailand
1992-1994	Armed Forced Academy Preparatory school, Bangkok, Thailand
1994-1995	Chulachomklao Royal Military Academy, Nakhonnayok, Thailand
1995-1999	Virginia Military Institute (B.S. in Physics) , Virginia, USA
1999-2001	University of Rochester (M.S. in Optics), New York, USA

Career

2001-2002	Low altitude aircraft detection radar platoon leader, 3th Anti Aircraft Artillery Battalion, Lopburi, Thailand.
2002-2004	Artillery battery commander, 3th Anti Aircraft Artillery Battalion, Lopburi, Thailand.
2004-present	Lecturer, Department of Physics, Chulachomklao Royal Military Academy, Nakhonnayok, Thailand